YAG ($Y_3Al_5O_{12}$) as a SCAVENGER for Si and Ca

by

YENER KURU

Submitted to the Graduate School of Engineering and Natural Sciences
in partial fulfillment of
the requirements for the degree of
Master of Science

Sabancı University
July 2004

YAG ($Y_3Al_5O_{12}$) as a SCAVENGER for Si and Ca

APPROVED BY:

Assist. Prof. Mehmet Ali Gülgün ……………………………………
(Dissertation Supervisor)

Assist. Prof. Cleva Ow-Yang ……………………………………

Assoc. Prof. Mehmet Somer ……………………………………

DATE OF APPROVAL: ……………………………………

ABSTRACT

General garnet structure (Ia3-d) is a forgiving host and can accommodate cations of varying sizes and valence states. Yttrium aluminate garnet (YAG, $Y_3Al_5O_{12}$) forms with the substitution of yttrium for manganese in the original garnet mineral spessartite ($Mn_3Al_2(SiO_4)_3$), if aluminum simultaneously substitute for silicon such that the charge neutrality is maintained. Studies on highly yttrium doped alumina ceramics with Si and Ca contamination indicated that YAG precipitates in the ceramic had a propensity to allow simultaneous incorporation of small amounts of Si and Ca impurities in their structure. In this study, using chemical synthesis techniques it was shown that YAG can accommodate up to approximately 10 cation % Si^{4+} and Ca^{2+} (i.e. Si^{4+}/Y^{3+} and Ca^{2+}/Y^{3+}) amount in YAG if they are incorporated together. Equilibrium conditions are established by calcining samples at 900°C for 2 hours and cooling the samples to room temperature in the furnace. Disappearing-phase method and EDS analysis were used to determine solubility and co-solubility limits. Beyond the solubility limit phase separation occured and three crystalline yttrium aluminate phases (YAG, YAP (yttrium aluminate perovskite, $YAlO_3$), YAM (yttrium aluminate monoclinic, $Y_4Al_2O_9$)) were observed. It is believed that the excess Si and Ca above co-solubility limit precipitate out in the form of an x-ray amorphous anorthite like glass in the system.

ÖZET

Genel garnet yapısında (Ia3-d) değişik büyüklükte ve yükte birçok katyonu rahatlıkla barındırabilir. İtriyum alüminat garnet (YAG, $Y_3Al_5O_{12}$) eğer itriyum ile mangan ve alüminyum ile silikon aynı anda yer değiştirirlerse orijinal garnet yapılı spessartite ($Mn_3Al_2(SiO_4)_3$) mineralinden üretilebilir. Bu yer değiştirmeler sırasında yapıdaki yük dengesi korunmuş olur. Yüksek miktarda itriyum eklenmiş alümina seramiklerinin Si ve Ca ile kirletilmesi üzerine çalışmalar, seramikte çökelen YAG fazının yapısına düşük miktarda Si ve Ca girişine izin verdiğini göstermiştir. Bu çalışmada, kimyasal sentez yöntemleri kullanılarak, yapıya birlikte girmeleri durumunda, YAG fazının Y^{3+} katyonlarının yaklaşık %10'u kadar Si^{4+} ve Ca^{2+} katyonlarını barındırabildiği gösterilmiştir. Denge koşullarının sağlanması için 900°C de 2 saat ısıl işlem uygulanmıştır ve numuneler fırında oda sıcaklığına kadar soğutulmuştur. Çözünürlük limitlerinin bulunması için kaybolan faz ve EDS elementel analiz yöntemleri kullanılmıştır. Çözünürlük sınırı aşıldığında faz ayrımı oluşmuştur ve üç kristal faz (YAG, YAP (itriyum alüminat peroskit, $YAlO_3$), YAM (itriyum alüminat monoklinik, $Y_4Al_2O_9$)) gözlenmiştir. Ortak çözünürlük sınırını aşan Si ve Ca katyonlarının x-ışını amorf anorthite benzeri camsı bir faz olarak çökeldiğine inanılmaktadır.

To my family and my Gülgün

ACKNOWLEDGEMENTS

I would like to thank my supervisor, Assist. Prof. Mehmet Ali Gülgün, for his guidance and advice throughout this study. Without his ideas and support, I would not have been even able to start this project. It was a great relief during my days at Sabancı University, to have a professor and a big brother like him.

I would like to thank Assist. Prof. Canan Baysal, for her encouraging attitude and kindness from my interview to my graduation.

I would like to thank my laboratory partner Erdem Onur Savaşır for his excellent assistance throughout this study.

I am also grateful to my friends Serkan Baş, Özgür Bozat, Karahan Bulut, Burcu Kaplan, Çınar Öncel, İstem Özen, Güngör Özer, Gözde İ. Öztürk, Ünal Şen and Mesut Ünal for their support and help through the past two years.

Finally, I would like to thank faculty members Prof. Yusuf Ziya Menceloğlu and Prof. Alpay Taralp and students at the Materials Science and Engineering Program, for making things a lot easier.

TABLE OF CONTENTS

ABBREVIATIONS

AHC: NH_4HCO_3

BSE: Back scattered electron

CN: Coordination number

EDS: Energy dispersive spectrometer

G.B.: Grain boundary

n_A: mole number of A

nm: nanometer

PEG: Poly ethylene glycol

pm: picometer

ppm: parts per million

PVA: Poly vinyl alcohol

SEM: Scanning electron microscope

T: Temperature

TEM: Transmission electron microscope

TEOS: Tetra ethyl orto silicate

XRD: X-ray diffraction

YAG: Yttrium aluminate garnet

YAM: Yttrium aluminate monoclinic

YAP: Yttrium aluminate perovskite

a_B: Activity of B

LIST OF FIGURES

LIST OF TABLES

YAG ($Y_3Al_5O_{12}$) as a SCAVENGER for Si and Ca

by

YENER KURU

Submitted to the Graduate School of Engineering and Natural Sciences
in partial fulfillment of
the requirements for the degree of
Master of Science

Sabancı University
July 2004

YAG ($Y_3Al_5O_{12}$) as a SCAVENGER for Si and Ca

APPROVED BY:

Assist. Prof. Mehmet Ali Gülgün ……………………………………
(Dissertation Supervisor)

Assist. Prof. Cleva Ow-Yang ……………………………………

Assoc. Prof. Mehmet Somer ……………………………………

DATE OF APPROVAL: ……………………………………

ABSTRACT

General garnet structure (Ia3-d) is a forgiving host and can accommodate cations of varying sizes and valence states. Yttrium aluminate garnet (YAG, $Y_3Al_5O_{12}$) forms with the substitution of yttrium for manganese in the original garnet mineral spessartite ($Mn_3Al_2(SiO_4)_3$), if aluminum simultaneously substitute for silicon such that the charge neutrality is maintained. Studies on highly yttrium doped alumina ceramics with Si and Ca contamination indicated that YAG precipitates in the ceramic had a propensity to allow simultaneous incorporation of small amounts of Si and Ca impurities in their structure. In this study, using chemical synthesis techniques it was shown that YAG can accommodate up to approximately 10 cation % Si^{4+} and Ca^{2+} (i.e. Si^{4+}/Y^{3+} and Ca^{2+}/Y^{3+}) amount in YAG if they are incorporated together. Equilibrium conditions are established by calcining samples at 900°C for 2 hours and cooling the samples to room temperature in the furnace. Disappearing-phase method and EDS analysis were used to determine solubility and co-solubility limits. Beyond the solubility limit phase separation occured and three crystalline yttrium aluminate phases (YAG, YAP (yttrium aluminate perovskite, $YAlO_3$), YAM (yttrium aluminate monoclinic, $Y_4Al_2O_9$)) were observed. It is believed that the excess Si and Ca above co-solubility limit precipitate out in the form of an x-ray amorphous anorthite like glass in the system.

ÖZET

Genel garnet yapısında (Ia3-d) değişik büyüklükte ve yükte birçok katyonu rahatlıkla barındırabilir. İtriyum alüminat garnet (YAG, $Y_3Al_5O_{12}$) eğer itriyum ile mangan ve alüminyum ile silikon aynı anda yer değiştirirlerse orijinal garnet yapılı spessartite ($Mn_3Al_2(SiO_4)_3$) mineralinden üretilebilir. Bu yer değiştirmeler sırasında yapıdaki yük dengesi korunmuş olur. Yüksek miktarda itriyum eklenmiş alümina seramiklerinin Si ve Ca ile kirletilmesi üzerine çalışmalar, seramikte çökelen YAG fazının yapısına düşük miktarda Si ve Ca girişine izin verdiğini göstermiştir. Bu çalışmada, kimyasal sentez yöntemleri kullanılarak, yapıya birlikte girmeleri durumunda, YAG fazının Y^{3+} katyonlarının yaklaşık %10'u kadar Si^{4+} ve Ca^{2+} katyonlarını barındırabildiği gösterilmiştir. Denge koşullarının sağlanması için 900°C de 2 saat ısıl işlem uygulanmıştır ve numuneler fırında oda sıcaklığına kadar soğutulmuştur. Çözünürlük limitlerinin bulunması için kaybolan faz ve EDS elementel analiz yöntemleri kullanılmıştır. Çözünürlük sınırı aşıldığında faz ayrımı oluşmuştur ve üç kristal faz (YAG, YAP (itriyum alüminat peroskit, $YAlO_3$), YAM (itriyum alüminat monoklinik, $Y_4Al_2O_9$)) gözlenmiştir. Ortak çözünürlük sınırını aşan Si ve Ca katyonlarının x-ışını amorf anorthite benzeri camsı bir faz olarak çökeldiğine inanılmaktadır.

To my family and my Gülgün

ACKNOWLEDGEMENTS

I would like to thank my supervisor, Assist. Prof. Mehmet Ali Gülgün, for his guidance and advice throughout this study. Without his ideas and support, I would not have been even able to start this project. It was a great relief during my days at Sabancı University, to have a professor and a big brother like him.

I would like to thank Assist. Prof. Canan Baysal, for her encouraging attitude and kindness from my interview to my graduation.

I would like to thank my laboratory partner Erdem Onur Savaşır for his excellent assistance throughout this study.

I am also grateful to my friends Serkan Baş, Özgür Bozat, Karahan Bulut, Burcu Kaplan, Çınar Öncel, İstem Özen, Güngör Özer, Gözde İ. Öztürk, Ünal Şen and Mesut Ünal for their support and help through the past two years.

Finally, I would like to thank faculty members Prof. Yusuf Ziya Menceloğlu and Prof. Alpay Taralp and students at the Materials Science and Engineering Program, for making things a lot easier.

TABLE OF CONTENTS

ABBREVIATIONS

AHC: NH_4HCO_3

BSE: Back scattered electron

CN: Coordination number

EDS: Energy dispersive spectrometer

G.B.: Grain boundary

n_A: mole number of A

nm: nanometer

PEG: Poly ethylene glycol

pm: picometer

ppm: parts per million

PVA: Poly vinyl alcohol

SEM: Scanning electron microscope

T: Temperature

TEM: Transmission electron microscope

TEOS: Tetra ethyl orto silicate

XRD: X-ray diffraction

YAG: Yttrium aluminate garnet

YAM: Yttrium aluminate monoclinic

YAP: Yttrium aluminate perovskite

a_B: Activity of B

LIST OF FIGURES

LIST OF TABLES

1 INTRODUCTION

Yttrium aluminum garnet, $Y_3Al_5O_{12}$ (YAG), drew considerable attention as a host for solid-state industrial, medical and scientific laser applications. YAG is known to be a very forgiving host material and can be heavily doped with cations of different sizes and valence states. In addition to this YAG is one of the best high temperature structural oxides known[1]. The lasing substances such as neodymium, erbium, ytterbium, chromium, thulium, or holmium can be incorporated into the matrix of YAG in suitable concentrations. Nd:YAG is one of the best laser materials for the high power, high energy and Q-switched pulse laser systems since its upper level has a long lifetime and population buildup can occur. It is used for distance measuring, chemical large-distance analysis, laser drilling, pointer for electronic vision etc[2]. Compared with the commonly used Nd:YAG crystal, another doped crystal Yb: YAG has a larger absorption bandwidth and it is known as a good laser gain material. In the case of Yb:YAG doping level as high as 50at.% was recently reported[3]. Yet another laser crystal, Er:YAG produces “eye-safe” wavelengths for many applications where human eyes could be injured. Their excellent optical, high temperature mechanical properties and chemical stability, suggest YAG ceramics as the most promising materials for solid-state laser application. Moreover, some of its high temperature mechanical properties open YAG new application fields like fiber reinforcements in ceramic and metal-matrix composites that withstand very high temperatures as advanced structural materials[4-6].

Several methods were reported to synthesize YAG powders in the literature. Although solid-state reaction method[7-14] is more suitable than wet chemical synthesis methods for large scale production, it has several drawbacks such as high processing temperature(T>1200°C), contamination due to extensive ball milling and large particle size. Alternative fabrication methods are hydrothermal synthesis[15-17], co-precipitation[18-20], sol-gel process[21-24], Pechini method[25,26], polymerized organic-inorganic synthesis [27] and mixed solvothermal method[28].

One way of substituting cations is introduction of a cation similar in size and charge to one of the original cations. Another way is to include the substitution of two cations that have similar sizes but different charges, one greater and the other less than those of the original cations[29]. It was shown by Yoder and Keith[30] that there is a complete solid solution series between garnet mineral spessartite ($Mn_3Al_2(SiO_4)_3$) and yttrium aluminate garnet (YAG, $Y_3Al_5O_{12}$). Yoder and Keith showed that yttrium can be substituted for manganese if aluminum is simultaneously substituted for Si to maintain charge balance in the structure[30]. Carda pointed out that garnet solid solutions can be synthesized between $Y_3Al_2Al_3O_{12}$ (YAG) and $Ca_3Cr_2Si_3O_{12}$ (uvarovite) although there is incomplete substitution in small sites[31].

In this thesis, we report that YAG can be contaminated by relatively large amounts of Si and Ca when they are simultaneously incorporated in contrast to their low elemental solubilities in the ceramic. Figure1.1 depicts a hypothetical crystal structure of Si and Ca co-doped YAG and possible positions of Ca and Si impurities in the lattice. Existence of $Y_3Al_2Al_3O_{12}$ (YAG) and $Ca_3Al_2Si_3O_{12}$ (grossular) compounds that have same crystal structure and conservation of charge balance in the structure during the substitution may be responsible for this increased co-solubility limit.

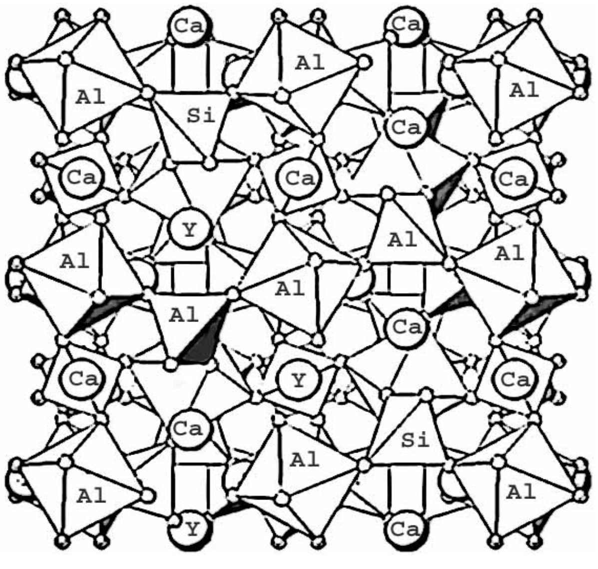

Figure 1.1. Possible positions of Ca and Si ions in crystal structure of YAG after http://unit.aist.go.jp/greenlife/ii/STRUCIMAGES/Grossular.gif[32].

2 OVERVIEW

In the first part of this chapter, methods especially the wet chemical ones, that are used to produce mixed oxide ceramics were explained. Detailed information about the three intermediate compounds in Y_2O_3-Al_2O_3 system, YAG, YAP and YAM, were given in the second part.

2.1 Methods for YAG Production

2.1.1 Solid State Reaction Method

Solid state reaction method is a basic and well known technique to produce mixed oxide ceramic materials. Oxides and/or carbonates of the cations are usually used as starting materials. Starting materials are weighed and mixed according to the stoichiometry of the ceramic that will be synthesized. This mixture is wet ball milled and resulting slurry is dried[7]. Final step in the procedure is annealing the mixture at high temperatures in order to increase atomic mobilities and reaction rate to facilitate atomic scale mixing. Solid-state reaction method is a suitable method for large scale production but it has some disadvantages like high processing temperature($T>1200°C$), contamination due to extensive ball milling and large particle size. It also requires repeated cycles of grinding and high temperature treatment to assure phase purity.

2.1.2 Wet Chemical Methods

In wet chemical methods, molecular level mixing is obtained by dissolving precursors in a liquid medium. Better homogeneity, lower process temperature due to shorter diffusion distances, lower energy consumption and lower initial investment cost are some important advantages of these methods over conventional high temperature, solid state methods[33].

2.1.2.1 Sol-Gel Method

Sol-gel process is a wet chemical method. It has advantages such as better composition control (molecular level) and better homogeneity. In addition, it is an economical process due to lower process temperature, which directly determines the energy consumed, and equipment needed for production. This lower capital investment cost also made this technique attractive for processing of multication oxide ceramics[34].

Materials which are used in modern ceramic and device technologies require high purity and close control over composition and microstructure. Since the chemical reactants for sol-gel process can be purified conveniently by distillation and crystallization, final powders can be obtained with high chemical and phase purity.

A very important advantage of sol-gel and other wet chemical processes is that since the elements that will form the final compound are mixed at the molecular level, the diffusion distances are very short. Therefore thermodynamically stable phases are easily formed. This ultimate mixing and high reactivity results in homogeneous and pure oxide powders.

There are essentially two kinds of sol-gel technology. The first is colloidal method which involves the dispersion of colloidal particles in a liquid to form a sol and then gel is formed due to the destabilization of the sol. The second method is polymerization of organometallic compounds such as alkoxides to produce a gel with a continuous network. Uniform particles, fibers, aerogels, thin films and dense ceramics can be obtained by sol-gel process. Figure 2.1 describes production routes to different final products by using sol-gel process.

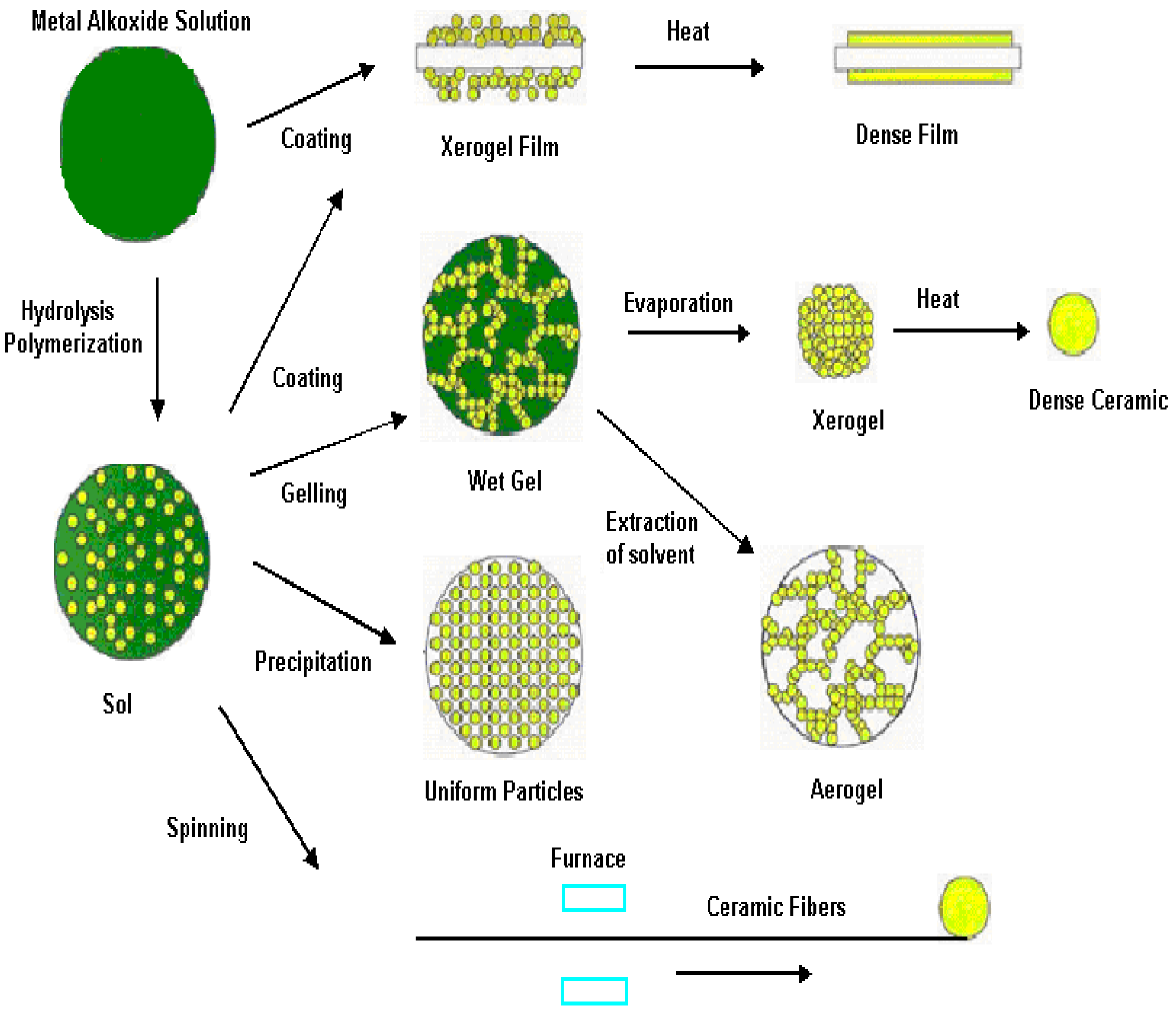

Figure 2.1. Production routes of various types of final products by sol-gel process[35].

Alkoxides, whose general composition is $M(O\text{-}R)_n$, are the typical precursors for making solid solutions where R is an alkyl radical (CH_3, C_2H_5, etc.). Properties of precursors have important effects on process route and product properties. The ideal compounds to be used as precursors should have following properties:

- It should have high metal content in order to minimize the volume change during the change from metalorganic solution to inorganic product.
- It should have a high solubility in common solvents with other precursor compounds.

- It should thermally decompose and form -M-O-M- (Metal-Oxygen-Metal) network without leaving the system due to evaporation or melting.
- Cost of the precursor should be low.

The ideal solvent for sol-gel process should satisfy the conditions listed below :

- Solvent should evaporate and leave the system in a short time.
- Solvent should produce a stable solution with solute, gelation of solution should not occur quickly in storage conditions.
- Solvent should dissolve high amounts of precursors, it should have proper surface tension and viscosity according to final product of the process[36].

2.1.2.2 Co-precipitation

In co-precipitation method, nitrate or chloride salts of cation(s) are usually dissolved in distilled water. Hydroxides of cations are obtained after precipitation process with a suitable precipitant such as urea, ammonia and AHC (NH_4HCO_3). Then, hydroxides are generally washed and dried. Finally oxide powers are produced by calcination of hydroxides at high temperatures in this method.

Wang et al. synthesized YAG powders by co-precipitation method. Yttrium nitrate and aluminum nitrate were dissolved in distilled water. Hydroxides of cations ($Al(OH)_3$ and $Y(OH)_3$) were obtained after precipitation with ammonia. Then hydroxides were washed and dried in oven at 100 °C. Finally, dried hydroxide precursors were heat treated at various temperatures in order to produce YAG powders. Pure YAG phase was obtained when calcination temperature was 900 °C or higher[18].

YAG powders were produced from yttria, aluminum nitrate, urea and AHC by Li et al. also using co-precipitation method. Yttria was dissolved in nitric acid and some distilled water. Aluminum nitrate was dissolved in distilled water, then hydroxides were formed after precipitation by urea and AHC. Hydroxides were dried by an infrared lamp and precursors were calcined at different temperatures. Pure YAG phase was obtained after calcination at 900 °C for 2 hours[37].

2.1.2.3 Hydrothermal Synthesis

In hydrothermal synthesis, solution or suspension of reactants such as metal salts, hydroxides, metal powders and oxides are prepared in a liquid (usually in water). Ceramic powders are produced by heating this solution or suspension at elevated temperatures and pressures. Sub-micron sized oxides, non-oxides and metallic particles can be formed with controlled size and shape by nucleation and growth processes that occur under fabrication temperature and pressure.[38]

Homogeneous nucleation due to forced hydrolysis and phase transformations in hydrothermal synthesis method allow fabrication of advanced ceramics like stabilized zirconia in the form of isolated sub-micron sized oxide particles with controlled shape, size and high chemical purity. Low process temperature and ability to use impure reactants are important advantages of this technique. [38]

Yu et al. synthesized $ZnFe_2O_4$ ultrafine particles by the interface reaction between a metal zinc sheet and $FeCl_2$ as reactants in ammonia solutions at 180 °C.[39] Spinel-type lithium manganese oxide nanocrystals were produced from LiOH, $Mn(NO_3)_2$ and H_2O_2 at 90 °C –110 °C for 8 hours by Zhang et al.[40] Zhang et al. also reported the production of MnS crystallites at 60 °C-130 °C via the reaction of manganese acetate and thioacetamide in water.[41]

2.1.2.4 Solution Polymerization Techniques

2.1.2.4.1. Polymerizable Complex Method

Polmerizable complex method is based on the polyesterification reaction between citric acid and ethylene glycol. Metal ions are immobilized in the polyester network. Segregation of a particular metal during process is greatly reduced.[42] Citric acid is dissolved in water. The mixture is magnetically stirred after the metal precursors are added into citric acid solution. After complete dissolution, ethylene glycol is added. Final solution is slowly heated to 90 °C in order to remove excess water and to accelerate polyesterification reaction. The resulting resin is heat treated at 400°C-450°C for the removal of highly combustible organics. Oxide powders are obtained after the final heat treatment at 500 °C-900 °C for 6 hours.[43]

Synthesis of $LaCoO_3$ powders were reported by Popa et al. Polymeric precursor was treated at 600 °C for 6 hours. [44] $LaMeO_3$ (Me: Mn, Fe) powders were also produced by polmerizable complex method after calcination at 900 °C for 6 hours. [43]

This method provides an easy control over final stoichiometry, low processing temperature and high surface areas of the resulting material. Intermediate grinding steps are not necessary for this process.[44]

2.1.2.4.2. Pechini Method

Pechini process is a solution polymerization technique. It is arguably one of the most successful processes for production of single phase mixed oxide powders. Although it is not the only mechanism, chelation of metal ions by certain organic acids is the main stabilizing mechanism of this technique[27]. When the solution is heated chelates undergo polyesterification reaction. The result is that cations are homogeneously distributed in the polymeric resin. Mixed oxide powders are obtained after calcinations of the preceramic powder. [27]

Generally nitrates are used as cation source. Stoichiometric amounts of nitrates were added into citric acid and metal citrates are formed. Proper amount of ethylene glycol is added to start polyesterification reaction and solution is heat at 120 °C-200 °C to evaporate the water in the solution. Ceramic powders were obtained after the final calcination step at 550 °C-800 °C for 8-12 hours.[45]

Wu et al. produced $LiMn_2O_4$ powders by Pechini process. Molar ratio of citric acid to ethylene glycol was 1:4, drying treatment was done at 200 °C for 6 hours. Calcination was carried out between 600 °C and 800 °C for 8 hours.[46] $ZnGa_2O_4:Tb^{3+}$ phosphors were synthesized by Xu et al. Citric acid to ethylene glycol molar ratio was 1:1 in the experiment. Solution was dried at 120 °C for 14 hours and resulting polymeric resin was calcined at various temperatures. Single phase $ZnGa_2O_4$ could produced when calcination temperature is 550 °C or higher.[47]

2.1.2.4.3 Polymerized Organic-Inorganic Synthesis

Polymerized organic-inorganic route uses simple, long chain polymers like PVA and PEG that do not have special chelating end groups. This process is a viable and inexpensive technique for production of metal oxide powders. Many ceramic powders can be produced successfully by this new method. [27]

Since there is not any chelating organics in the solution factors other than chemical linking should stabilize the metal ions in the polymer structure. The following mechanism was proposed by Gülgün et al. about the physical entrapment of cations in the network structure of polymers that do not have chelating end groups. Metal ions that are not connected to hydroxyl groups are free in the solution. Water molecules make bridges between the metal ions that are linked to the hydroxyl group and the free cations in the solution. During heating water starts to evaporate, viscosity of the solution increases and polymer chains come closer to each other. Free space between polymer chains decreases and polymer entanglement occurs. As a result mobility of the cations is greatly reduced and they remain entangled in the polymer network. [27]

Selection of a cation source whose aqueous solubility is high is an important factor for the process to be successful. Nitrate sources are highly soluble in cold water and are strong oxidizing agents so that they help with pyrolysis of the organics and reduce the amount of carbonates that are formed. Gülgün et al. mentioned that samples which were calcined at temperatures below 900 °C contained amorphous carbonate like compounds. As calcination temperature was increased, the amount of carbonate phases observed by IR spectroscopy decreased. They also reported that the morphology of the powders were influenced by chain length of the polymeric carrier. When smaller chain lengths were used agglomerates were round and hollow. On the other hand, star shaped dendritic agglomerates were produced if longer chains were used.[27]

2.2 Intermediate Compounds in Y_2O_3-Al_2O_3 System

Y_2O_3-Al_2O_3 phase diagram and reported studies on the existence, stability and formation mechanisms of three intermediate compounds in the Y_2O_3-Al_2O_3 system are inconsistent in literature and this enigma is not resolved yet completely.

Chronological development of Y_2O_3-Al_2O_3 phase diagram is shown in Figure 2.2. and the main difference between them is about the existence and stability range of $YAlO_3$ (YAP) phase[48]. Most recent one was published by Abell et al. and it accepts $YAlO_3$ (YAP) phase as a stable phase. Information about crystal structures, atomic positions, X-ray peaks and reported data related to their existence and stability is given in following sections.

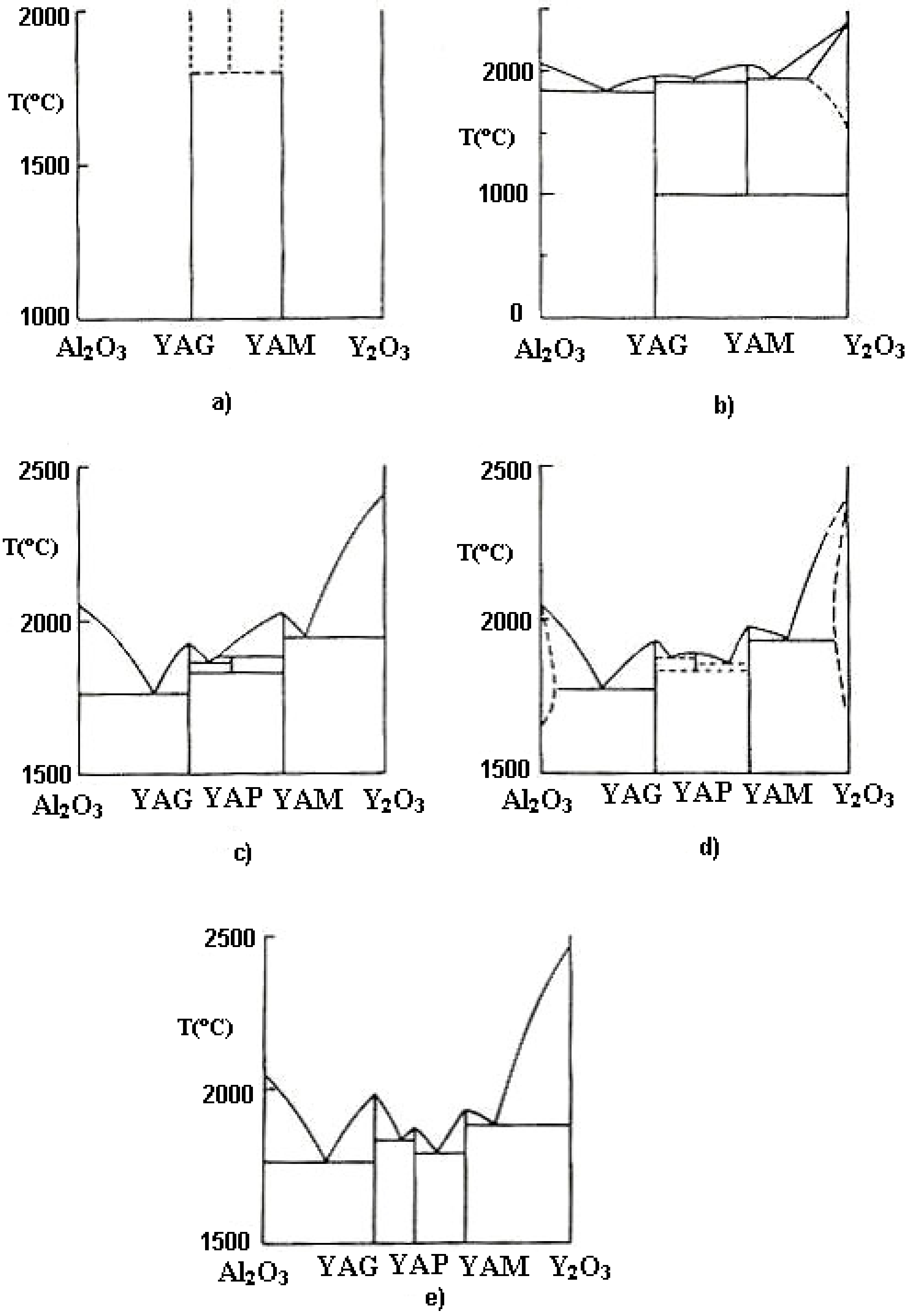

Figure 2.2. Chronological development of Y_2O_3-Al_2O_3 phase diagram[48] a) Schneider et al.[48] b) Olds et al.[49] c) Toropov et al.[50] d) Mizuno et al.[48] e) Abell et al.[51].

2.2.1. $Y_3Al_5O_{12}$ (YAG)

YAG has cubic garnet structure that has 160 atoms in each unit cell[48]. Garnet crystal structure can be seen in Figure 2.3 and Appendix A. Table 2.1. shows the atomic positions in YAG structure. Calculated X-ray diffraction spectrum of YAG is given in Figure 2.4.

Atom	**# of Atom**	**Oxi**	**Wy**	**x**	**y**	**Z**
Al	1	+3	16a	0.0	0.0	0.0
Al	2	+3	24d	0.375	0.0	0.25
Y	1	+3	24c	0.125	0.0	0.25
O	1	-2	96h	-0.029	0.053	0.1510

Table 2.1. Atomic positions in YAG structure.[52]

YAG is one of the stable intermediate phases in the Y_2O_3-Al_2O_3 binary phase system. Both fused and sintered samples and single crystals are stable when system is cooled to room temperature and annealed at temperatures below the melting point. Its stability stretches from room temperature to its melting point at 1970 °C[48].

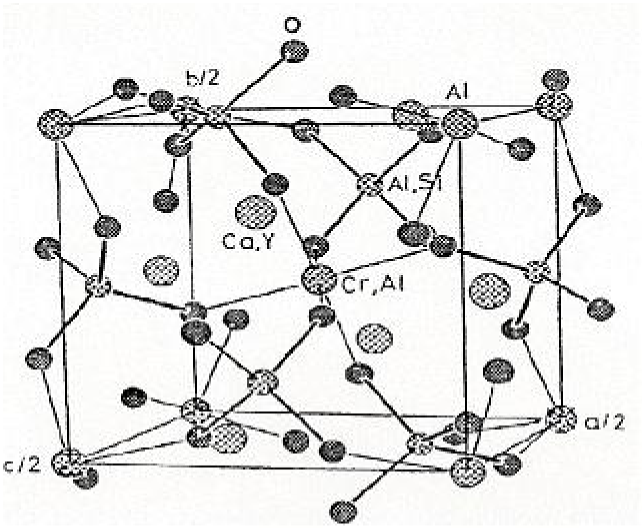

Figure 2.3. Garnet crystal structure[31].

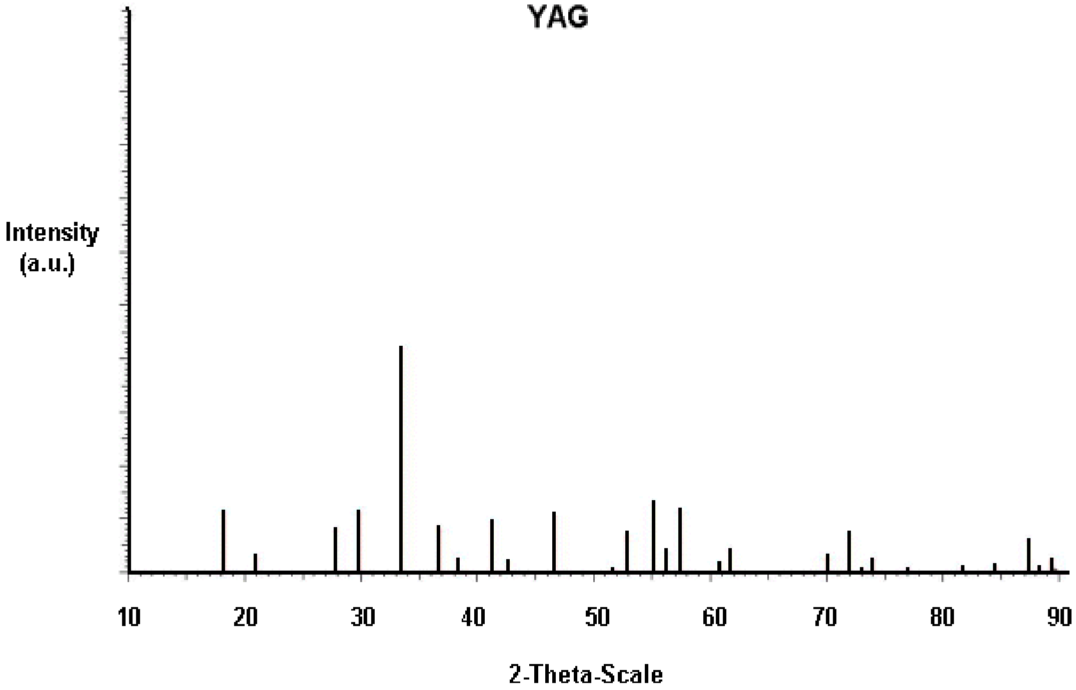

Figure 2.4. Calculated XRD peak positions of YAG.

Interesting thing about solidification behavior of YAG is that the phase formation and the final phase composition is kinetically controlled. It was observed that nucleation of solid phase from the melt determines the transparency of the sample. When heterogeneous nucleation occurs, low undercooling is sufficient for transformation.

Phase transformation happens at a high temperature. As a result mobility of atoms is high enough to form the YAG phase which has a complex structure with 160 atoms in a unit cell. When homogeneous nucleation is the mechanism, the YAG phase nucleates without the help of an external surface and a larger surface area must be created. The transformation should occur at a lower temperature because undercooling is the driving force for nucleation and a larger driving force is necessary to create a larger surface area. As a result, diffusion is limited and mobility of atoms are not sufficient to form the complex YAG phase instead simpler YAP and Al_2O_3 phases with only 20 and 10 atoms per unit cell form, respectively[48].

Data published by Hess et al.[53] also confirms this conclusion. They synthesized YAG by using glycine-nitrate process depending on temperature and time. They sometimes observed pure YAG or YAG and YAP phases when they prepared starting materials according to YAG composition. Although the balance of the starting composition would require Al_2O_3-rich phase formation, they did not observe any other crystalline phases in the XRD spectra. They underlined that formation of amorphous Al_2O_3 phase could explain production of YAP phase although they started with YAG stoichiometry. Figure 2.5 shows time and temperature intervals where certain phases are obtained starting with YAG composition. It can be seen that when time or temperature is low and when fast heating rates are applied, YAP and YAG phases are produced. This region is the diffusion limited region. At high temperatures and/or long processing times, YAG phase is observed. Under such conditions diffusion rate is high and enough time is given to the atoms to arrange themselves in the complex 160 atom unit cells of YAG in these parts of the diagram.

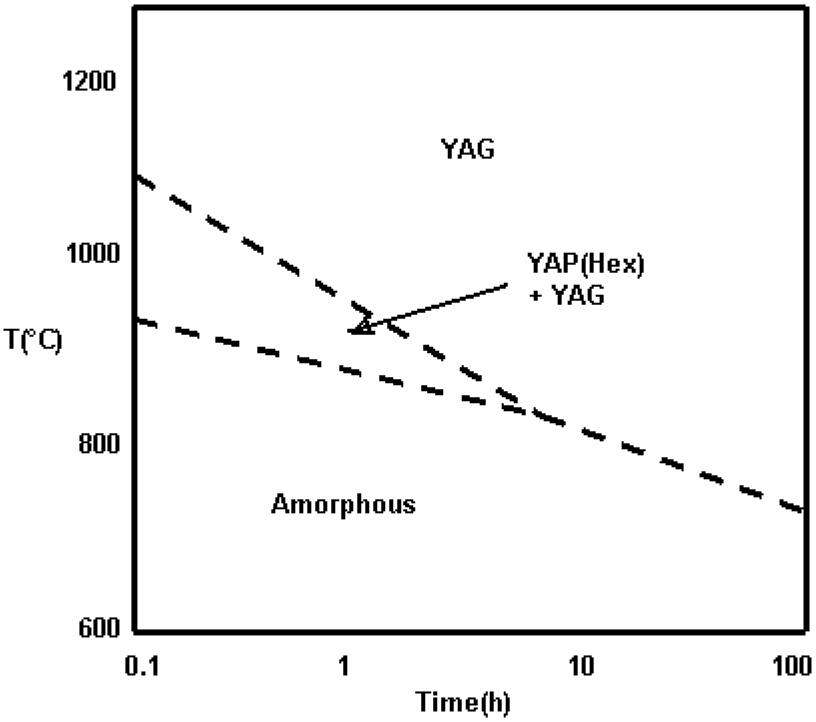

Figure 2.5. Time and temperature intervals where certain phases are obtained started with YAG composition.

2.2.2. $YAlO_3$ (YAP)

YAP is a dimorphic phase in the binary system. In other words, same composition has two crystal structures. The first one is orthorhombic perovskite structure that has 20 atoms in each unit cell[48] and the second one is a hexagonal structure. Crystal structures of YAP can be seen in Appendix A. Table 2.2. and Table 2.3. show the atomic positions in YAP structures. Figure 2.6 and Figure 2.7 give 2θ values of YAP phases.

Atom	**# of Atom**	**Oxi**	**Wy**	**x**	**Y**	**z**
Y	1	+3	4c	0.0526	0.250	0.9896
Al	1	+3	4b	0.0	0.0	0.5
O	1	-2	4c	0.475	0.250	0.086
O	2	-2	8d	0.293	0.044	0.703

Table 2.2. Atomic positions in orthorhombic YAP structure.[54]

Atom	**# of Atom**	**Oxi**	**Wy**	**x**	**Y**	**z**
Y	1	+3	2a	0.0	0.0	0.0
Al	1	+3	2c	0.3333	0.6667	0.25
O	1	-2	2b	0.0	0.0	0.250
O	2	-2	4f	0.3333	0.6667	0.077

Table 2.3. Atomic positions in hexagonal YAP structure.[55]

Doubts about the existence, stability, crystal structure and composition of YAP phase are the main causes of the conflicting results in the literature about Y_2O_3-Al_2O_3 system. After its production as a single crystal by Czochralski method, it was accepted as a stable phase and shown as such in the Y_2O_3-Al_2O_3 phase diagram[48].

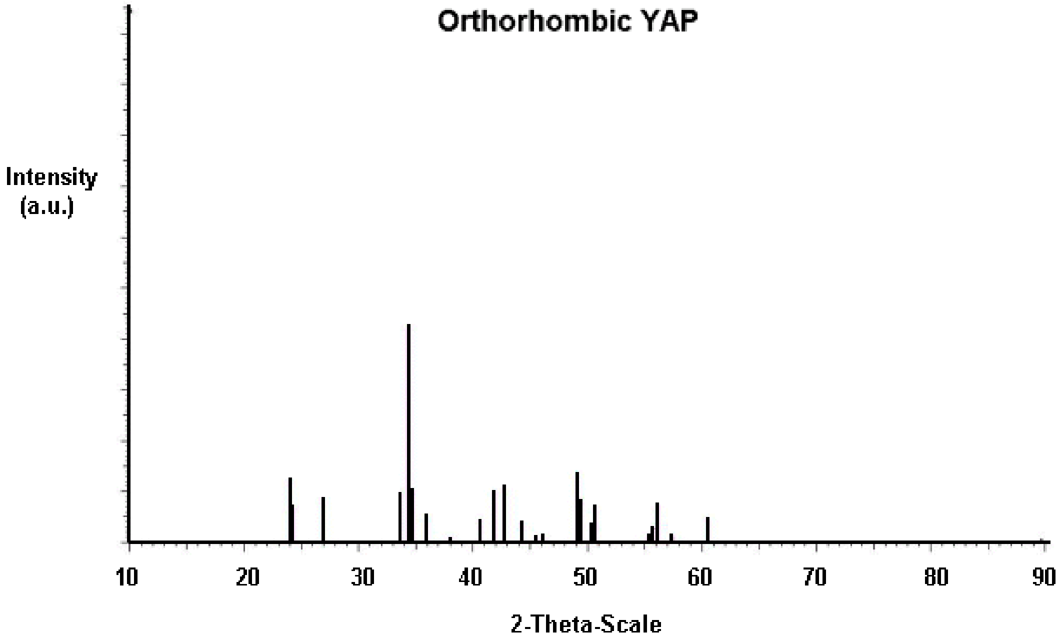

Figure 2.6. Calculated XRD peak positions of orthorhombic YAP.

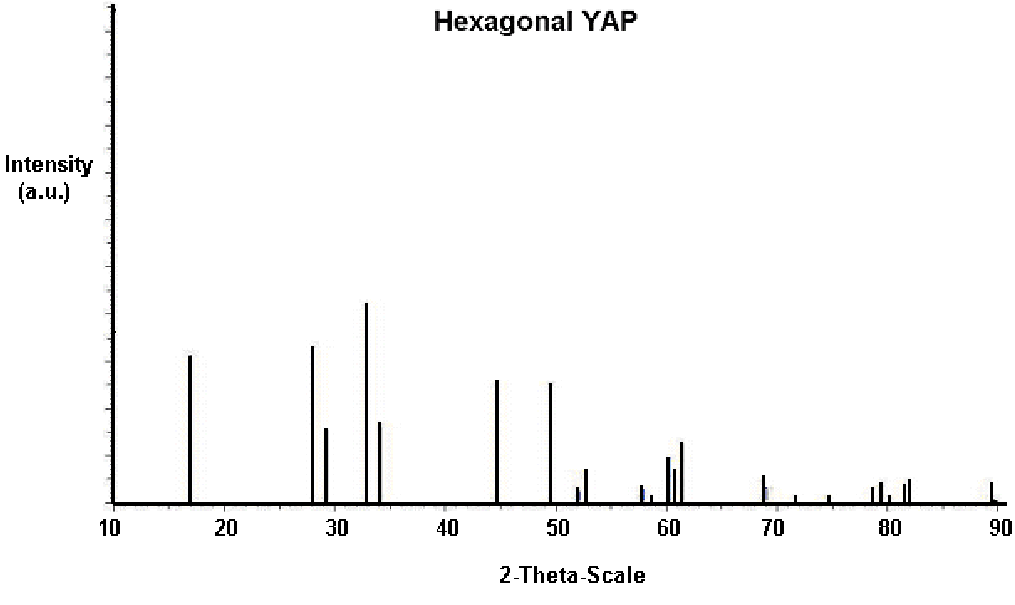

Figure 2.7. Calculated XRD peak positions of hexagonal YAP.

Czochralski growth is not always an equilibrium process so stability of YAP needed to be confirmed by annealing. Abell et al. observed the decomposition of the surface of YAP single crystal into two phases. The first phase was YAG and the second phase could not be identified. Further decomposition did not occur after the surface film had decomposed. Decomposition was probably diffusion limited. Possible reason of the decomposition process was claimed to be oxygen loss[48]. However, Abell et al. proved that decomposition process was not affected by vacuum or reducing atmosphere while remelting the decomposed parts in an oxygen atmosphere regenerated the YAP phase[51]. The key factor in the whole decomposition process was shown to be the surface area. When the surface area was greater, the tendency for decomposition was greater. As a result if YAP is produced from powders by sintering or by fusion, amount of YAP that is decomposed is much more than the single crystal case. Therefore YAP was thought to be a metastable phase. This appears to be the reason of the confusion in the literature[48].

Hess et al. synthesized YAP by glycine-nitrate process. Figure 2.8 shows time and temperature intervals where certain phases are obtained starting with YAP composition. They showed that crystallization of YAP involves three intermediate phases: hexagonal YAP, YAG and YAM. Mostly orthorhombic YAP and detectable amounts of YAG and YAM were observed at high temperatures and long processing times. They suggested that the sequence of crystallization of YAP may occur according to the reaction below.

Amorphous YAP→ YAM→ Hexagonal YAP→ YAG→ Orthorhombic YAP

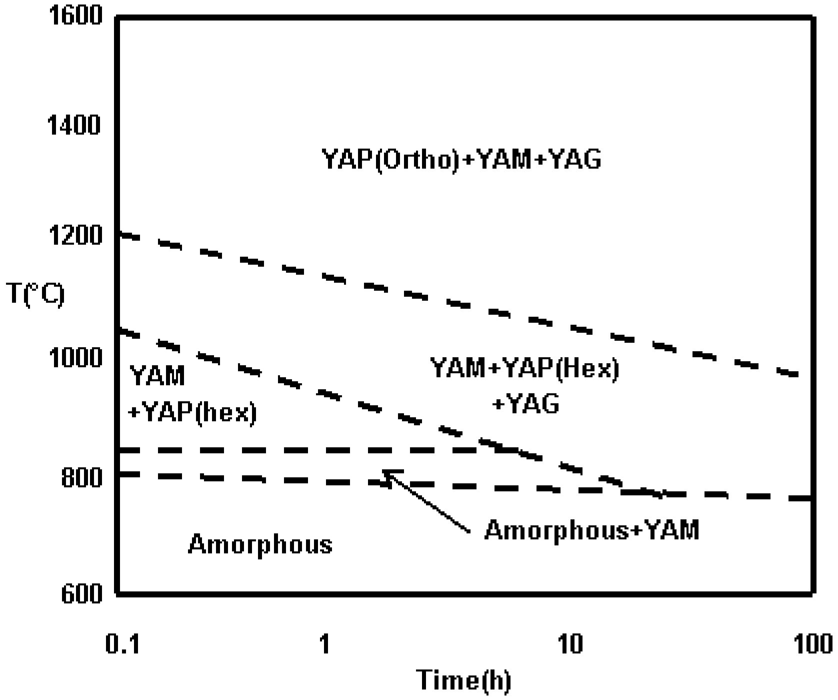

Figure 2.8. Time and temperature intervals where certain phases are obtained started with YAP composition.

They suggested that crystallization of YAP could follow different routes depending on the starting materials and heat treatment procedure taken to produce it[53].

2.2.3. $Y_4Al_2O_9$ (YAM)

YAM has monoclinic structure with $\alpha=\gamma=90$, $\beta=108,888$, a=7.4706, b=10.5350 and c=11.1941[56]. YAM melts congruently at 2030 °C[57]. Crystal structure of YAM is illustrated in Appendix A. Table 2.4. shows the atomic positions in YAM structure. Figure 2.9 gives 2θ values of YAM phase.

Atom	**# of Atom**	**Oxi**	**Wy**	**x**	**y**	**z**
Y	1	+3	4e	0.532	0.094	0.799
Y	2	+3	4e	0.014	0.099	0.797
Y	3	+3	4e	0.342	0.117	0.414
Y	4	+3	4e	0.834	0.124	0.434
Al	1	+3	4e	0.174	0.158	0.113
Al	2	+3	4e	0.675	0.196	0.135
O	1	-2	4e	0.211	0.007	0.143
O	2	-2	4e	0.733	0.051	0.176
O	3	-2	4e	0.034	-0.012	0.403
O	4	-2	4e	0.583	0.005	0.381
O	5	-2	4e	0.248	0.255	0.238
O	6	-2	4e	0.079	0.248	0.956
O	7	-2	4e	0.752	0.286	0.288
O	8	-2	4e	0.645	0.201	0.985
O	9	-2	4e	0.415	0.210	0.096

Table 2.4. Atomic positions in monoclinic YAM structure.[56]

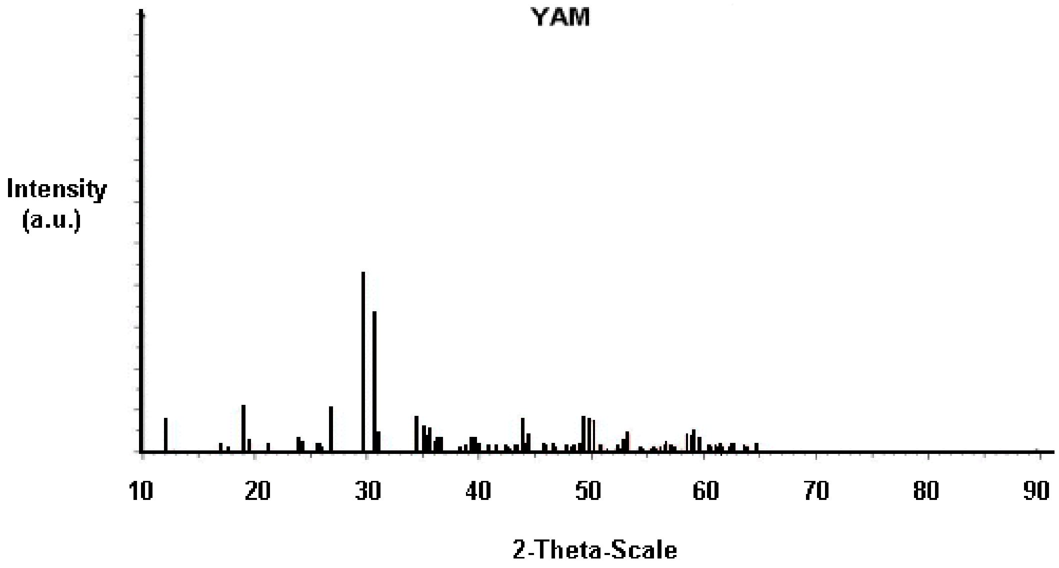

Figure 2.9. Calculated XRD peak positions of YAM.

Single crystal of YAM phase was fabricated by Abell et al. [51]. Papadopoulos et al. reported that they could not produce single crystal of YAM phase by Czochralski method from melt and second phase could not be identified[58]. Hess et al. used glycine-nitrate process. When they heat treated the sample at 1200 °C for 1 hour, they observed orthorhombic YAP phase and YAM phase although they started with YAM composition. Pure YAM phase was obtained after extended heat treatment at 1500 °C. They explained the crystallization process of YAM according to the reaction shown below[53].

$$\text{Amorphous YAM} \rightarrow \text{Hexagonal YAP} \rightarrow \text{Orthorhombic YAP} \rightarrow \text{YAM}$$

Although many studies agree that YAM phase becomes unstable under 1000 °C[48] Warshaw et al. stated that YAM phase appears stable below 800 °C but difficulties about attaining equilibrium and the rapid production of YAP prevent the determination of whether YAM is stable below 1000 °C or not[57].

Cracking of transparent YAM single crystals when it is cooled to 1000 °C is an important observation about instability of YAM under 1000 °C. Cracking in complex oxide systems is generally related to polymorphism. Abell et al. reported decomposition of the surface layer of the single crystal of YAM to YAG and alumina phases after annealing process above 1400 °C. Polymorphism and decomposition were proposed as two possible mechanisms responsible for instability[48]. The enigma about the instability has not yet been resolved.

3 EXPERIMENTAL DETAILS

3.1 Chemicals

Aluminum nitrate nanohydrate ($Al(NO_3)_3.9H_2O$, purity> 98%, Fluka Chemie, Buchs, Switzerland), calcium nitrate tetrahydrate ($Ca(NO_3)_2.4H_2O$, purity> 99%, Merck KgaA, Darmstadt, Germany), yttrium nitrate hexahydrate($Y(NO_3)_3.6H_2O$, purity>99,9 %, Aldrich Chemical Company, Milwaukee, U.S.A.) and tetraethylortosilicate (TEOS, $(C_2H_5O)_4Si$, purity> 98%, Merck-Schuchardt, Hohenbrunn, Germany) were used as starting materials. As the reaction medium, 2 wt% polyvinyl alcohol (PVA, A.M.W. 70.000-100.000, Sigma Chemical Company, St.Louis, U.S.A.) solution in distilled water was used.

3.2 Experimental Procedure

Required amount of PVA was dissolved in distilled water and 2 wt% clear solution was obtained after stirring 20 minutes at 80°C. In each experiment 200ml solution was used to produce 3g $Y_3Al_5O_{12}$. Yttrium nitrate hexahydrate ($Y(NO_3)_3.6H_2O$) and Aluminum nitrate nanohydrate ($Al(NO_3)_3.9H_2O$) were added to the PVA solution according to the stoichiometry of YAG ($n_Y/n_{Al}=3/5$). $Ca(NO_3)_2.4H_2O$ and TEOS were dissolved in this solution to obtain required n_{Ca}/n_Y and n_{Si}/n_Y ionic ratios. We used equal moles of $Ca(NO_3)_2.4H_2O$ and TEOS to determine co-solubility of Ca and Si in YAG. Pure YAG sample and 300ppm Ca, 400ppm Ca, 500ppm Ca, 2000ppm Ca, 5000ppm Ca, 1% Ca, 5% Ca, 10% Ca, 15% Ca, 150ppm Si, 1% Si, 2% Si, 7% Si, 2% Si+Ca, 5% Si+Ca, 8% Si+Ca, 9% Si+Ca, 10% Si+Ca and 15% Si+Ca doped samples were prepared to find the solubility and co-solubility limits.

Solutions were heated and stirred continuously until solution viscosity increased and yellowish jelly liquid was formed. Further heating on a hot plate resulted in a sponge-like bulk solid, whose color changed from yellow to brown. After this crisp solid was ground for 15 minutes, a very fine powder was obtained. Finally, the powder was calcined at 900°C for 2 hours in a Pt crucible in air. After the calcination process, white and fine YAG powders were obtained. The flowchart of the process can be seen in Figure 3.1.

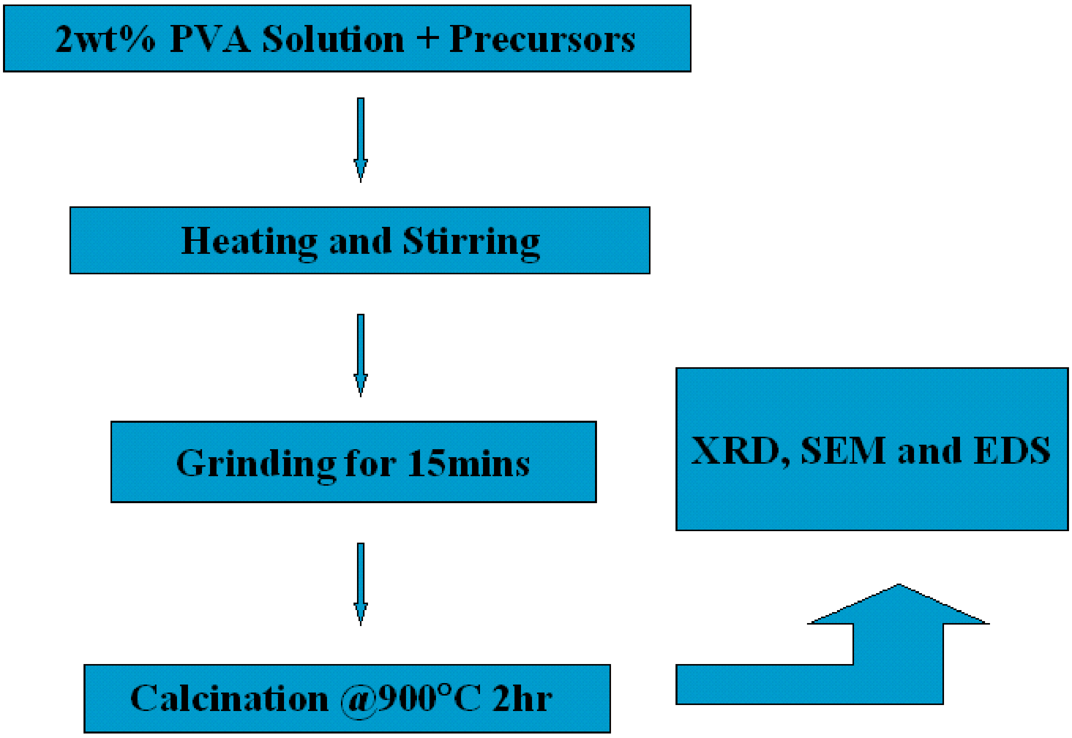

Figure 3.1. Flowchart of the experimental procedure.

When the solubility limit is exceeded, phase separation is expected to occur due to the large strain and the high vacancy concentration in the structure. The amounts of preexisting phases are expected to decrease and new phases, which can allow higher amounts of the dopant in its structure, are formed. The solubility limits of Ca, Si and their co-solubility limit in YAG were determined within 1% accuracy using the disappearing-phase method[59].

X-ray diffraction analysis was carried out by an X-ray diffractometer (XRD; Bruker AXS GmbH D8 Advance, Karlsruhe, Germany). The X-ray generator voltage and current were held constant at 40kV and 40mA, respectively. The 2θ was varied continuously from 10° to 90° in locked-couple mode with a rate of 0.015°/s. DIFFRAC PLUS Evaluation software was used to analyze diffraction data. The chemical composition of the powders were determined by using an energy dispersive spectrometer (EDS; Roentech, QuanTax, Berlin, Germany) attached to a field emission scanning electron microscope (FEG-SEM; Leo Supra 35 VP, Oberkochen, Germany) that is used to monitor powder morphology and particle size. Quantification of EDS results was done using a standardless routine incorporated in the QuanTax program (Roentech, QuanTax, Berlin, Germany). A quantitative evaluation that is carried out by the QuanTax software always follows the evaluation steps listed below:

- Correction of the detector effects (Escape, Shelf, Tail)
- Identification of the elements and selection of a line series
- Selection of the background manually by the user and calculation of the bremsstrahlung background by the QuanTax software.
- Development of overlaid lines and production of the net intensity identification
- Concentration calculation
- Result presentation

4 RESULTS

In order to determine the solubility limits of Ca and Si in YAG and their co-solubility limit, various amounts of the dopants were added to the YAG composition. The results are presented in this section.

4.1 Calcium Doping

In order to find the solubility limit of Ca in yttrium aluminum garnet, the calcium amount that was added to the stoichiometric YAG precursor solution was varied between Ca/Y=300ppm and Ca/Y=15% as cation ratios. The XRD spectra of Ca doped samples are shown in Figure 4.1. YAP peaks start to appear when Ca addition is 5000ppm. Intensities of YAP peaks increase with the amount of the dopant. Any other additional crystalline phase was not detected with XRD. As the amount of added dopant was increased, there were no significant peak shifts in the two-theta values of the YAG peaks within the experimental error limits (Table 4.1).

Ca Amount	*2θ (Degrees)*
Pure YAG	17.956
300ppm	17.960 ± 0.03
400ppm	17.951 ± 0.03
500ppm	17.965 ± 0.03
2000ppm	18.021 ± 0.03
5000ppm	18.033 ± 0.03
1%	18.004 ± 0.03
5%	17.966 ± 0.03
15%	17.974 ± 0.03

Table 4.1. 2θ values of pure YAG and Ca doped YAG samples.

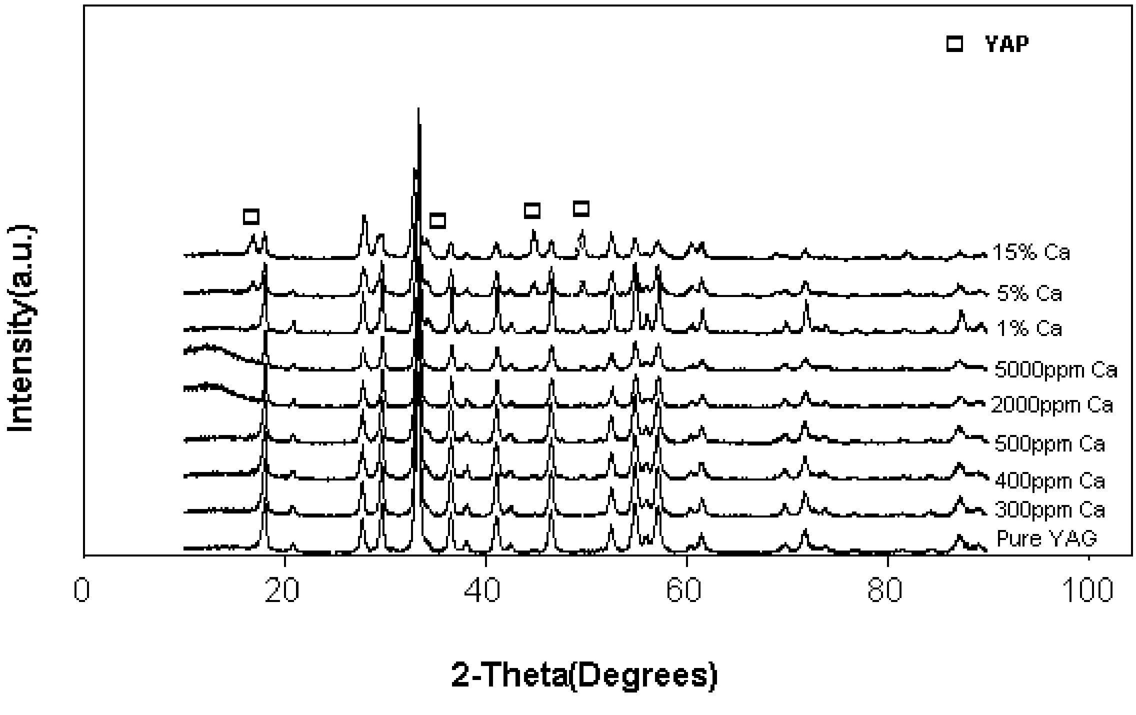

Figure 4.1. XRD graph of samples that are doped with various amounts of Ca.

Regions with high Ca content were observed during EDS analysis (Figure 4.2). Significant amounts of Y, Al and Ca are present in these Ca rich regions. The results of quantitative elemental analysis are shown in Table 4.2.

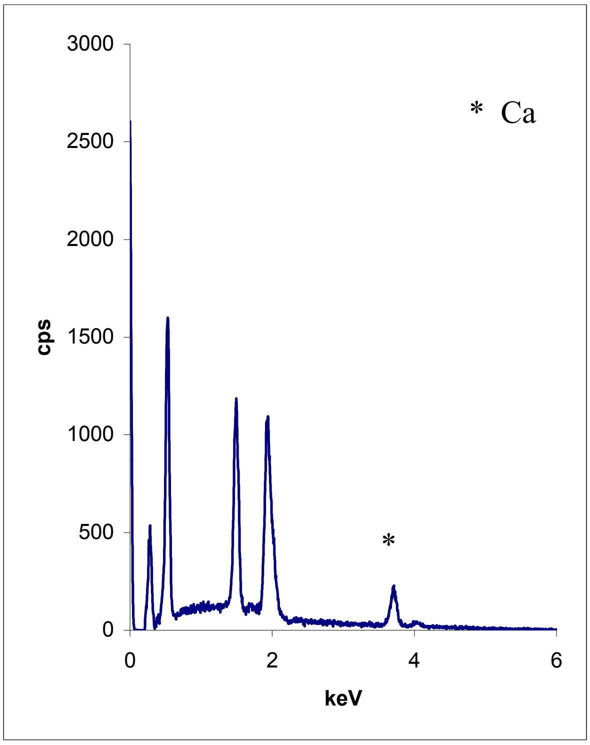

Figure 4.2. EDS spectra of the region that has high Ca content.

Element	***At.%***
Y	34.30 ± 3.53
Al	42.44 ± 1.61
Ca	23.27 ± 4.17

Table 4.2. Result of quantitative elemental analysis from Ca rich zone.

Figure 4.3 shows SEM image and result of EDS analysis taken from a 10% Ca doped sample. According to the EDS results, the YAG phase does not contain any detectable amount of Ca. The result of quantitative elemental analysis from the region which has YAG stoichiometry is shown in Table 4.3.

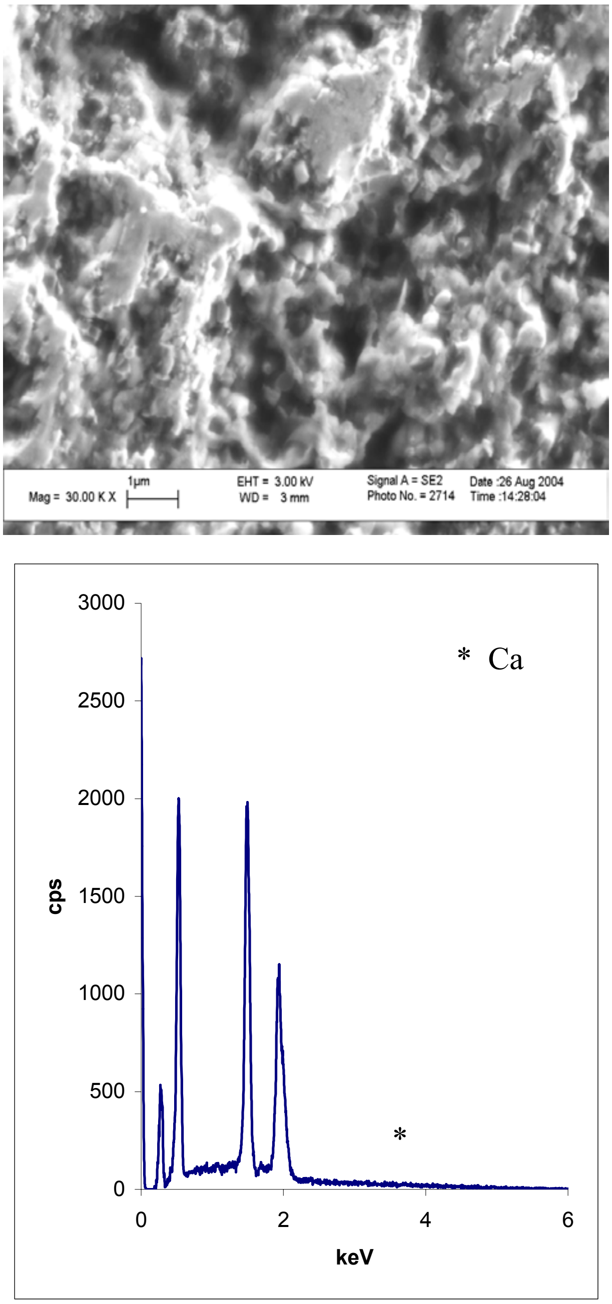

Figure 4.3. SEM image and EDS result of 10% Ca doped sample.

Element	*At.%*
Y	22.12 ± 4.06
Al	33.42 ± 7.34
Ca	N.D.*
O	44.48 ± 11.46

* Not detectable.

Table 4.3. Results of quantitative elemental analysis taken from the region that has YAG stoichiometry in 10% Ca doped sample.

4.2 Silicon Doping

In order to find the solubility limit of silicon in YAG, the amount of Si added was varied between Si/Y=150ppm and Si/Y=7%. The XRD spectra of Si-doped samples are shown in Figure 4.4. When the amount of dopant is 150ppm only YAG peaks are observable. Peaks of YAG and YAP crystalline phases are present in XRD spectra of 1%, 2% and 7% Si doped samples. Intensities of YAP peaks increased while amount of Si addition increases. Figure 4.4 also shows that there is a bump between 10° and 16° and its height is increasing when the amount of Si addition increases. As the amount of added dopant was increased, there were no significant peak shifts in the two-theta values of the YAG peaks within the experimental error limits (Table 4.4).

Si Amount	***2θ (Degrees)***
Pure YAG	17.956
150ppm	17.953 ± 0.03
1%	17.953 ± 0.03
2%	17.959 ± 0.03
5%	17.986 ± 0.03
7%	17.970 ± 0.03

Table 4.4. The 2θ values of pure YAG and Si doped YAG samples.

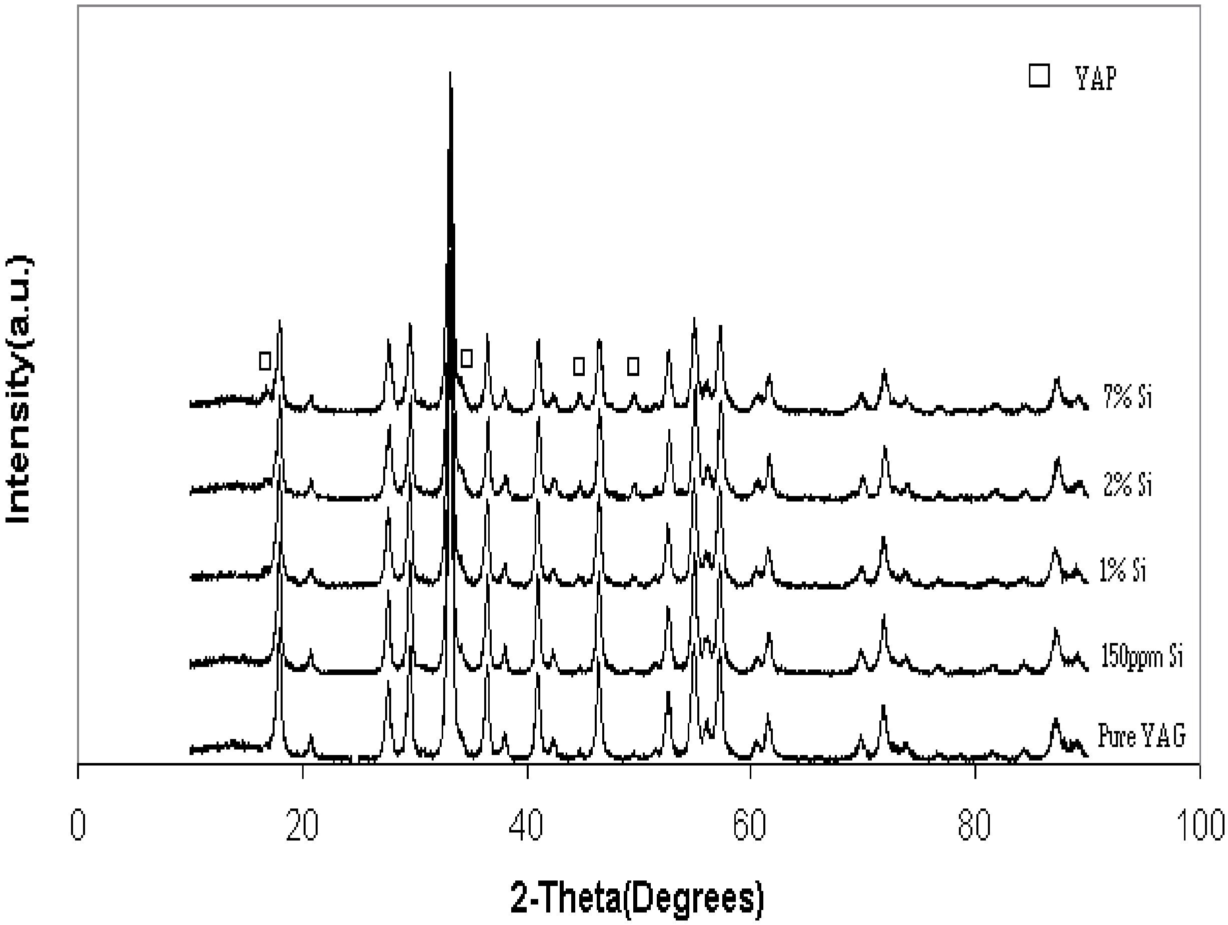

Figure 4.4. XRD graph of Si doped samples.

The highly Si-rich regions that were identified by Si mapping and EDS analysis are shown in Figure 4.5.

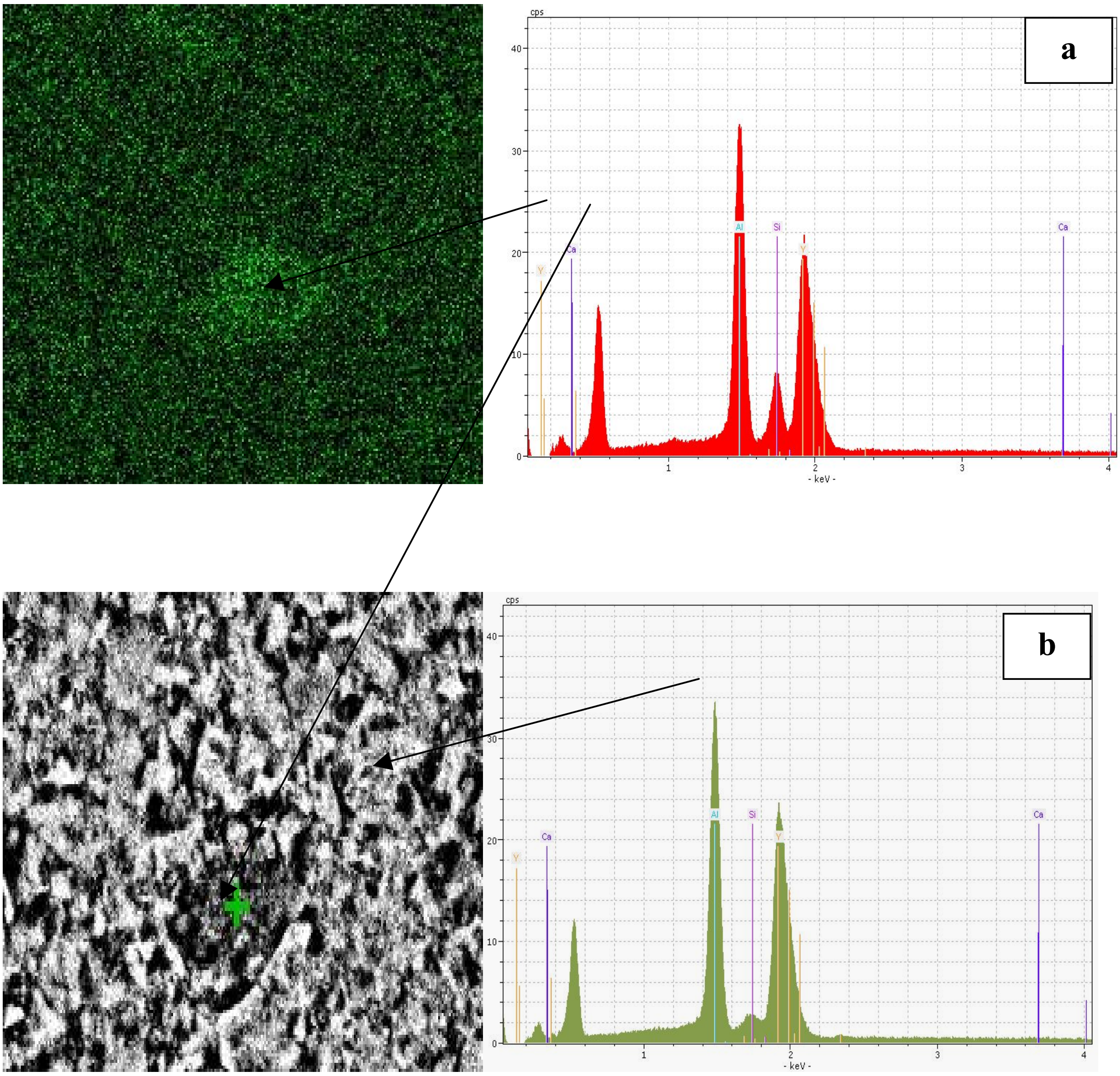

Figure 4.5. a) Si map and EDS result from Si rich region. b) BSE image and EDS result from outside of Si rich region.

Figure 4.6 is the SEM image and EDS result of 7% Si doped sample. Result of the quantitative elemental analysis from the region which has YAG stoichiometry is shown in Table 4.5.

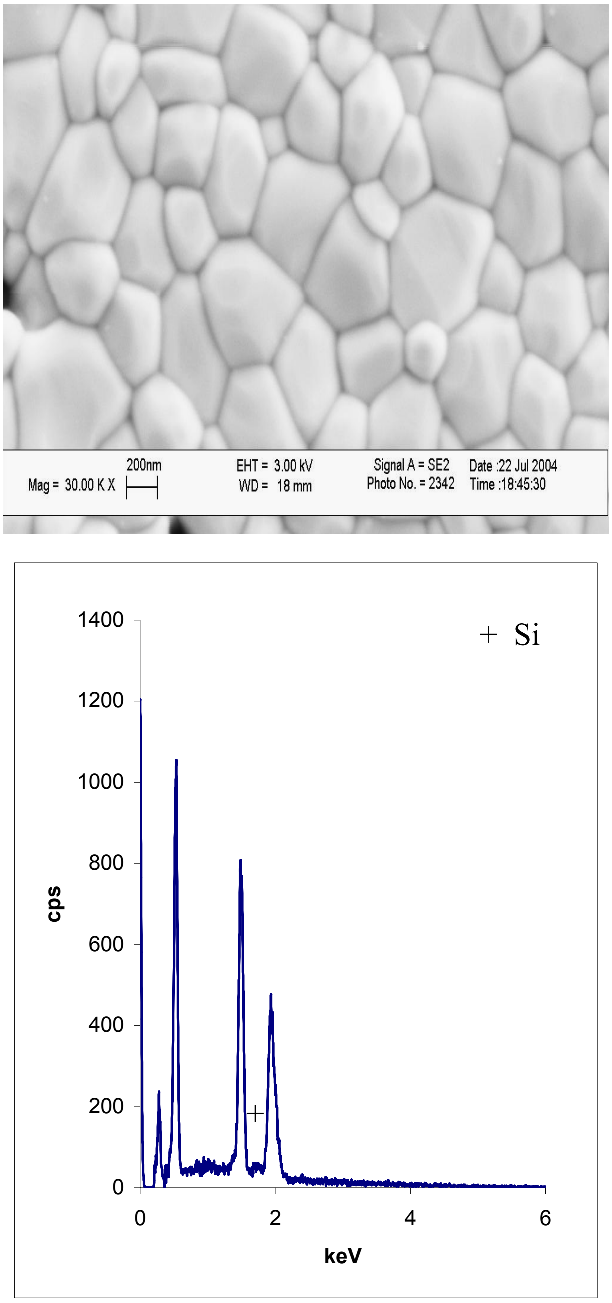

Figure 4.6. SEM image and EDS result of 7% Si doped sample.

Element	*At.%*
Y	13.38 ± 0.79
Al	24.34 ± 2.76
Si	N.D.*
O	62.28 ± 3.49

* Not detectable.

Table 4.5. Results of quantitative elemental analysis taken from the region that has YAG stoichiometry in 7% Si doped sample.

4.3 Co-doping of Calcium and Silicon

Amounts of Si and Ca were varied between Ca(or Si)/Y=2% and Ca(or Si)/Y=15% to find co-solubility limit of silicon and calcium in YAG. The XRD spectra of co-doped samples are shown in Figure 4.7. Only two crystalline phases (YAG and YAP) are present up to 9% Ca+Si addition. Intensities of YAP peaks increase when amounts of dopants increase. Intensities of YAP peaks decrease and YAM peaks start to appear when amounts of dopants exceed 9%. There are again no observable peak-shift for the peaks of the YAG phase within the experimental error limits.

Si +Ca Amount	*2θ (Degrees)*
Pure YAG	17.956
2%	17.966 ± 0.03
5%	17.957 ± 0.03
8%	17.953 ± 0.03
9%	17.950 ± 0.03
10%	18.010 ± 0.03
15%	18.040 ± 0.03

Table 4.6. 2θ values of pure YAG and Ca and Si co-doped YAG samples.

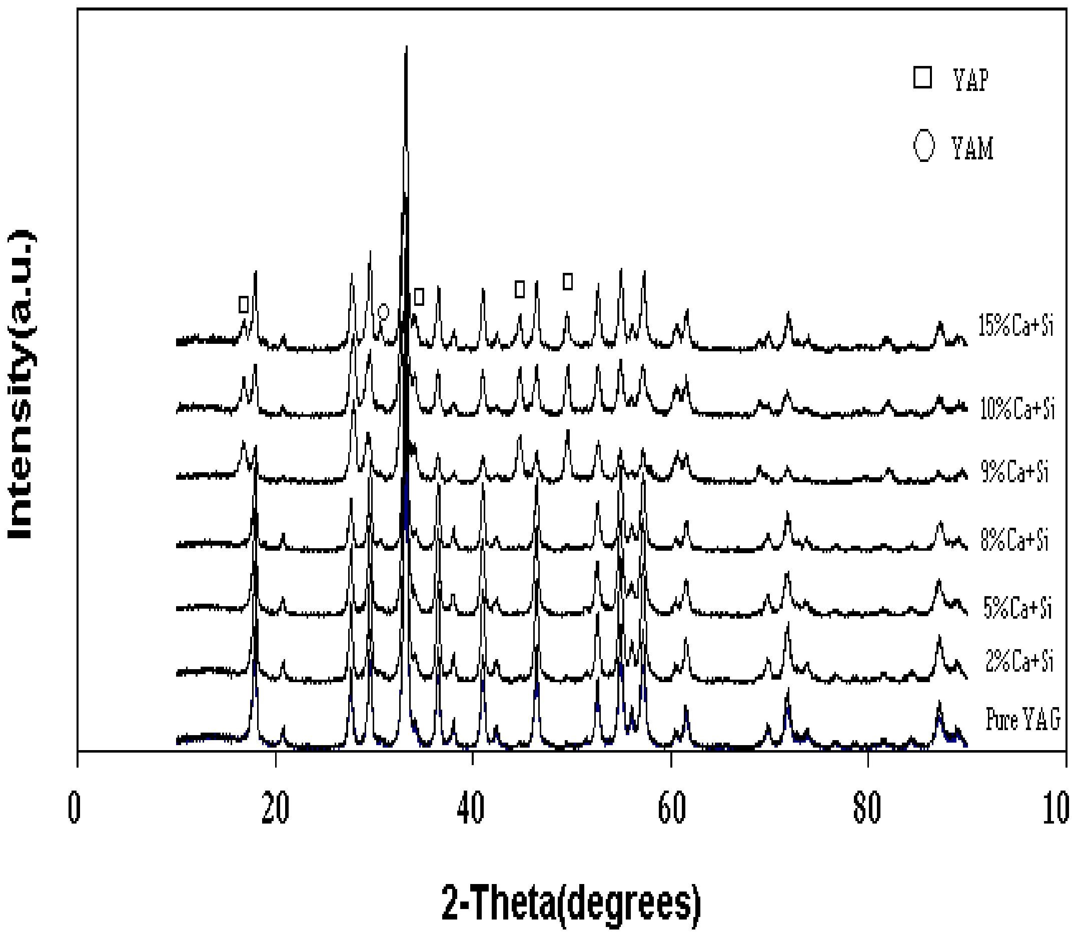

Figure 4.7. XRD graph of samples which were doped with both Si and Ca.

Regions with high Ca content were observed during EDS analysis (Figure 4.8). These regions also include high amount of silicon nearly 5% of the yttrium amount. Results of quantitative elemental analysis from the calcium rich zone are shown in Table 4.7.

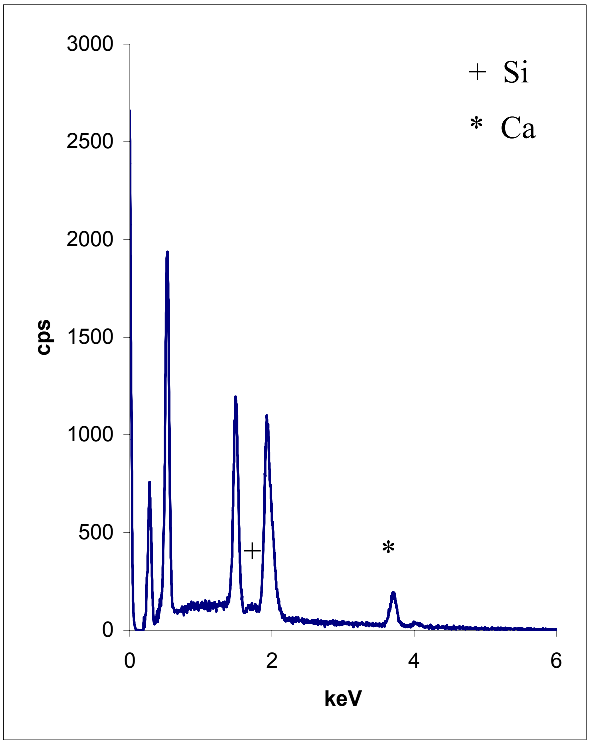

Figure 4.8. EDS spectra of the region that has high Ca content in the 15% Ca+Si doped sample.

Element	*At.%*
Y	36.36 ± 0.18
Al	37.89 ± 2.22
Si	1.89 ± 0.18
Ca	23.86 ± 2.51

Table 4.7. Results of quantitative elemental analysis from Ca rich zone in the 15% Ca+Si doped sample.

Figure 4.9 is the SEM image and EDS result of 15% Ca+Si doped sample. Results of quantitative elemental analysis from the region which has YAG stoichiometry are shown in Table 4.8. Ca and Si amounts in these regions are between 8% and 10% of the yttrium amount in YAG.

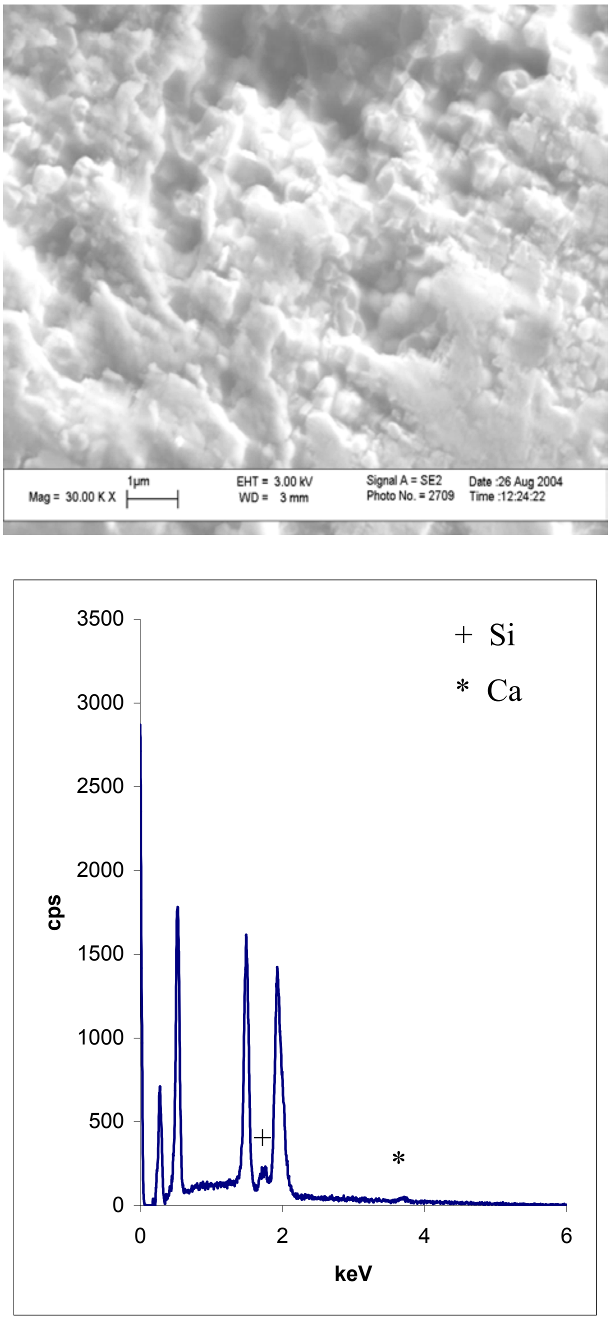

Figure 4.9. SEM image and EDS result of 15% Si +15% Ca doped sample.

Element	***At.%***
Y	37.38 ± 0.51
Al	56.88 ± 0.44
Si	2.67 ± 0.42
Ca	3.07 ± 0.33

Table 4.8. Results of quantitative elemental analysis from the region that has YAG stoichiometry in the 15% Ca+Si doped sample.

5 DISCUSSION

5.1 Calcium Doping

Defect reaction in terms of Kröger-Vink notation during Ca addition can be written as;

$$2CaO \xrightarrow{YAG} 2Ca_Y^{'} + 2O_O^{X} + V_O^{\bullet\bullet} \ (1)$$

Ionic radii of Ca, Y, Al and Si ions for different coordination numbers are listed in Table 5.1. Ca has an ionic radius of 114pm, when its coordination number (CN) is 6. It is approximately two times larger than Al ions. On the other hand, the ionic radius of Ca is very similar to that of Y, when their coordination numbers are 8. Therefore, it is more likely that Ca replaces Y according to reaction(1). Excess yttrium atoms produced during this reaction may react with YAG according to reaction(2) and form $YAlO_3$ (YAP) as predicted by the Y_2O_3-Al_2O_3 phase diagram in Figure 5.1.

$$Y_2O_3 + Y_3Al_5O_{12} \rightarrow 5YAlO_3 \ (2)$$

Consequently, YAG and YAP phases should coexist before the saturation of YAG with Ca. The practical detection limit for a second phase in the XRD system used in this investigation is about 0.5 at%. When the amount of Ca addition is lower than 2000ppm, peaks of the second phase (YAP) may not be observed, since 5 moles of $YAlO_3$ is formed for every 2 moles of Ca-Y replacement. Beyond the solubility limit, the amount of Ca atoms exceeding the solubility limit may combine with Al ions to form calcium aluminate phase(s). When some of Al atoms are used in this new phase, the excess Y^{+3} ions may have reacted with the existing YAG phase to form an additional $YAlO_3$ (YAP) phase.

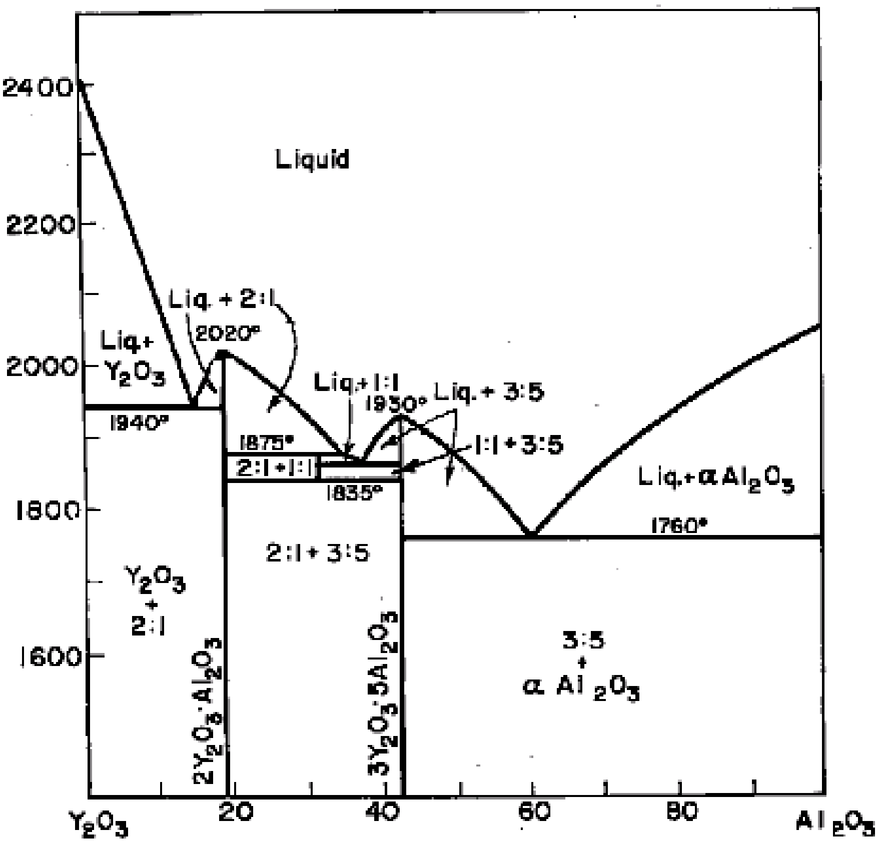

Figure 5.1. Phase diagram of Y_2O_3-Al_2O_3 system[50]

As a result, the amount of secondary YAP phase was expected to increase as the calcium doping level was increased beyond the solubility limit. The same two phases are present above and below the solubility limit but their amounts are changing according to doping level. Thus, the saturation limit of YAG with Ca can not be determined by XRD, while EDS analysis gives a more accurate value of the solubility.

Ion Type	***Coordination***	***Ionic Radius(pm)***
Ca(II)	6	114
Ca(II)	8	126
Y(III)	6	104
Y(III)	8	115.9
Al(III)	4	53
Al(III)	6	67.5
Si(IV)	4	40
Si(IV)	6	54

Table 5.1. Ionic radii of Ca, Y, Al and Si ions for different coordination states[60].

According to the EDS results, the YAG phase does not contain any detectable amount of Ca. The detection limit of EDS is approximately 0.5 % of total atoms in the specimen. If the detection limit of EDS is used to find the upper limit of solubility, the amount of Ca atoms that can be accommodated in YAG should be lower than 2.76 % of yttrium amount in YAG. On the other hand, Vrolijk reported that solubility limit of Ca is less than 170ppm of yttrium amount in YAG[61]. Therefore, the statement that YAG phase does not contain any detectable amount of Ca agrees with previously reported data since EDS can not detect 170ppm Ca distributed uniformly in the specimen.

5.2 Silicon Doping

Ionic radii of silicon are 40pm and 54pm, ionic radii of aluminum are 53pm and 67.5pm, if their coordination numbers are 4 or 6, respectively. Si may substitute for Al according to equation (3). On the other hand, Si can sit on an interstitial site and dissolve in YAG as described in equation (4).

$$3SiO_2 \xrightarrow{YAG} 3\,Si^{\bullet}_{Al} + 6O^{X}_{O} + V'''_{Al} \quad (3)$$

$$3SiO_2 \xrightarrow{YAG} 3\,Si_i^{\bullet\bullet\bullet\bullet} + 6O_O^X + 4V_{Al}^{'''}\ (4)$$

Reaction (4) appears to be less favorable compared to reaction (3) because a larger number of aluminum vacancies needs to be produced. In addition to this, the Si atom will most likely produce a large strain when it sits on an interstitial site. However, from the phase formation point of view, results of both reactions (3 and 4) are the same in terms of the phases produced. There will be free aluminum ions in the reaction medium, and they will react with some Si so that the activity of the dissolved Si (a_{Si}) in YAG is equal to the activity of Si in amorphous aluminum silicate phase ($Al_{2x}Si_yO_{3x+2y}$). The two phases are present under solubility limit, and $a_{Si}^{YAG} = a_{Si}^{Glass}$ condition should be satisfied at equilibrium.

Beyond the solubility limit, phases produced can be found using the ternary phase diagram of SiO_2-Y_2O_3-Al_2O_3 system that is shown in Figure 5.2. The composition is in the compatibility triangle of YAG-Al_2O_3-$Y_2O_3.2SiO_2$, and these three phases are expected to exist when the system is cooled to room temperature under equilibrium conditions. We did not see peaks of Al_2O_3 or $Y_2O_3.2SiO_2$ phases in any of our XRD spectra, as shown in Figure 4.4. These two phases may react to form YAP and $Al_2Si_3O_9$ according to reactions (5) and (6) under non-equilibrium conditions. The synthesis temperature and time may not enough for the production of equilibrium phases.

$$100\ Y_3Al_5O_{12} + x\ SiO_2 \rightarrow x/2\ (Y_2O_3.2SiO_2) + (100-x/3)\ Y_3Al_5O_{12} + 5x/6\ Al_2O_3\ (5)$$

$$x/2\ (Y_2O_3.2SiO_2) + 5x/6\ Al_2O_3 \rightarrow x\ YAlO_3 + x/3\ Al_2Si_3O_9\ (6)$$

YAP peaks in the XRD pattern are an indicator of saturation of YAG with Si. YAP peaks are not observed for Si/Y= 150ppm sample. However, for YAG samples doped with Si/Y= 1%, Si/Y= 2 % and Si/Y= 7%, YAP peaks are observed. Hence, the solubility limit of Si in YAG is predicted to lie between Si/Y= 150ppm and Si/Y= 1%. The highly Si-rich regions were readily identified by Si mapping and EDS analysis. The amorphous bump between 10° and 16° may also be indicative of an amorphous alumina silicate-rich phase.

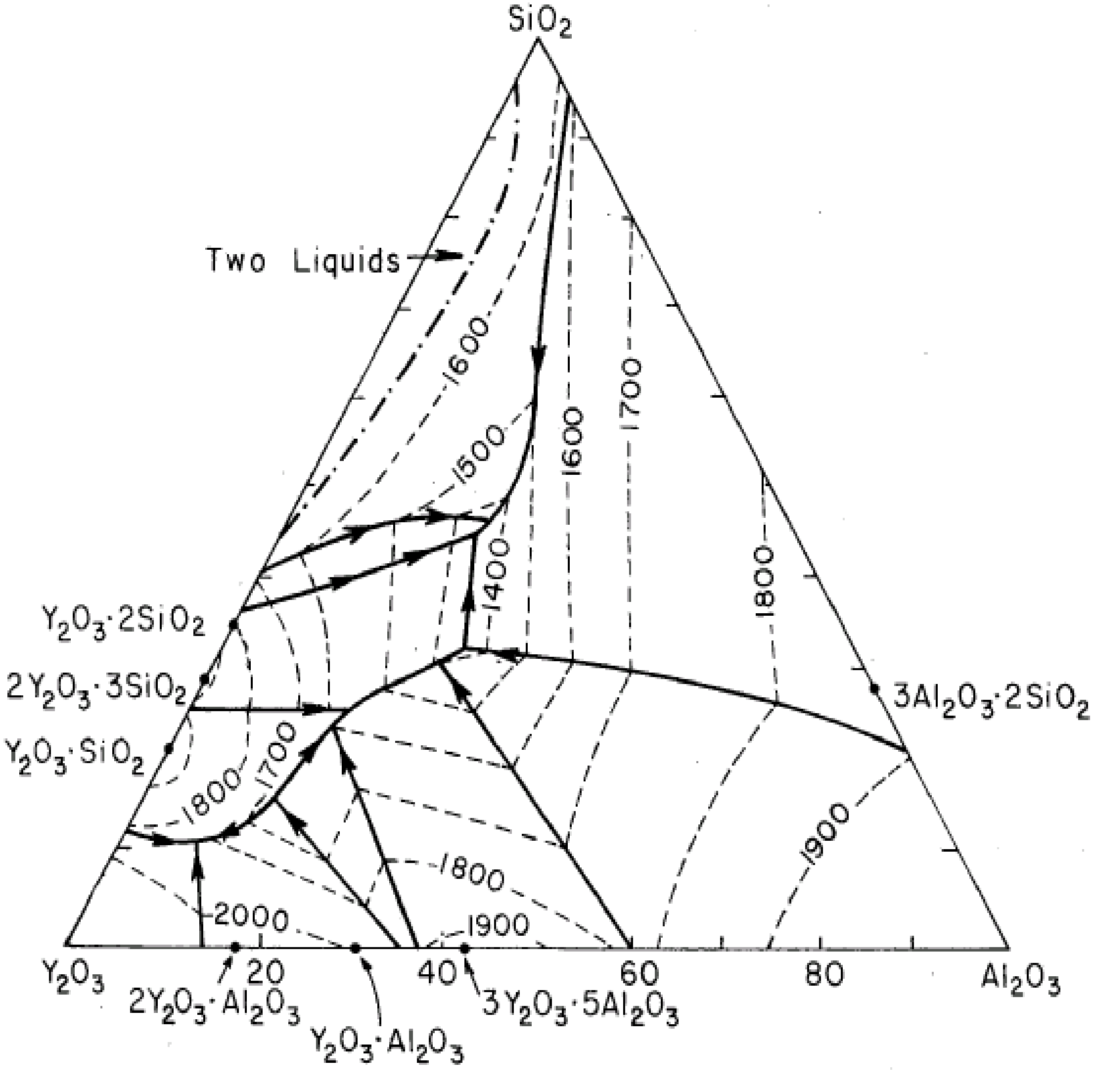

Figure 5.2. Phase diagram of the SiO_2-Al_2O_3-Y_2O_3 system[62]

EDS analysis indicated that Si was not detected in YAG. The amount of Si that can be accommodated in YAG structure should be lower than the detection limit of the EDS spectrometer, which is 0.5 at.% of the total elements in the sample. Vrolijk reported that the solubility limit of Si is more than 166ppm of yttrium amount in YAG[61], and it is consistent with our results. As a result, the solubility of Si in YAG is estimated to be between 150ppm and 1% of yttrium amount in YAG.

5.3 Co-doping of Calcium and Silicon

Equal moles of Si and Ca were added simultaneously to find the co-solubility limit of these atoms in YAG. Equation (7) is the defect reaction of this addition, when the amount of the dopants is less than co-solubility limit.

$$CaO + SiO_2 \xrightarrow{YAG} Ca_Y' + Si_{Al}^{\bullet} + 3O_O^X + YAlO_3 \quad (7)$$

Calcium exchanges with yttrium while silicon replaces aluminum. The free aluminum and yttrium ions produced during this reaction may form YAP phase and/or an amorphous glassy phase that is composed of Y, Al, Ca and Si. The amounts of YAP phase and glassy phase are related to the amount of addition before saturation of YAG. The maximum amounts of YAP phase and the amorphous phase are expected to form at solubility limit.

Beyond the solubility limit, free calcium and silicon ions may combine with some aluminum and may form an anorthite-like glassy phase. The yttrium removed from the YAG composition may further react with the existing YAP phase. The amount of YAP phase decreased, and a yttrium richer phase, yttrium aluminate monoclinic (YAM, $Y_4Al_2O_9$), formed, since some of the aluminum, which would be used in production of YAP phase, was used during the formation of this glassy phase.

Consequently, YAM peaks in XRD graph indicate that the co-solubility limit of Ca and Si in YAG was exceeded. According to the XRD spectra from different samples that are shown in Figure 4.7, YAG and YAP phases were present, and the amount of YAP phase was increasing in the XRD plot of samples up to 9% Ca+Si addition. YAM peaks started to appear, while the amount of YAP phase decreased above 9% Ca+Si. A similar behavior was observed in 10% Ca+Si doped samples. More Ca and Si addition leads to an increase in the intensity of YAM peaks. These data show that co-solubility limit of Ca and Si in YAG is most likely between 8% and 9% of yttrium amount in YAG.

Two phases are present before the solubility limit is exceeded for both solubility and co-solubility experiments, since YAG stochiometry was maintained, and excess Ca and Si were introduced to the system during synthesis. As a result, some of the calcium and the silicon may also enter the lattice of the second phase. Ca and Si are shared between the two phases such that activities of Ca(a_{Ca}) and Si(a_{Si}) are same in both phases, so $a_{Ca}^{YAG} = a_{Ca}^{2nd\ Phase}$ and $a_{Si}^{YAG} = a_{Si}^{2nd\ Phase}$ at the equilibrium. Amounts of second phases are negligible compared to amount of YAG. Thus, most of the Ca and Si additions can be considered as being captured by YAG phase. Nevertheless, tertiary phases(YAM or YAP) were produced after saturation of both YAG and second phases, so there should be a small difference between exact solubility limits and solubility limit ranges obtained from our XRD data.

EDS results indicate that the solubility of Ca is between 7.23 % and 9.22 % and the solubility of Si is between 5.94 % and 8.38 % of yttrium amount in YAG, when they are added simultaneously. This result is consistent with the previously predicted co-solubility limit from Figure 4.7.

Whenever there is a substitutional defect in the lattice, a strain is produced according to differences between the ionic sizes of substituting elements. Ca has a larger ionic radius than Y. On the other hand, the ionic radius of Si is smaller than the host Al. If these two substitutions occur at the same time, they compensate the effects of each other.

Like every material YAG has an equilibrium vacancy concentration with respect to the temperature[63]. The defect reactions (1), (3) and (4) produce vacancies as substitution occurs. When the vacancy concentration in the structure reaches the limit, the Gibbs free energy of vacancy formation is positive, and formation of one more vacancy is impossible. As a result, no more substitution can be made, and phase separation occurs. This is the case if we add only Ca or only Si to the structure. During reaction (7), vacancies are not created, because two replacements occur at the same time. The charge of Si is one greater, and the charge of Ca is one less than those of the original cations, and charge neutrality is maintained. The vacancy limit of YAG is not an obstacle for the dissolving of Si and Ca when they enter to the structure at the same time as described in reaction (7).

The size difference between Ca and Y ions is 8.71 % of the size of host Y ion. On the other hand, the size difference between Al and Si is 24.5 % of the size of host Al ion, when their coordination numbers are 4. EDS analysis of 15 % Ca+Si doped sample shows that YAG can accommodate approximately equal amounts of Ca and Si in its structure, which indicates that one Ca-Y replacement for each Si-Al substitution. Consequently, Ca-Y replacement may not totally compensate for the size and strain effect of Si-Al substitution. This reason may limit the co-solubility of Ca and Si in YAG and may hinder the 100 % co-solubility.

6 CONCLUSION

Results presented in the fourth chapter indicate that the co-solubility of Si (with Ca in YAG) is at least 6 times of its solubility in YAG. According to the solubility limit of Ca reported by Vrolijk, co-solubility of Ca (with Si in YAG) is at least 425 times of its solubility. On the other hand, according to the solubility range of Ca that we predicted from quantitative EDS analysis, co-solubility of Ca when it enters to YAG structure with Si, is at least 2.62 times of its solubility.

Ca has a larger ionic radius than the host Y. On the other hand, ionic radius of Si is smaller than the host Al. When these two substitutions occur simultaneously they compensate the effects of each other. During co-solubility, vacancies are not created because two replacements occur at the same time, charge of Si is one greater and charge of Ca is one less than those of the original cations and charge neutrality is maintained. Compensation of the size and vacancy effects may be the reasons of increased co-solubility of Ca and Si in YAG.

The large size difference between Al and Si cations may not be fully compensated by Y-Ca replacement. This may be the reason of existence of a co-solubility limit instead of 100% co-solubility.

7 REFERENCES

1. J. K. R. Weber, B. Cho, A. D. Hixson, J. G. Abadie, P. C. Nordine, W. M. Kriven, B. R. Johnson and D. Zhu, Growth and Crystallization of YAG- and Mullite-composition Glass Fibers, Journal of the European Ceramic Society **19** (1999) 2543-2550.

2. http://www.td.anl.gov/Programs/ti/lal/

3. X. Xu, Z. Zhao, P. Song, J. Xu and P. Deng, Growth of High-quality Single Crystal of 50 at.% Yb:YAG and Its Spectral Properties, Journal of Alloys and Compounds **364** (2004) 311-314.

4. L. Gao, H. Wang, H. Kawaoka, T. Sekino and K. Niihara, Fabrication of YAG-SiC Nanocomposites by Spark Plasma Sintering, Journal of the European Ceramic Society **22** (2002) 785-789.

5. T.A. Parthasarathy, T. Mah and K. Keller, Creep Mechanism of Polycrystalline Yttrium Aluminum Garnet, Journal of the American Ceramic Society **75** (1992) 1756-1759.

6. K. Keller, T. Mah and T.A. Parthasarathy, Processing and Mechanical Properties of Polycrystalline $Y_3Al_5O_{12}$, Ceramic Engineering and Science Proceeding **12** (1990) 1122-1133.

7. A. Ikesue, I. Furusato and K. Kamata, Fabrication of Polycrystalline, Transparent YAG Ceramics by a Solid-State Reaction Method, Journal of the American Ceramic Society **78** [1] (1995) 225-228.

8. Q. Zhang and F. Saito, Mechanochemical Solid Reaction of Yttrium Oxide Alumina Leading to the Synthesis of Yttrium Aluminum Garnet, Powder Technology **129** (2003) 86-91.

9. S.M. Sim, K.A. Keller and T.I. Mah, Phase Formation in Yttrium Aluminum Garnet Powders Synthesized by Chemical Methods, Journal of Materials Science **35** (2000) 713-717.

10. A. Ikesue, T. Kinoshita, K. Kamata and Y. Yoshida, Fabrication and Optical-Properties of High-Performance Polycrystalline Nd-YAG Ceramics for Solid State Lasers, Journal of the American Ceramic Society **78** (1995) 1033-1040.

11. G.S. Corman, High-temperature Creep of Some Single Crystal Oxides, Ceramic Engineering and Science Proceeding **12** (1991) 1745-1766.

12. T.A. Parthasarathy, T. Mah and K. Keller, High-Temperature Deformation Behaviour of Polycrystalline Yttrium Aluminum Garnet (YAG), Ceramic Engineering and Science Proceeding **12** (1991) 1767-1773.

13. D.R. Messier and G.E. Gazza, Synthesis of $MgAl_2O_4$ and $Y_3Al_5O_{12}$ by Thermal Decomposition of Hydrated Nitrate Mixtures, American Ceramic Society Bulletin **51** (1972) 692-694.

14. L. Wen, X. Sun, Z. Xiu, S. Chen and C. Tsai, Synthesis of Nanocrystalline Yttria Powder and Fabrication of Transparent YAG Ceramics, Journal of the European Ceramic Society **24** (2004) 2681-2688.

15. Y. Hakuta, T. Haganuma, K. Sue, T. Adschiri and K. Arai, Continuous Production of Phosphor YAG:Tb Nanoparticles by Hydrothermal Synthesis in Supercritical Water, Materials Research Bulletin **38** [7] (2003) 1257-1265.

16. Y. Hakuta, K. Seino, H. Ura, T. Adschiri, H. Takizawa and K. Arai, Production of Phosphor (YAG:Tb) Fine Particles by Hydrothermal Synthesis in Supercritical Water, Journal of Materials Chemistry **9** (1999) 2671-2674.

17. T. Takamori and L.D. David, Controlled Nucleation for Hydrothermal Growth of Yttrium-Aluminum Garnet Powders, American Ceramic Society Bulletin **65** (9) (1986)1282-1286.

18. H. Wang, L. Gao and K. Niihara, Synthesis of Nanoscaled Yttrium Aluminum Garnet Powder by the Co-precipitation Method, Materials Science and Engineering A **288** [1] (2000) 1-4.

19. J.-y. Park, S.-G. Oh, U. Paik and S.-K. Moon, Preparation of Aluminum Oxide Particles Using Ammonium Acetate as Precipitating Agent, Materials Letters **56** (2002) 429-434.

20. I. Matsubara, M. Paranthaman, S.W. Allison, M.R. Cates, D.L. Beshears and D.E. Holcomb, Preparation of Cr-Doped $Y_3Al_5O_{12}$ Phosphors by Heterogeneous Precipitation Methods and Their Luminescent Properties, Materials Research Bulletin **35** (2000) 217-224.

21. D. Hreniak and W. Strek, Synthesis and Optical Properties of Nd^{+3}-doped $Y_3Al_5O_{12}$ Nanoceramics, Journal of Alloys and Compounds **341** [1-2] (2002) 183-186.

22. M. Veith, S. Mathur, A. Kareiva, M. Jilavi, M. Zimmer and V. Huch, Low Temperature Synthesis of Nanocrystalline Y3Al5O12 (YAG) and Ce-doped Y3Al5O12 via Different Sol-Gel Methods, Journal of Materials Chemistry **9** (1999) 3069-3079.

23. P. Vaqueiro and M.A. Lopez-Quintela, Influence of Complexing Agents and Ph on Yttrium-Iron Garnet Synthesized by the Sol-Gel Method, Chemistry of Materials **9** (1997) 2836-2841.

24. T. Tachiwaki, M. Yoshinaka, K. Hirota, T. Ikegami and O. Yamaguchi, Novel Synthesis of Y3Al5O12 (YAG) Leading to Transparent Ceramics, Solid State Communications **119** (2001) 603-606.

25. M. A. Gülgün, O. O. Popoola and W. M. Kriven, Chemical Synthesis and Characterization of Calcium Aluminate Powders, Journal of the American Ceramic Society **77** [2] (1994) 531-539.

26. M. Pechini, Method of Preparing Lead and Alkaline-Earth Titanates and Niobates and Coating Method Using the Same to Form a Capacitor, U.S. Pat. No. 3 330 697 July 11, 1967.

27. M. A. Gülgün, M. H. Nguyen and W. M. Kriven, Polymerized Organic-Inorganic Synthesis of Mixed Oxides, Journal of the American Ceramic Society **82** [3] (1999) 556-560.

28. X. Zhang, H. Liu, W. He, J. Wang, X. Li and R. I. Boughton, Synthesis of Monodisperse and Spherical YAG Nanopowder by a Mixed Solvothermal Method, Journal of Alloys and Compounds, **372** [1-2] (2004) 300-303.

29. M. L. Keith and R. Roy, Structural Relations among Double Oxides of Trivalent Elements, Journal of the Mineralogical Society of America, **39** January- February, (1954) Nos. 1 and 2.

30. H. S. Yoder and M. L. Keith, Complete Substitution of Aluminum for Silicon: The System $3MnO.Al_2O_3.3SiO_2$-$3Y_2O_3.5Al_2O_3$, Journal of the Mineralogical Society of America, **36** July- August, (1951) Nos. 7 and 8.

31. J. Carda, M. A. Tena, G. Monros, V. Esteve, M. M. Reventos and J. M. Amigo, A Rietveld Study of the Cation Substitution between Uvarovite and Yttrium-Aluminum Synthetic Garnets, Obtained by Sol-Gel Method, Crystal Research and Technology **29** (1994) 3 387-391.

32. http://unit.aist.go.jp/greenlife/ii/STRUCIMAGES/Grossular.gif

33. M. Yoshimura and W. Suchanek, In Situ Fabrication of Morphology-Controlled Advanced Ceramic Materials by Soft Solution Processing, Solid State Ionics **98** (1997) 197-208.

34. U. Adem, Preparation of $Ba_xSr_{1-x}TiO_3$ Thin Films by Chemical Solution Deposition and Their Electrical Characterization (2003), p.27.

35. http://www.chemat.com/html/solgel.html

36. C.J. Brinker and G.W. Scherer, Sol-Gel Science, Academic Press, (1990) p.4 and p.21-30.

37. X. Li, H. Liu, J. Wang, X. Zhang and H. Cui, Preparation and Properties of YAG Nano-sized Powder from Different Precipitating Agent, Optical Materials **25** [4] (2004) 407-412.

38. D. Segal, Chemical Synthesis of Advanced Ceramic Materials, Cambridge University Press, (1991) p. 23.

39. S-H. Yu, T. Fujino and M. Yoshimura, Hydrothermal Synthesis of $ZnFe_2O_4$ Ultrafine Particles with High Magnetization, Journal of Magnetism and Magnetic Materials **256** (2003) 420-424.

40. Y.C. Zhang, H. Wang, H.Y. Xu, B. Wang, H. Yan, A. Ahniyaz and M. Yoshimura, Low-Temperature Hydrothermal Synthesis of Spinel-Type Lithium Manganese Oxide Nanocrystallites, Solid State Ionics **158** (2003) 113-117.

41. Y.C. Zhang, H. Wang, B. Wang, H.Y. Xu, H. Yan and M. Yoshimura, Hydrothermal Synthesis of Metastable γ-Manganese Sulfide Crystallites, Optical Materials **23** (2003) 433-437.

42. M. Popa, J. Frantti and M. Kakihana, Lanthanum Ferrite $LaFeO_{3+d}$ Nanopowders Obtained by the Polymerizable Complex Method, Solid State Ionics **154-155** (2002) 437-445.

43. M. Popa, J. Frantti and M. Kakihana, Characterization of $LaMeO_3$ (Me: Mn, Co, Fe) Perovskite Powders Obtained by Polymerizable Complex Method, Solid State Ionics **154-155** (2002) 135-141.

44. M. Popa and M. Kakihana, Synthesis of Lanthanum Cobaltite ($LaCoO_3$) by the Polymerizable Complex Route, Solid State Ionics **151** (2002) 251-257.

45. A. Abrue Jr., S.M. Zanetti, M.A.S. Oliveira and G.P. Thim, Effect of Urea on Lead Zirconate Titanate –$Pb(Zr_{0.52}Ti_{0.48})O_3$- Nanopowders Synthesized by the Pechini Method, Journal of the European Ceramic Society **xxx** (2004) xxx-xxx.

46. S. Wu and H. Chen, The Effects of Heat-Treatment Temperature on the Retention Capacities of Spinels Prepared by the Pechini Process, Journal of Power Sources **119-121** (2003) 134-138.

47. Z. Xu, Y. Li, Z. Liu and Z. Xiong, Low-Temperature Synthesis of Nanocrystalline $ZnGa_2O_4:Tb^{3+}$ Phosphors via the Pechini Method, Materials Science and Engineering B **110** (2004) 302-306.

48. B. Cockayne, The Uses and Enigmas of the Al_2O_3-Y_2O_3 Phase System, Journal of the Less-Common Metals, **114** (1985) 199-206.

49. L.E. Olds and H.E. Otto, in E.M. Levin et al. (eds.), Phase Diagrams for Ceramicists, American Ceramics Society, (1987), Fig. 311.

50. N. A. Toropov, I. A. Bondar, F. Ya. Galakhov, X. S. Nikogosyan and N. V. Vinogradova, Phase Diagrams for Ceramists, American Ceramic Society, (1987) Fig. 2344.

51. J.S. Abell, I.R. Harris, B. Cockayne and B. Lent, An Investigation of Phase Stability in the Y_2O_3-Al_2O_3 System, Journal of Materials Science, **9** (1974) 527-537.

52. E. Prince, Neutron Diffraction Measurements on Yttrium-Iron and Yttriumaluminium Garnets, Acta Crystallographica B, **31** (1975) 2233-2240.

53. N.J. Hess, G.D. Maupin, L.A. Chick, D.S. Sunberg, D.E. McCreedy and T.R. Armstrong, Synthesis and Crystallization of Yttrium-Aluminium Garnet and Related Compounds, Journal of Materials Science **29** (1994) 1873-1878.

54. R. Diehl and G. Brandt, Crystal Structure Refinement of $YAlO_3$, a Promising Laser Material, Materials Research Bulletin, **10** (1975) 85-90.

55. F. Bertaut and J. Mareschal, Un Nouveau Type de Structure Hexagonale: Al T O3 (T= Y, Eu, Gd, Tb, Dy, Ho, Er), Comptes Rendus Hebdomadaires des Seances de l' A cademie des Sciences, **257** (1963) 867-870.

56. H. Yamane, M. Omori and T. Hirai, Thermogravimetry and Rietveld Analysis for the High-Temperature X-ray Powder Diffraction Pattern of Y4 Al2 O9, Journal of Materials Science. Letters, **14** (1995) 470-473.

57. I. Warshaw and R. Roy, Stable and Metastable Equilibria in the Systems Y_2O_3-Al_2O_3 and Gd_2O_3-Fe_2O_3, Journal of the American Ceramic Society, **42** [9] (1959) 434-438.

58. I. Papadopoulos, On the Existence and Formation of $Y_4Al_2O_9$, Crystal Research and Technology **26** [4] (1991) 409-411.

59. B.D. Cullity, Elements of X-Ray Diffraction, Addison-Wesley Publishing Company, Inc., (1978) p. 377-379.

60. www.webelements.com

61. J. W. G. A. Vrolijk, S. van den Cruysem and R. Metselaar, The Influence of MgO and SiO_2 Dopants on the Sintering Behaviour of Yttrium Aluminium Garnet Ceramics, Ceramic Processing Science and Technology, American Ceramic Society, (1995) p. 573-577.

62. I.A. Bondar and F. Ya. Galakhov, Phase Diagrams for Ceramists, American Ceramic Society, (1987) Fig. 2586.

63. J.D. Verhoeven, Fundamentals of Physical Metallurgy, John Wiley & Sons, (1975) p. 127-129.

APPENDIX A

Crystal Structure of YAP

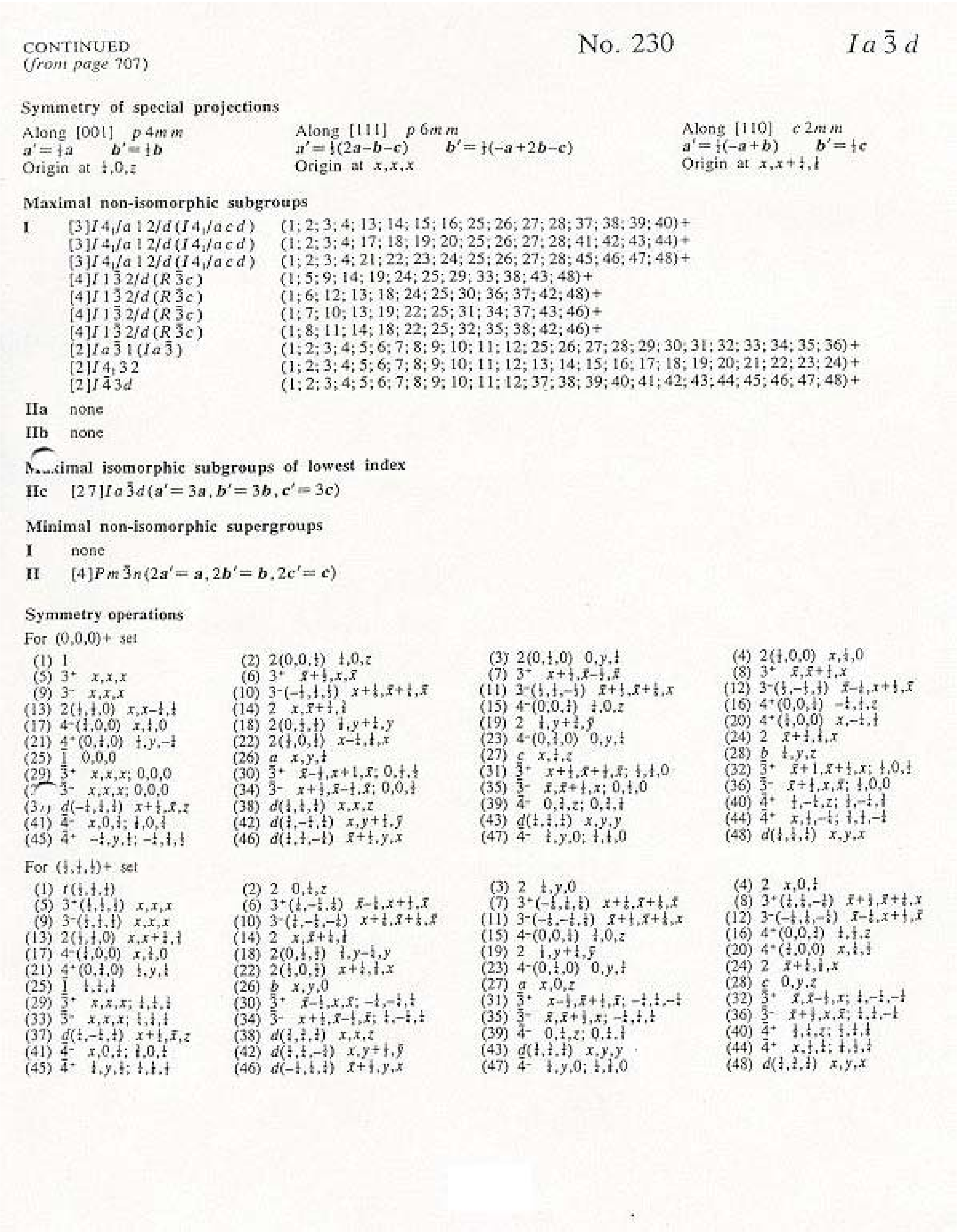

CONTINUED
(*from page* 707)

No. 230 $Ia\bar{3}d$

Symmetry of special projections

Along [001] $p4mm$
$a'=\frac{1}{2}a \quad b'=\frac{1}{2}b$
Origin at $\frac{1}{4},0,z$

Along [111] $p6mm$
$a'=\frac{1}{3}(2a-b-c) \quad b'=\frac{1}{3}(-a+2b-c)$
Origin at x,x,x

Along [110] $c2mm$
$a'=\frac{1}{2}(-a+b) \quad b'=\frac{1}{2}c$
Origin at $x,x+\frac{1}{4},\frac{1}{8}$

Maximal non-isomorphic subgroups

I	$[3]I4_1/a\,1\,2/d\,(I4_1/acd)$	(1; 2; 3; 4; 13; 14; 15; 16; 25; 26; 27; 28; 37; 38; 39; 40)+
	$[3]I4_1/a\,1\,2/d\,(I4_1/acd)$	(1; 2; 3; 4; 17; 18; 19; 20; 25; 26; 27; 28; 41; 42; 43; 44)+
	$[3]I4_1/a\,1\,2/d\,(I4_1/acd)$	(1; 2; 3; 4; 21; 22; 23; 24; 25; 26; 27; 28; 45; 46; 47; 48)+
	$[4]I\,1\,\bar{3}\,2/d\,(R\bar{3}c)$	(1; 5; 9; 14; 19; 24; 25; 29; 33; 38; 43; 48)+
	$[4]I\,1\,\bar{3}\,2/d\,(R\bar{3}c)$	(1; 6; 12; 13; 18; 24; 25; 30; 36; 37; 42; 48)+
	$[4]I\,1\,\bar{3}\,2/d\,(R\bar{3}c)$	(1; 7; 10; 13; 19; 22; 25; 31; 34; 37; 43; 46)+
	$[4]I\,1\,\bar{3}\,2/d\,(R\bar{3}c)$	(1; 8; 11; 14; 18; 22; 25; 32; 35; 38; 42; 46)+
	$[2]Ia\bar{3}\,1\,(Ia\bar{3})$	(1; 2; 3; 4; 5; 6; 7; 8; 9; 10; 11; 12; 25; 26; 27; 28; 29; 30; 31; 32; 33; 34; 35; 36)+
	$[2]I4_1\,3\,2$	(1; 2; 3; 4; 5; 6; 7; 8; 9; 10; 11; 12; 13; 14; 15; 16; 17; 18; 19; 20; 21; 22; 23; 24)+
	$[2]I\bar{4}\,3d$	(1; 2; 3; 4; 5; 6; 7; 8; 9; 10; 11; 12; 37; 38; 39; 40; 41; 42; 43; 44; 45; 46; 47; 48)+
IIa	none	
IIb	none	

Maximal isomorphic subgroups of lowest index

IIc $[27]Ia\bar{3}d\,(a'=3a, b'=3b, c'=3c)$

Minimal non-isomorphic supergroups

I none

II $[4]Pm\bar{3}n\,(2a'=a, 2b'=b, 2c'=c)$

Symmetry operations

For (0,0,0)+ set

(1) 1
(2) $2(0,0,\frac{1}{2})\quad \frac{1}{4},0,z$
(3) $2(0,\frac{1}{2},0)\quad 0,y,\frac{1}{4}$
(4) $2(\frac{1}{2},0,0)\quad x,\frac{1}{4},0$
(5) $3^{+}\quad x,x,x$
(6) $3^{+}\quad \bar{x}+\frac{1}{2},x,\bar{x}$
(7) $3^{+}\quad x+\frac{1}{2},\bar{x}-\frac{1}{2},\bar{x}$
(8) $3^{+}\quad \bar{x},\bar{x}+\frac{1}{2},x$
(9) $3^{-}\quad x,x,x$
(10) $3^{-}(-\frac{1}{3},\frac{1}{3},\frac{1}{3})\quad x+\frac{1}{6},\bar{x}+\frac{1}{6},\bar{x}$
(11) $3^{-}(\frac{1}{3},\frac{1}{3},-\frac{1}{3})\quad \bar{x}+\frac{1}{3},\bar{x}+\frac{1}{6},x$
(12) $3^{-}(\frac{1}{3},-\frac{1}{3},\frac{1}{3})\quad \bar{x}-\frac{1}{6},x+\frac{1}{3},\bar{x}$
(13) $2(\frac{1}{2},\frac{1}{2},0)\quad x,x-\frac{1}{4},\frac{1}{8}$
(14) $2\quad x,\bar{x}+\frac{3}{4},\frac{3}{8}$
(15) $4^{-}(0,0,\frac{3}{4})\quad \frac{1}{4},0,z$
(16) $4^{+}(0,0,\frac{1}{4})\quad -\frac{1}{4},\frac{1}{2},z$
(17) $4^{-}(\frac{3}{4},0,0)\quad x,\frac{1}{4},0$
(18) $2(0,\frac{1}{2},\frac{1}{2})\quad \frac{1}{8},y+\frac{1}{4},y$
(19) $2\quad \frac{3}{8},y+\frac{3}{4},\bar{y}$
(20) $4^{+}(\frac{1}{4},0,0)\quad x,-\frac{1}{4},\frac{1}{2}$
(21) $4^{+}(0,\frac{1}{4},0)\quad \frac{1}{2},y,-\frac{1}{4}$
(22) $2(\frac{1}{2},0,\frac{1}{2})\quad x-\frac{1}{4},\frac{1}{8},x$
(23) $4^{-}(0,\frac{3}{4},0)\quad 0,y,\frac{1}{4}$
(24) $2\quad \bar{x}+\frac{3}{4},\frac{3}{8},x$
(25) $\bar{1}\quad 0,0,0$
(26) $a\quad x,y,\frac{1}{4}$
(27) $c\quad x,\frac{1}{4},z$
(28) $b\quad \frac{1}{4},y,z$
(29) $\bar{3}^{+}\quad x,x,x;\ 0,0,0$
(30) $\bar{3}^{+}\quad \bar{x}-\frac{1}{2},x+1,\bar{x};\ 0,\frac{1}{2},\frac{1}{2}$
(31) $\bar{3}^{+}\quad x+\frac{1}{2},\bar{x}+\frac{1}{2},\bar{x};\ \frac{1}{2},\frac{1}{2},0$
(32) $\bar{3}^{+}\quad \bar{x}+1,\bar{x}+\frac{1}{2},x;\ \frac{1}{2},0,\frac{1}{2}$
(33) $\bar{3}^{-}\quad x,x,x;\ 0,0,0$
(34) $\bar{3}^{-}\quad x+\frac{1}{2},\bar{x}-\frac{1}{2},\bar{x};\ 0,0,\frac{1}{2}$
(35) $\bar{3}^{-}\quad \bar{x},\bar{x}+\frac{1}{2},x;\ 0,\frac{1}{2},0$
(36) $\bar{3}^{-}\quad \bar{x}+\frac{1}{2},x,\bar{x};\ \frac{1}{2},0,0$
(37) $d(-\frac{1}{4},\frac{1}{4},\frac{3}{4})\quad x+\frac{1}{2},\bar{x},z$
(38) $d(\frac{1}{4},\frac{1}{4},\frac{1}{4})\quad x,x,z$
(39) $\bar{4}^{-}\quad 0,\frac{3}{4},z;\ 0,\frac{3}{4},\frac{1}{8}$
(40) $\bar{4}^{+}\quad \frac{1}{2},-\frac{1}{4},z;\ \frac{1}{2},-\frac{1}{4},\frac{3}{8}$
(41) $\bar{4}^{-}\quad x,0,\frac{3}{4};\ \frac{1}{8},0,\frac{3}{4}$
(42) $d(\frac{3}{4},-\frac{1}{4},\frac{1}{4})\quad x,y+\frac{1}{2},\bar{y}$
(43) $d(\frac{1}{4},\frac{1}{4},\frac{1}{4})\quad x,y,y$
(44) $\bar{4}^{+}\quad x,\frac{1}{2},-\frac{1}{4};\ \frac{3}{8},\frac{1}{2},-\frac{1}{4}$
(45) $\bar{4}^{+}\quad -\frac{1}{4},y,\frac{1}{2};\ -\frac{1}{4},\frac{3}{8},\frac{1}{2}$
(46) $d(\frac{1}{4},\frac{3}{4},-\frac{1}{4})\quad \bar{x}+\frac{1}{2},y,x$
(47) $\bar{4}^{-}\quad \frac{3}{4},y,0;\ \frac{3}{4},\frac{1}{8},0$
(48) $d(\frac{1}{4},\frac{1}{4},\frac{1}{4})\quad x,y,x$

For $(\frac{1}{2},\frac{1}{2},\frac{1}{2})$+ set

(1) $t(\frac{1}{2},\frac{1}{2},\frac{1}{2})$
(2) $2\quad 0,\frac{1}{4},z$
(3) $2\quad \frac{1}{4},y,0$
(4) $2\quad x,0,\frac{1}{4}$
(5) $3^{+}(\frac{1}{2},\frac{1}{2},\frac{1}{2})\quad x,x,x$
(6) $3^{+}(\frac{1}{6},-\frac{1}{6},\frac{1}{6})\quad \bar{x}-\frac{1}{6},x+\frac{1}{3},\bar{x}$
(7) $3^{+}(-\frac{1}{6},\frac{1}{6},\frac{1}{6})\quad x+\frac{1}{6},\bar{x}+\frac{1}{6},\bar{x}$
(8) $3^{+}(\frac{1}{6},\frac{1}{6},-\frac{1}{6})\quad \bar{x}+\frac{1}{3},\bar{x}+\frac{1}{6},x$
(9) $3^{-}(\frac{1}{2},\frac{1}{2},\frac{1}{2})\quad x,x,x$
(10) $3^{-}(\frac{1}{6},-\frac{1}{6},-\frac{1}{6})\quad x+\frac{1}{6},\bar{x}+\frac{1}{6},\bar{x}$
(11) $3^{-}(-\frac{1}{6},-\frac{1}{6},\frac{1}{6})\quad \bar{x}+\frac{1}{3},\bar{x}+\frac{1}{6},x$
(12) $3^{-}(-\frac{1}{6},\frac{1}{6},-\frac{1}{6})\quad \bar{x}-\frac{1}{6},x+\frac{1}{3},\bar{x}$
(13) $2(\frac{1}{2},\frac{1}{2},0)\quad x,x+\frac{1}{4},\frac{3}{8}$
(14) $2\quad x,\bar{x}+\frac{1}{4},\frac{1}{8}$
(15) $4^{-}(0,0,\frac{1}{4})\quad \frac{3}{4},0,z$
(16) $4^{+}(0,0,\frac{3}{4})\quad \frac{1}{4},\frac{1}{2},z$
(17) $4^{-}(\frac{1}{4},0,0)\quad x,\frac{3}{4},0$
(18) $2(0,\frac{1}{2},\frac{1}{2})\quad \frac{3}{8},y-\frac{1}{4},y$
(19) $2\quad \frac{1}{8},y+\frac{1}{4},\bar{y}$
(20) $4^{+}(\frac{3}{4},0,0)\quad x,\frac{1}{4},\frac{1}{2}$
(21) $4^{+}(0,\frac{3}{4},0)\quad \frac{1}{2},y,\frac{1}{4}$
(22) $2(\frac{1}{2},0,\frac{1}{2})\quad x+\frac{1}{4},\frac{3}{8},x$
(23) $4^{-}(0,\frac{1}{4},0)\quad 0,y,\frac{3}{4}$
(24) $2\quad \bar{x}+\frac{1}{4},\frac{1}{8},x$
(25) $\bar{1}\quad \frac{1}{4},\frac{1}{4},\frac{1}{4}$
(26) $b\quad x,y,0$
(27) $a\quad x,0,z$
(28) $c\quad 0,y,z$
(29) $\bar{3}^{+}\quad x,x,x;\ \frac{1}{4},\frac{1}{4},\frac{1}{4}$
(30) $\bar{3}^{+}\quad \bar{x}-\frac{1}{2},x,\bar{x};\ -\frac{1}{4},-\frac{1}{4},\frac{1}{4}$
(31) $\bar{3}^{+}\quad x-\frac{1}{2},\bar{x}+\frac{1}{2},\bar{x};\ -\frac{1}{4},\frac{1}{4},-\frac{1}{4}$
(32) $\bar{3}^{+}\quad \bar{x},\bar{x}-\frac{1}{2},x;\ \frac{1}{4},-\frac{1}{4},-\frac{1}{4}$
(33) $\bar{3}^{-}\quad x,x,x;\ \frac{1}{4},\frac{1}{4},\frac{1}{4}$
(34) $\bar{3}^{-}\quad x+\frac{1}{2},\bar{x}-\frac{1}{2},\bar{x};\ \frac{1}{4},-\frac{1}{4},\frac{1}{4}$
(35) $\bar{3}^{-}\quad \bar{x},\bar{x}+\frac{1}{2},x;\ -\frac{1}{4},\frac{1}{4},\frac{1}{4}$
(36) $\bar{3}^{-}\quad \bar{x}+\frac{1}{2},x,\bar{x};\ \frac{1}{4},\frac{1}{4},-\frac{1}{4}$
(37) $d(\frac{1}{4},-\frac{1}{4},\frac{1}{4})\quad x+\frac{1}{2},\bar{x},z$
(38) $d(\frac{3}{4},\frac{3}{4},\frac{3}{4})\quad x,x,z$
(39) $\bar{4}^{-}\quad 0,\frac{1}{4},z;\ 0,\frac{1}{4},\frac{3}{8}$
(40) $\bar{4}^{+}\quad \frac{1}{2},\frac{1}{4},z;\ \frac{1}{2},\frac{1}{4},\frac{1}{8}$
(41) $\bar{4}^{-}\quad x,0,\frac{1}{4};\ \frac{3}{8},0,\frac{1}{4}$
(42) $d(\frac{1}{4},\frac{1}{4},-\frac{1}{4})\quad x,y+\frac{1}{2},\bar{y}$
(43) $d(\frac{3}{4},\frac{3}{4},\frac{3}{4})\quad x,y,y$
(44) $\bar{4}^{+}\quad x,\frac{1}{2},\frac{1}{4};\ \frac{1}{8},\frac{1}{2},\frac{1}{4}$
(45) $\bar{4}^{+}\quad \frac{1}{4},y,\frac{1}{2};\ \frac{1}{4},\frac{1}{8},\frac{1}{2}$
(46) $d(-\frac{1}{4},\frac{1}{4},\frac{1}{4})\quad \bar{x}+\frac{1}{2},y,x$
(47) $\bar{4}^{-}\quad \frac{1}{4},y,0;\ \frac{1}{4},\frac{3}{8},0$
(48) $d(\frac{3}{4},\frac{3}{4},\frac{3}{4})\quad x,y,x$

$Ia\bar{3}d$ O_h^{10} $m\bar{3}m$ Cubic

No. 230 $I4_1/a\,\bar{3}\,2/d$ Patterson symmetry $Im\bar{3}m$

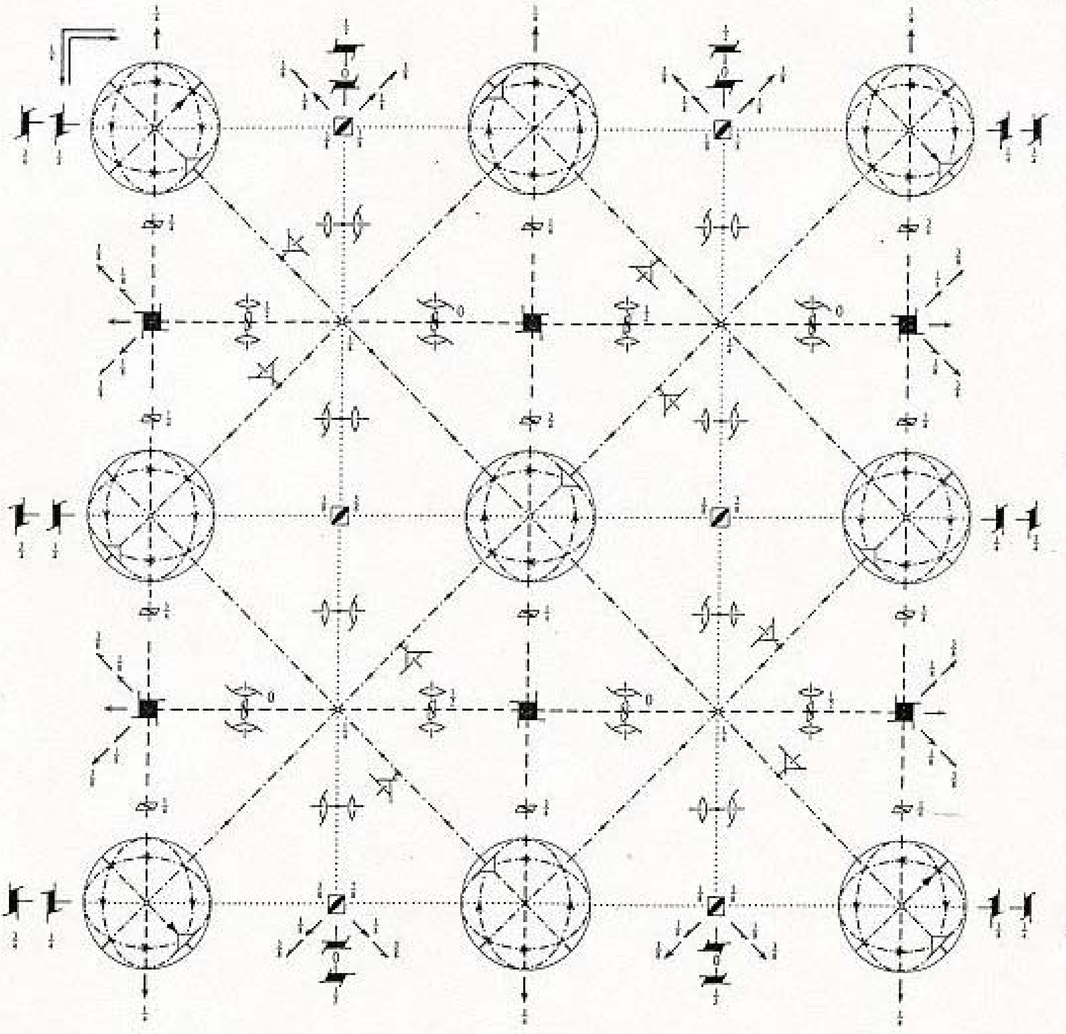

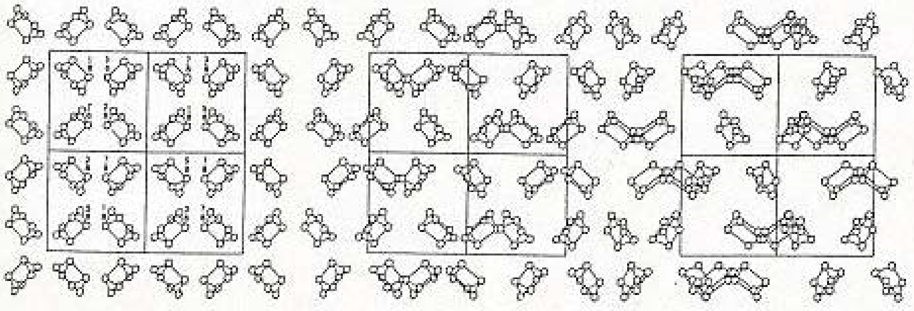

Origin at centre ($\bar{3}$)

Asymmetric unit $-\frac{1}{8}\leq x\leq\frac{1}{8}$; $-\frac{1}{8}\leq y\leq\frac{1}{8}$; $0\leq z\leq\frac{1}{4}$; $\max(x,-x,y,-y)\leq z$

Vertices $0,0,0$ $\frac{1}{8},\frac{1}{8},\frac{1}{8}$ $-\frac{1}{8},\frac{1}{8},\frac{1}{8}$ $-\frac{1}{8},-\frac{1}{8},\frac{1}{8}$ $\frac{1}{8},-\frac{1}{8},\frac{1}{8}$
$\frac{1}{8},\frac{1}{8},\frac{1}{4}$ $-\frac{1}{8},\frac{1}{8},\frac{1}{4}$ $-\frac{1}{8},-\frac{1}{8},\frac{1}{4}$ $\frac{1}{8},-\frac{1}{8},\frac{1}{4}$

Symmetry operations
(*given on page* 703)

Generators selected (1); $t(1,0,0)$; $t(0,1,0)$; $t(0,0,1)$; $t(\frac{1}{2},\frac{1}{2},\frac{1}{2})$; (2); (3); (5); (13); (25)

Positions

Multiplicity,
Wyckoff letter,
Site symmetry

Coordinates

$(0,0,0)+$ $(\frac{1}{2},\frac{1}{2},\frac{1}{2})+$

Reflection conditions

h,k,l permutable

96 h 1

(1) x,y,z	(2) $\bar{x}+\frac{1}{2},\bar{y},z+\frac{1}{2}$	(3) $\bar{x},y+\frac{1}{2},\bar{z}+\frac{1}{2}$	(4) $x+\frac{1}{2},\bar{y}+\frac{1}{2},\bar{z}$
(5) z,x,y	(6) $z+\frac{1}{2},\bar{x}+\frac{1}{2},\bar{y}$	(7) $\bar{z}+\frac{1}{2},\bar{x},y+\frac{1}{2}$	(8) $\bar{z},x+\frac{1}{2},\bar{y}+\frac{1}{2}$
(9) y,z,x	(10) $\bar{y},z+\frac{1}{2},\bar{x}+\frac{1}{2}$	(11) $y+\frac{1}{2},\bar{z}+\frac{1}{2},\bar{x}$	(12) $\bar{y}+\frac{1}{2},\bar{z},x+\frac{1}{2}$
(13) $y+\frac{3}{4},x+\frac{1}{4},\bar{z}+\frac{1}{4}$	(14) $\bar{y}+\frac{3}{4},\bar{x}+\frac{3}{4},\bar{z}+\frac{3}{4}$	(15) $y+\frac{1}{4},\bar{x}+\frac{1}{4},z+\frac{3}{4}$	(16) $\bar{y}+\frac{1}{4},x+\frac{3}{4},z+\frac{1}{4}$
(17) $x+\frac{3}{4},z+\frac{1}{4},\bar{y}+\frac{1}{4}$	(18) $\bar{x}+\frac{1}{4},z+\frac{3}{4},y+\frac{1}{4}$	(19) $\bar{x}+\frac{3}{4},\bar{z}+\frac{3}{4},\bar{y}+\frac{3}{4}$	(20) $x+\frac{1}{4},\bar{z}+\frac{1}{4},y+\frac{3}{4}$
(21) $z+\frac{3}{4},y+\frac{1}{4},\bar{x}+\frac{1}{4}$	(22) $z+\frac{1}{4},\bar{y}+\frac{1}{4},x+\frac{3}{4}$	(23) $\bar{z}+\frac{1}{4},y+\frac{3}{4},x+\frac{1}{4}$	(24) $\bar{z}+\frac{3}{4},\bar{y}+\frac{3}{4},\bar{x}+\frac{3}{4}$
(25) $\bar{x},\bar{y},\bar{z}$	(26) $x+\frac{1}{2},y,\bar{z}+\frac{1}{2}$	(27) $x,\bar{y}+\frac{1}{2},z+\frac{1}{2}$	(28) $\bar{x}+\frac{1}{2},y+\frac{1}{2},z$
(29) $\bar{z},\bar{x},\bar{y}$	(30) $\bar{z}+\frac{1}{2},x+\frac{1}{2},y$	(31) $z+\frac{1}{2},x,\bar{y}+\frac{1}{2}$	(32) $z,\bar{x}+\frac{1}{2},y+\frac{1}{2}$
(33) $\bar{y},\bar{z},\bar{x}$	(34) $y,\bar{z}+\frac{1}{2},x+\frac{1}{2}$	(35) $\bar{y}+\frac{1}{2},z+\frac{1}{2},x$	(36) $y+\frac{1}{2},z,\bar{x}+\frac{1}{2}$
(37) $\bar{y}+\frac{1}{4},\bar{x}+\frac{3}{4},z+\frac{3}{4}$	(38) $y+\frac{1}{4},x+\frac{1}{4},z+\frac{1}{4}$	(39) $\bar{y}+\frac{3}{4},x+\frac{3}{4},\bar{z}+\frac{1}{4}$	(40) $y+\frac{3}{4},\bar{x}+\frac{1}{4},\bar{z}+\frac{3}{4}$
(41) $\bar{x}+\frac{1}{4},\bar{z}+\frac{3}{4},y+\frac{3}{4}$	(42) $x+\frac{3}{4},\bar{z}+\frac{1}{4},\bar{y}+\frac{3}{4}$	(43) $x+\frac{1}{4},z+\frac{1}{4},y+\frac{1}{4}$	(44) $\bar{x}+\frac{3}{4},z+\frac{3}{4},\bar{y}+\frac{1}{4}$
(45) $\bar{z}+\frac{1}{4},\bar{y}+\frac{3}{4},x+\frac{3}{4}$	(46) $\bar{z}+\frac{3}{4},y+\frac{3}{4},\bar{x}+\frac{1}{4}$	(47) $z+\frac{3}{4},\bar{y}+\frac{1}{4},\bar{x}+\frac{3}{4}$	(48) $z+\frac{1}{4},y+\frac{1}{4},x+\frac{1}{4}$

General:
$hkl: h+k+l=2n$
$0kl: k,l=2n$
$hhl: 2h+l=4n$
$h00: h=4n$

Special: as above, plus

48 g ..2

$\frac{1}{8},y,\bar{y}+\frac{1}{4}$	$\frac{3}{8},\bar{y},\bar{y}+\frac{3}{4}$	$\frac{7}{8},y+\frac{1}{2},y+\frac{1}{4}$	$\frac{5}{8},\bar{y}+\frac{1}{2},y+\frac{3}{4}$
$\bar{y}+\frac{1}{4},\frac{1}{8},y$	$\bar{y}+\frac{3}{4},\frac{3}{8},\bar{y}$	$y+\frac{1}{4},\frac{7}{8},y+\frac{1}{2}$	$y+\frac{3}{4},\frac{5}{8},\bar{y}+\frac{1}{2}$
$y,\bar{y}+\frac{1}{4},\frac{1}{8}$	$\bar{y},\bar{y}+\frac{3}{4},\frac{3}{8}$	$y+\frac{1}{2},y+\frac{1}{4},\frac{7}{8}$	$\bar{y}+\frac{1}{2},y+\frac{3}{4},\frac{5}{8}$
$\frac{7}{8},\bar{y},y+\frac{3}{4}$	$\frac{5}{8},y,y+\frac{1}{4}$	$\frac{1}{8},\bar{y}+\frac{1}{2},\bar{y}+\frac{3}{4}$	$\frac{3}{8},y+\frac{1}{2},\bar{y}+\frac{1}{4}$
$y+\frac{3}{4},\frac{7}{8},\bar{y}$	$y+\frac{1}{4},\frac{5}{8},y$	$\bar{y}+\frac{3}{4},\frac{1}{8},\bar{y}+\frac{1}{2}$	$\bar{y}+\frac{1}{4},\frac{3}{8},y+\frac{1}{2}$
$\bar{y},y+\frac{3}{4},\frac{7}{8}$	$y,y+\frac{1}{4},\frac{5}{8}$	$\bar{y}+\frac{1}{2},\bar{y}+\frac{3}{4},\frac{1}{8}$	$y+\frac{1}{2},\bar{y}+\frac{1}{4},\frac{3}{8}$

$hkl: h=2n+1$
or $h=4n$

48 f 2..

$x,0,\frac{1}{4}$	$\bar{x}+\frac{1}{2},0,\frac{3}{4}$	$\frac{1}{4},x,0$	$\frac{3}{4},\bar{x}+\frac{1}{2},0$	$0,\frac{1}{4},x$	$0,\frac{3}{4},\bar{x}+\frac{1}{2}$
$\frac{3}{4},x+\frac{1}{4},0$	$\frac{3}{4},\bar{x}+\frac{3}{4},\frac{1}{2}$	$x+\frac{3}{4},\frac{1}{2},\frac{1}{4}$	$\bar{x}+\frac{1}{4},0,\frac{1}{4}$	$0,\frac{1}{4},\bar{x}+\frac{1}{4}$	$\frac{1}{2},\frac{1}{4},x+\frac{3}{4}$
$\bar{x},0,\frac{3}{4}$	$x+\frac{1}{2},0,\frac{1}{4}$	$\frac{3}{4},\bar{x},0$	$\frac{1}{4},x+\frac{1}{2},0$	$0,\frac{3}{4},\bar{x}$	$0,\frac{1}{4},x+\frac{1}{2}$
$\frac{1}{4},\bar{x}+\frac{3}{4},0$	$\frac{1}{4},x+\frac{1}{4},\frac{1}{2}$	$\bar{x}+\frac{1}{4},\frac{1}{2},\frac{3}{4}$	$x+\frac{3}{4},0,\frac{3}{4}$	$0,\frac{3}{4},x+\frac{3}{4}$	$\frac{1}{2},\frac{3}{4},\bar{x}+\frac{1}{4}$

$hkl: 2h+l=4n$

32 e .3.

x,x,x	$\bar{x}+\frac{1}{2},\bar{x},x+\frac{1}{2}$	$\bar{x},x+\frac{1}{2},\bar{x}+\frac{1}{2}$	$x+\frac{1}{2},\bar{x}+\frac{1}{2},\bar{x}$
$x+\frac{3}{4},x+\frac{1}{4},\bar{x}+\frac{1}{4}$	$\bar{x}+\frac{3}{4},\bar{x}+\frac{3}{4},\bar{x}+\frac{3}{4}$	$x+\frac{1}{4},\bar{x}+\frac{1}{4},x+\frac{3}{4}$	$\bar{x}+\frac{1}{4},x+\frac{3}{4},x+\frac{1}{4}$
$\bar{x},\bar{x},\bar{x}$	$x+\frac{1}{2},x,\bar{x}+\frac{1}{2}$	$x,\bar{x}+\frac{1}{2},x+\frac{1}{2}$	$\bar{x}+\frac{1}{2},x+\frac{1}{2},x$
$\bar{x}+\frac{1}{4},\bar{x}+\frac{3}{4},x+\frac{3}{4}$	$x+\frac{1}{4},x+\frac{1}{4},x+\frac{1}{4}$	$\bar{x}+\frac{3}{4},x+\frac{3}{4},\bar{x}+\frac{1}{4}$	$x+\frac{3}{4},\bar{x}+\frac{1}{4},\bar{x}+\frac{3}{4}$

$hkl: h=2n+1$
or $h+k+l=4n$

24 d $\bar{4}$..

$\frac{3}{8},0,\frac{1}{4}$	$\frac{1}{8},0,\frac{3}{4}$	$\frac{1}{4},\frac{3}{8},0$	$\frac{3}{4},\frac{1}{8},0$	$0,\frac{1}{4},\frac{3}{8}$	$0,\frac{3}{4},\frac{1}{8}$
$\frac{3}{4},\frac{5}{8},0$	$\frac{3}{4},\frac{3}{8},\frac{1}{2}$	$\frac{1}{8},\frac{1}{2},\frac{1}{4}$	$\frac{7}{8},0,\frac{1}{4}$	$0,\frac{1}{4},\frac{7}{8}$	$\frac{1}{2},\frac{1}{4},\frac{1}{8}$

24 c 2.22

$\frac{1}{8},0,\frac{1}{4}$	$\frac{3}{8},0,\frac{3}{4}$	$\frac{1}{4},\frac{1}{8},0$	$\frac{3}{4},\frac{3}{8},0$	$0,\frac{1}{4},\frac{1}{8}$	$0,\frac{3}{4},\frac{3}{8}$
$\frac{7}{8},0,\frac{3}{4}$	$\frac{5}{8},0,\frac{1}{4}$	$\frac{3}{4},\frac{7}{8},0$	$\frac{1}{4},\frac{5}{8},0$	$0,\frac{3}{4},\frac{7}{8}$	$0,\frac{1}{4},\frac{5}{8}$

$hkl: h,k=2n,\ h+k+l=4n$
or $h,k=2n+1,\ l=4n+2$
or $h=8n,\ k=8n+4$ and
$h+k+l=4n+2$

16 b .32

$\frac{1}{8},\frac{1}{8},\frac{1}{8}$	$\frac{3}{8},\frac{7}{8},\frac{5}{8}$	$\frac{7}{8},\frac{5}{8},\frac{3}{8}$	$\frac{5}{8},\frac{3}{8},\frac{7}{8}$	$\frac{7}{8},\frac{7}{8},\frac{7}{8}$	$\frac{5}{8},\frac{1}{8},\frac{3}{8}$	$\frac{1}{8},\frac{3}{8},\frac{5}{8}$	$\frac{3}{8},\frac{5}{8},\frac{1}{8}$

$hkl: h,k=2n+1,\ l=4n+2$
or $h,k,l=4n$

16 a .$\bar{3}$.

$0,0,0$	$\frac{1}{2},0,\frac{1}{2}$	$0,\frac{1}{2},\frac{1}{2}$	$\frac{1}{2},\frac{1}{2},0$	$\frac{3}{4},\frac{1}{4},\frac{1}{4}$	$\frac{3}{4},\frac{3}{4},\frac{3}{4}$	$\frac{1}{4},\frac{1}{4},\frac{3}{4}$	$\frac{1}{4},\frac{3}{4},\frac{1}{4}$

$hkl: h,k=2n,\ h+k+l=4n$

(*Continued on page* 705)

Crystal Structure of Orthorhombic YAP

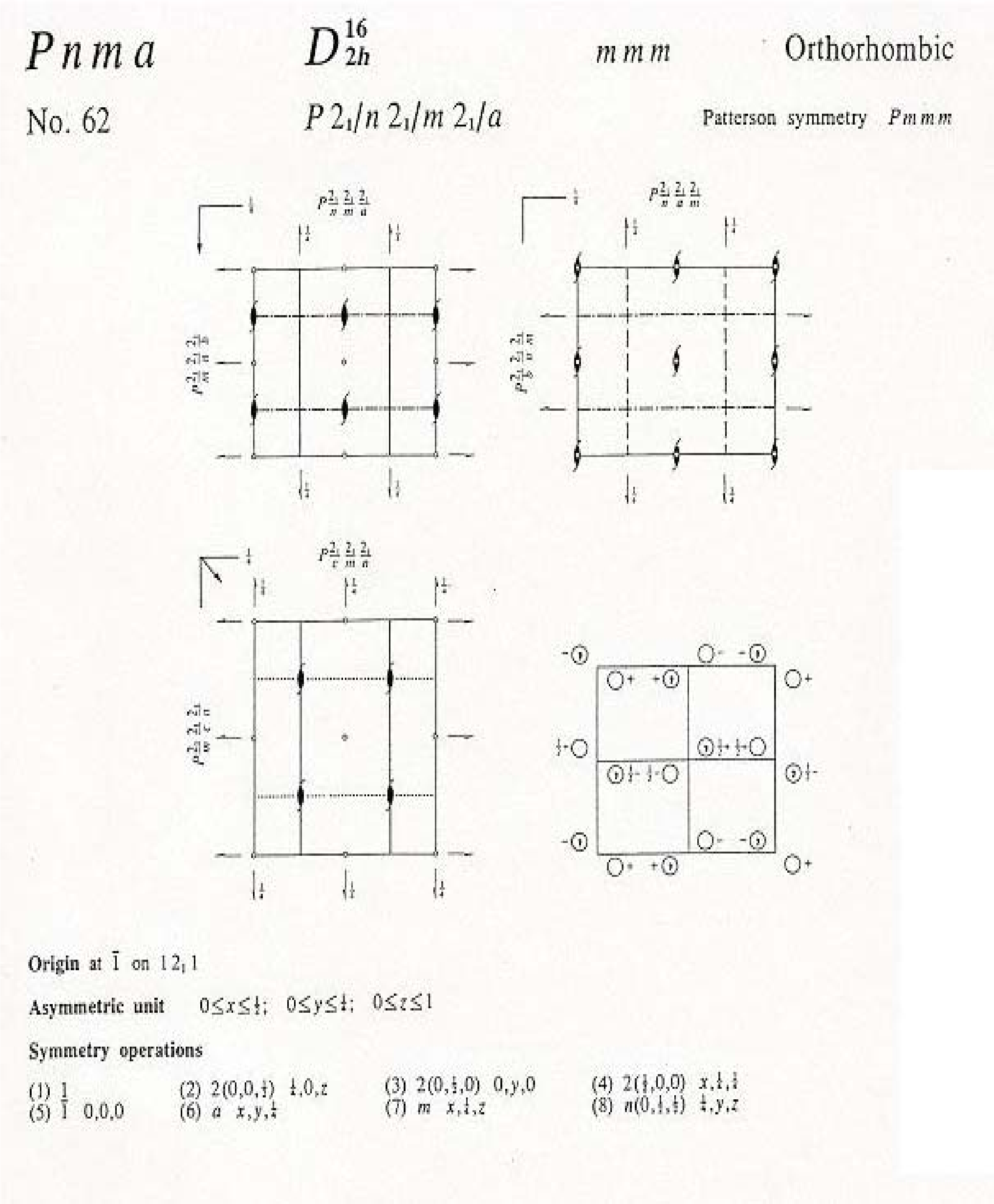

$Pnma$ D_{2h}^{16} mmm Orthorhombic

No. 62 $P\,2_1/n\,2_1/m\,2_1/a$ Patterson symmetry $Pmmm$

Origin at $\bar{1}$ **on** $1\,2_1\,1$

Asymmetric unit $0 \leq x \leq \frac{1}{2};\ 0 \leq y \leq \frac{1}{4};\ 0 \leq z \leq 1$

Symmetry operations

(1) 1
(2) $2(0,0,\frac{1}{2})\ \frac{1}{4},0,z$
(3) $2(0,\frac{1}{2},0)\ 0,y,0$
(4) $2(\frac{1}{2},0,0)\ x,\frac{1}{4},\frac{1}{4}$
(5) $\bar{1}\ 0,0,0$
(6) $a\ x,y,\frac{1}{4}$
(7) $m\ x,\frac{1}{4},z$
(8) $n(0,\frac{1}{2},\frac{1}{2})\ \frac{1}{4},y,z$

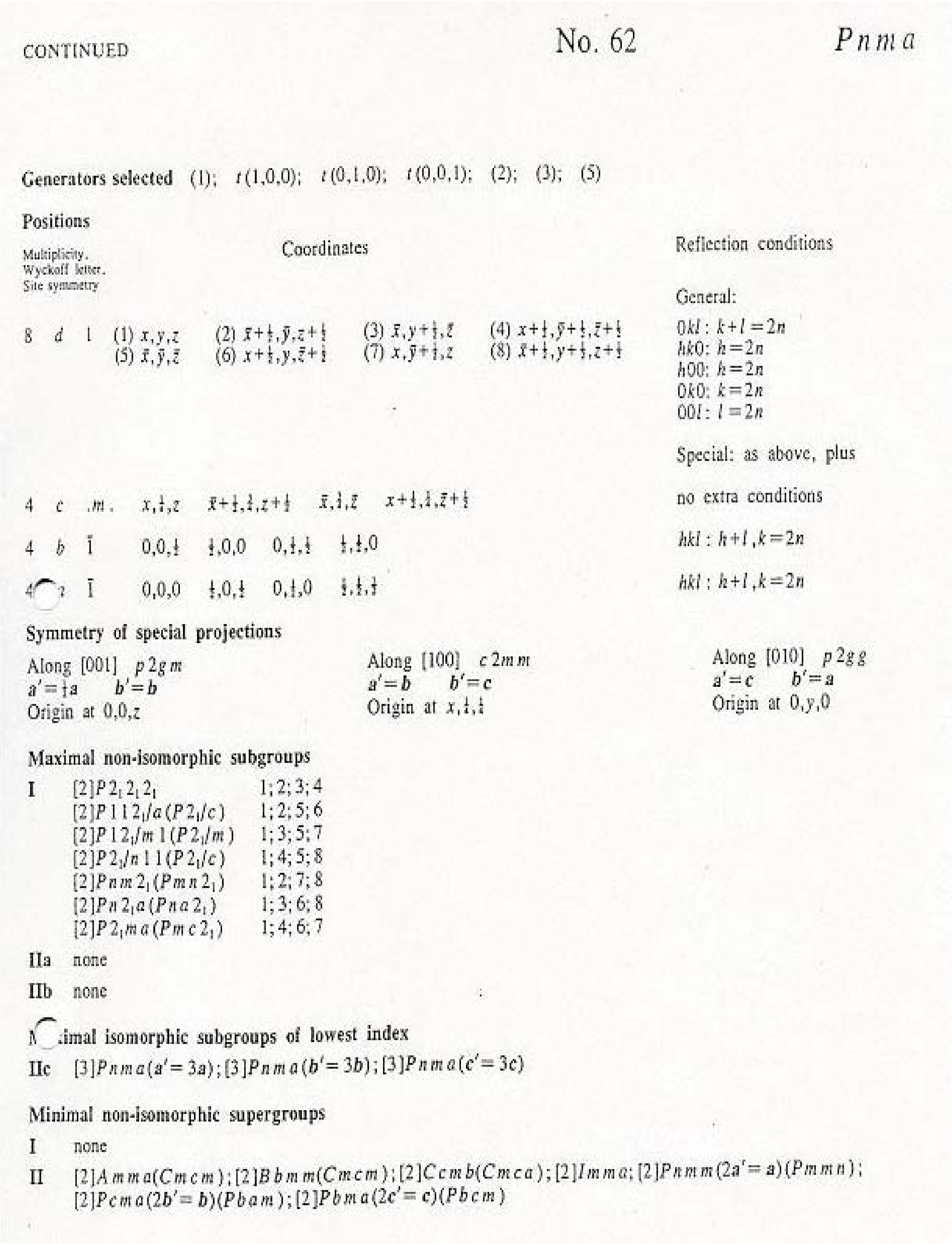

Generators selected (1); $t(1,0,0)$; $t(0,1,0)$; $t(0,0,1)$; (2); (3); (5)

Positions

Multiplicity, Wyckoff letter, Site symmetry			Coordinates				Reflection conditions
							General:
8	d	1	(1) x,y,z (5) $\bar{x},\bar{y},\bar{z}$	(2) $\bar{x}+\frac{1}{2},\bar{y},z+\frac{1}{2}$ (6) $x+\frac{1}{2},y,\bar{z}+\frac{1}{2}$	(3) $\bar{x},y+\frac{1}{2},\bar{z}$ (7) $x,\bar{y}+\frac{1}{2},z$	(4) $x+\frac{1}{2},\bar{y}+\frac{1}{2},\bar{z}+\frac{1}{2}$ (8) $\bar{x}+\frac{1}{2},y+\frac{1}{2},z+\frac{1}{2}$	$0kl: k+l=2n$ $hk0: h=2n$ $h00: h=2n$ $0k0: k=2n$ $00l: l=2n$
							Special: as above, plus
4	c	$.m.$	$x,\frac{1}{4},z$	$\bar{x}+\frac{1}{2},\frac{3}{4},z+\frac{1}{2}$	$\bar{x},\frac{3}{4},\bar{z}$	$x+\frac{1}{2},\frac{1}{4},\bar{z}+\frac{1}{2}$	no extra conditions
4	b	$\bar{1}$	$0,0,\frac{1}{2}$	$\frac{1}{2},0,0$	$0,\frac{1}{2},\frac{1}{2}$	$\frac{1}{2},\frac{1}{2},0$	$hkl: h+l,k=2n$
4	a	$\bar{1}$	$0,0,0$	$\frac{1}{2},0,\frac{1}{2}$	$0,\frac{1}{2},0$	$\frac{1}{2},\frac{1}{2},\frac{1}{2}$	$hkl: h+l,k=2n$

Symmetry of special projections

Along [001] $p2gm$	Along [100] $c2mm$	Along [010] $p2gg$
$a'=\frac{1}{2}a$ $b'=b$	$a'=b$ $b'=c$	$a'=c$ $b'=a$
Origin at $0,0,z$	Origin at $x,\frac{1}{4},\frac{1}{4}$	Origin at $0,y,0$

Maximal non-isomorphic subgroups

I	$[2]P2_12_12_1$	1; 2; 3; 4
	$[2]P112_1/a\,(P2_1/c)$	1; 2; 5; 6
	$[2]P12_1/m1\,(P2_1/m)$	1; 3; 5; 7
	$[2]P2_1/n11\,(P2_1/c)$	1; 4; 5; 8
	$[2]Pnm2_1\,(Pmn2_1)$	1; 2; 7; 8
	$[2]Pn2_1a\,(Pna2_1)$	1; 3; 6; 8
	$[2]P2_1ma\,(Pmc2_1)$	1; 4; 6; 7
IIa	none	
IIb	none	

M[illegible]imal isomorphic subgroups of lowest index

IIc $[3]Pnma\,(a'=3a)$; $[3]Pnma\,(b'=3b)$; $[3]Pnma\,(c'=3c)$

Minimal non-isomorphic supergroups

I none

II $[2]Amma\,(Cmcm)$; $[2]Bbmm\,(Cmcm)$; $[2]Ccmb\,(Cmca)$; $[2]Imma$; $[2]Pnmm\,(2a'=a)\,(Pmmn)$; $[2]Pcma\,(2b'=b)\,(Pbam)$; $[2]Pbma\,(2c'=c)\,(Pbcm)$

Crystal Structure of Hexagonal YAP

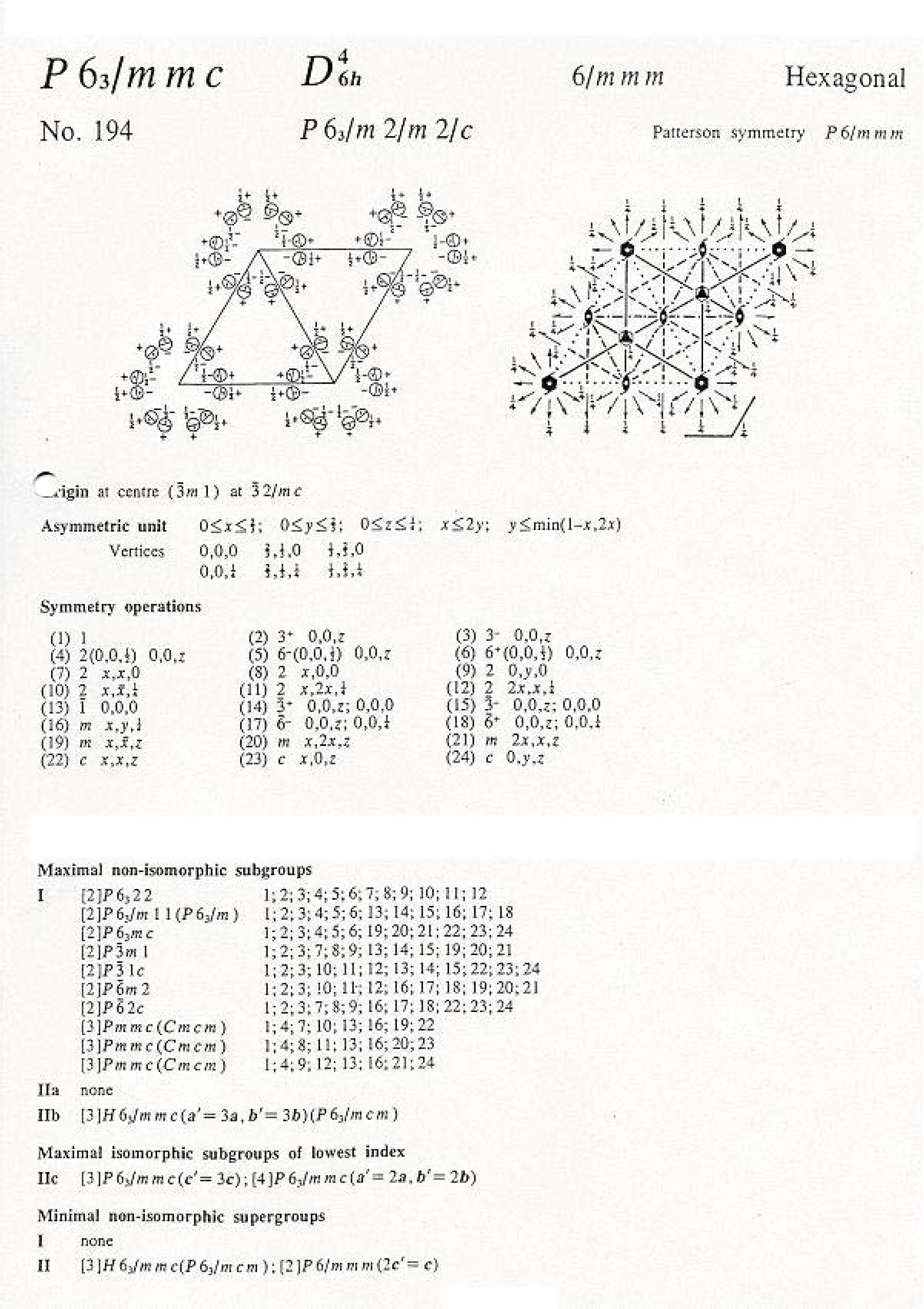

$P\,6_3/m\,m\,c$ D^4_{6h} $6/m\,m\,m$ Hexagonal

No. 194 $P\,6_3/m\,2/m\,2/c$ Patterson symmetry $P\,6/m\,m\,m$

igin at centre ($\bar{3}m\,1$) at $\bar{3}\,2/m\,c$

Asymmetric unit $0\le x\le\frac{2}{3};\quad 0\le y\le\frac{2}{3};\quad 0\le z\le\frac{1}{4};\quad x\le 2y;\quad y\le\min(1-x,2x)$

Vertices $0,0,0 \quad \frac{2}{3},\frac{1}{3},0 \quad \frac{1}{3},\frac{2}{3},0$

$0,0,\frac{1}{4} \quad \frac{2}{3},\frac{1}{3},\frac{1}{4} \quad \frac{1}{3},\frac{2}{3},\frac{1}{4}$

Symmetry operations

(1) 1	(2) 3^+ $0,0,z$	(3) 3^- $0,0,z$
(4) $2(0,0,\frac{1}{2})$ $0,0,z$	(5) $6^-(0,0,\frac{1}{2})$ $0,0,z$	(6) $6^+(0,0,\frac{1}{2})$ $0,0,z$
(7) 2 $x,x,0$	(8) 2 $x,0,0$	(9) 2 $0,y,0$
(10) 2 $x,\bar{x},\frac{1}{4}$	(11) 2 $x,2x,\frac{1}{4}$	(12) 2 $2x,x,\frac{1}{4}$
(13) $\bar{1}$ $0,0,0$	(14) $\bar{3}^+$ $0,0,z$; $0,0,0$	(15) $\bar{3}^-$ $0,0,z$; $0,0,0$
(16) m $x,y,\frac{1}{4}$	(17) $\bar{6}^-$ $0,0,z$; $0,0,\frac{1}{4}$	(18) $\bar{6}^+$ $0,0,z$; $0,0,\frac{1}{4}$
(19) m $x,\bar{x},z$	(20) m $x,2x,z$	(21) m $2x,x,z$
(22) c x,x,z	(23) c $x,0,z$	(24) c $0,y,z$

Maximal non-isomorphic subgroups

I	$[2]P\,6_3\,2\,2$	1; 2; 3; 4; 5; 6; 7; 8; 9; 10; 11; 12
	$[2]P\,6_3/m\,1\,1\,(P\,6_3/m)$	1; 2; 3; 4; 5; 6; 13; 14; 15; 16; 17; 18
	$[2]P\,6_3 m\,c$	1; 2; 3; 4; 5; 6; 19; 20; 21; 22; 23; 24
	$[2]P\,\bar{3}m\,1$	1; 2; 3; 7; 8; 9; 13; 14; 15; 19; 20; 21
	$[2]P\,\bar{3}\,1c$	1; 2; 3; 10; 11; 12; 13; 14; 15; 22; 23; 24
	$[2]P\,\bar{6}m\,2$	1; 2; 3; 10; 11; 12; 16; 17; 18; 19; 20; 21
	$[2]P\,\bar{6}\,2c$	1; 2; 3; 7; 8; 9; 16; 17; 18; 22; 23; 24
	$[3]P\,m\,m\,c\,(C\,m\,c\,m)$	1; 4; 7; 10; 13; 16; 19; 22
	$[3]P\,m\,m\,c\,(C\,m\,c\,m)$	1; 4; 8; 11; 13; 16; 20; 23
	$[3]P\,m\,m\,c\,(C\,m\,c\,m)$	1; 4; 9; 12; 13; 16; 21; 24

IIa none

IIb $[3]H\,6_3/m\,m\,c\,(a'=3a,\,b'=3b)(P\,6_3/m\,c\,m)$

Maximal isomorphic subgroups of lowest index

IIc $[3]P\,6_3/m\,m\,c\,(c'=3c)$; $[4]P\,6_3/m\,m\,c\,(a'=2a,\,b'=2b)$

Minimal non-isomorphic supergroups

I none

II $[3]H\,6_3/m\,m\,c\,(P\,6_3/m\,c\,m)$; $[2]P\,6/m\,m\,m\,(2c'=c)$

Generators selected (1); $t(1,0,0)$; $t(0,1,0)$; $t(0,0,1)$; (2); (4); (7); (13)

Positions

Multiplicity, Wyckoff letter, Site symmetry			Coordinates	Reflection conditions
				General:
24	l	1	(1) x,y,z (2) $\bar{y},x-y,z$ (3) $\bar{x}+y,\bar{x},z$ (4) $\bar{x},\bar{y},z+\frac{1}{2}$ (5) $y,\bar{x}+y,z+\frac{1}{2}$ (6) $x-y,x,z+\frac{1}{2}$ (7) $y,x,\bar{z}$ (8) $x-y,\bar{y},\bar{z}$ (9) $\bar{x},\bar{x}+y,\bar{z}$ (10) $\bar{y},\bar{x},\bar{z}+\frac{1}{2}$ (11) $\bar{x}+y,y,\bar{z}+\frac{1}{2}$ (12) $x,x-y,\bar{z}+\frac{1}{2}$ (13) $\bar{x},\bar{y},\bar{z}$ (14) $y,\bar{x}+y,\bar{z}$ (15) $x-y,x,\bar{z}$ (16) $x,y,\bar{z}+\frac{1}{2}$ (17) $\bar{y},x-y,\bar{z}+\frac{1}{2}$ (18) $\bar{x}+y,\bar{x},\bar{z}+\frac{1}{2}$ (19) $\bar{y},\bar{x},z$ (20) $\bar{x}+y,y,z$ (21) $x,x-y,z$ (22) $y,x,z+\frac{1}{2}$ (23) $x-y,\bar{y},z+\frac{1}{2}$ (24) $\bar{x},\bar{x}+y,z+\frac{1}{2}$	$hh2\bar{h}l$: $l=2n$ $000l$: $l=2n$
				Special: as above, plus
12	k	$.m.$	$x,2x,z$ $2\bar{x},\bar{x},z$ $x,\bar{x},z$ $\bar{x},2\bar{x},z+\frac{1}{2}$ $2x,x,z+\frac{1}{2}$ $\bar{x},x,z+\frac{1}{2}$ $2x,x,\bar{z}$ $\bar{x},2\bar{x},\bar{z}$ $\bar{x},x,\bar{z}$ $2\bar{x},\bar{x},\bar{z}+\frac{1}{2}$ $x,2x,\bar{z}+\frac{1}{2}$ $x,\bar{x},\bar{z}+\frac{1}{2}$	no extra conditions
12	j	$m..$	$x,y,\frac{1}{4}$ $\bar{y},x-y,\frac{1}{4}$ $\bar{x}+y,\bar{x},\frac{1}{4}$ $\bar{x},\bar{y},\frac{3}{4}$ $y,\bar{x}+y,\frac{3}{4}$ $x-y,x,\frac{3}{4}$ $y,x,\frac{3}{4}$ $x-y,\bar{y},\frac{3}{4}$ $\bar{x},\bar{x}+y,\frac{3}{4}$ $\bar{y},\bar{x},\frac{1}{4}$ $\bar{x}+y,y,\frac{1}{4}$ $x,x-y,\frac{1}{4}$	no extra conditions
12	i	$.2.$	$x,0,0$ $0,x,0$ $\bar{x},\bar{x},0$ $\bar{x},0,\frac{1}{2}$ $0,\bar{x},\frac{1}{2}$ $x,x,\frac{1}{2}$ $\bar{x},0,0$ $0,\bar{x},0$ $x,x,0$ $x,0,\frac{1}{2}$ $0,x,\frac{1}{2}$ $\bar{x},\bar{x},\frac{1}{2}$	$hkil$: $l=2n$
6	h	$mm2$	$x,2x,\frac{1}{4}$ $2\bar{x},\bar{x},\frac{1}{4}$ $x,\bar{x},\frac{1}{4}$ $\bar{x},2\bar{x},\frac{3}{4}$ $2x,x,\frac{3}{4}$ $\bar{x},x,\frac{3}{4}$	no extra conditions
6	g	$.2/m.$	$\frac{1}{2},0,0$ $0,\frac{1}{2},0$ $\frac{1}{2},\frac{1}{2},0$ $\frac{1}{2},0,\frac{1}{2}$ $0,\frac{1}{2},\frac{1}{2}$ $\frac{1}{2},\frac{1}{2},\frac{1}{2}$	$hkil$: $l=2n$
4	f	$3m.$	$\frac{1}{3},\frac{2}{3},z$ $\frac{2}{3},\frac{1}{3},z+\frac{1}{2}$ $\frac{2}{3},\frac{1}{3},\bar{z}$ $\frac{1}{3},\frac{2}{3},\bar{z}+\frac{1}{2}$	$hkil$: $l=2n$ or $h-k=3n+1$ or $h-k=3n+2$
4	e	$3m.$	$0,0,z$ $0,0,z+\frac{1}{2}$ $0,0,\bar{z}$ $0,0,\bar{z}+\frac{1}{2}$	$hkil$: $l=2n$
2	d	$\bar{6}m2$	$\frac{1}{3},\frac{2}{3},\frac{3}{4}$ $\frac{2}{3},\frac{1}{3},\frac{1}{4}$	$hkil$: $l=2n$ or $h-k=3n+1$ or $h-k=3n+2$
2	c	$\bar{6}m2$	$\frac{1}{3},\frac{2}{3},\frac{1}{4}$ $\frac{2}{3},\frac{1}{3},\frac{3}{4}$	
2	b	$\bar{6}m2$	$0,0,\frac{1}{4}$ $0,0,\frac{3}{4}$	$hkil$: $l=2n$
2	a	$\bar{3}m.$	$0,0,0$ $0,0,\frac{1}{2}$	$hkil$: $l=2n$

Symmetry of special projections

Along [001] $p6mm$	Along [100] $p2gm$	Along [210] $p2mm$
$a'=a$ $b'=b$	$a'=\frac{1}{2}(a+2b)$ $b'=c$	$a'=\frac{1}{2}b$ $b'=\frac{1}{2}c$
Origin at $0,0,z$	Origin at $x,0,0$	Origin at $x,\frac{1}{2}x,0$

(*Continued on preceding page*)

Crystal Structure of YAM

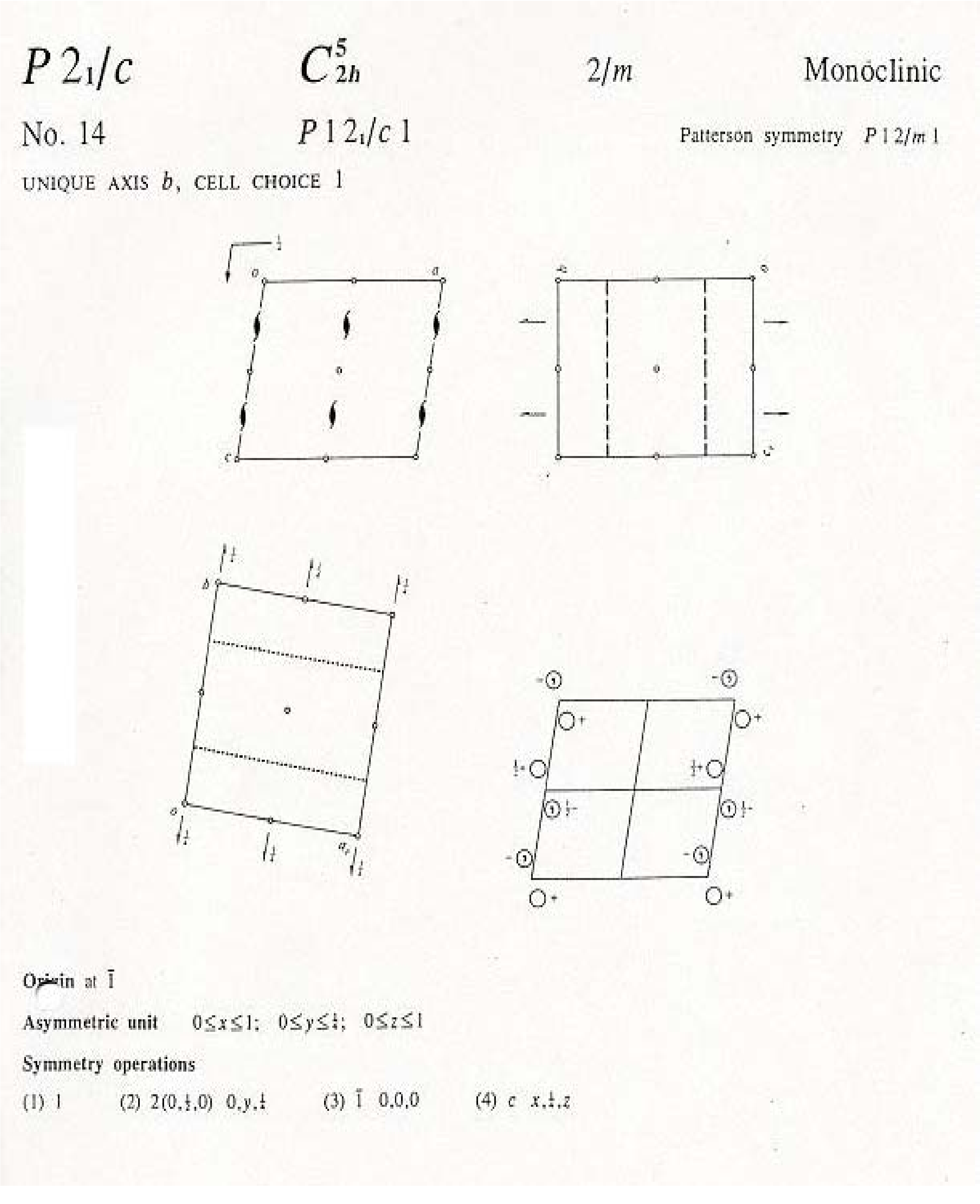

$P2_1/c$ C_{2h}^5 $2/m$ Monoclinic

No. 14 $P12_1/c1$ Patterson symmetry $P12/m1$

UNIQUE AXIS b, CELL CHOICE 1

Origin at $\bar{1}$

Asymmetric unit $0 \leq x \leq 1$; $0 \leq y \leq \frac{1}{4}$; $0 \leq z \leq 1$

Symmetry operations

(1) 1 (2) $2(0,\frac{1}{2},0)$ $0,y,\frac{1}{4}$ (3) $\bar{1}$ $0,0,0$ (4) c $x,\frac{1}{4},z$

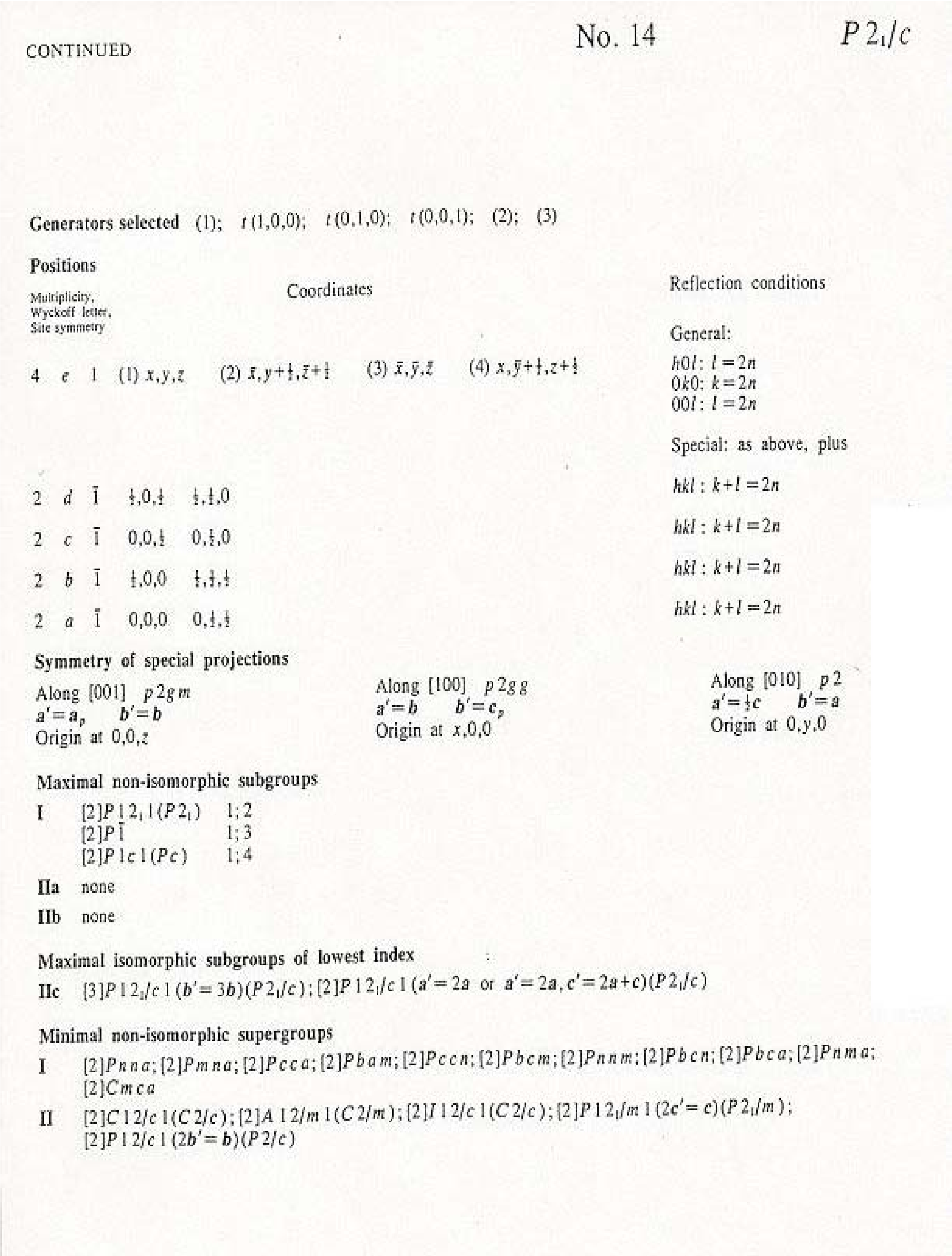

Generators selected (1); $t(1,0,0)$; $t(0,1,0)$; $t(0,0,1)$; (2); (3)

Positions

Multiplicity, Wyckoff letter, Site symmetry			Coordinates				Reflection conditions
							General:
4	e	1	(1) x,y,z	(2) $\bar{x},y+\frac{1}{2},\bar{z}+\frac{1}{2}$	(3) $\bar{x},\bar{y},\bar{z}$	(4) $x,\bar{y}+\frac{1}{2},z+\frac{1}{2}$	$h0l$: $l=2n$ $0k0$: $k=2n$ $00l$: $l=2n$
							Special: as above, plus
2	d	$\bar{1}$	$\frac{1}{2},0,\frac{1}{2}$	$\frac{1}{2},\frac{1}{2},0$			hkl : $k+l=2n$
2	c	$\bar{1}$	$0,0,\frac{1}{2}$	$0,\frac{1}{2},0$			hkl : $k+l=2n$
2	b	$\bar{1}$	$\frac{1}{2},0,0$	$\frac{1}{2},\frac{1}{2},\frac{1}{2}$			hkl : $k+l=2n$
2	a	$\bar{1}$	$0,0,0$	$0,\frac{1}{2},\frac{1}{2}$			hkl : $k+l=2n$

Symmetry of special projections

Along [001] $p2gm$
$a'=a_p$ $b'=b$
Origin at $0,0,z$

Along [100] $p2gg$
$a'=b$ $b'=c_p$
Origin at $x,0,0$

Along [010] $p2$
$a'=\frac{1}{2}c$ $b'=a$
Origin at $0,y,0$

Maximal non-isomorphic subgroups

I	$[2]P\,1\,2_1\,1\,(P2_1)$	1; 2
	$[2]P\bar{1}$	1; 3
	$[2]P\,1\,c\,1\,(Pc)$	1; 4
IIa	none	
IIb	none	

Maximal isomorphic subgroups of lowest index

IIc $[3]P\,1\,2_1/c\,1\,(b'=3b)(P2_1/c)$; $[2]P\,1\,2_1/c\,1\,(a'=2a$ or $a'=2a, c'=2a+c)(P2_1/c)$

Minimal non-isomorphic supergroups

I $[2]Pnna$; $[2]Pmna$; $[2]Pcca$; $[2]Pbam$; $[2]Pccn$; $[2]Pbcm$; $[2]Pnnm$; $[2]Pbcn$; $[2]Pbca$; $[2]Pnma$; $[2]Cmca$

II $[2]C\,1\,2/c\,1\,(C2/c)$; $[2]A\,1\,2/m\,1\,(C2/m)$; $[2]I\,1\,2/c\,1\,(C2/c)$; $[2]P\,1\,2_1/m\,1\,(2c'=c)(P2_1/m)$; $[2]P\,1\,2/c\,1\,(2b'=b)(P2/c)$

APPENDIX B

SEM Images and EDS Analysis Taken from 7% Si Doped Sample

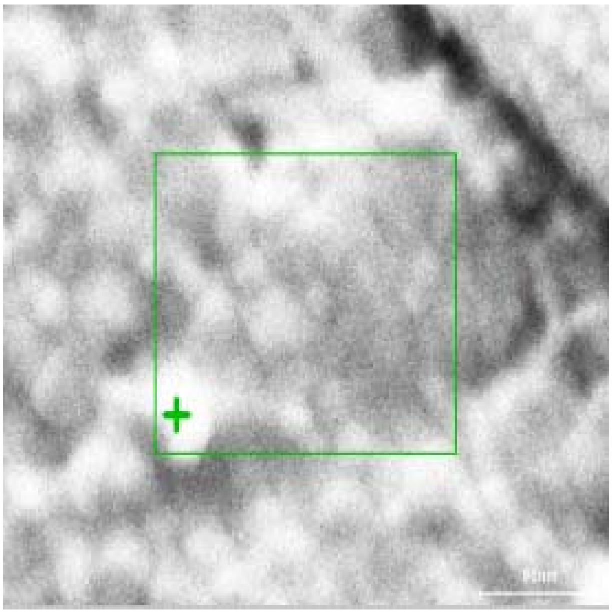

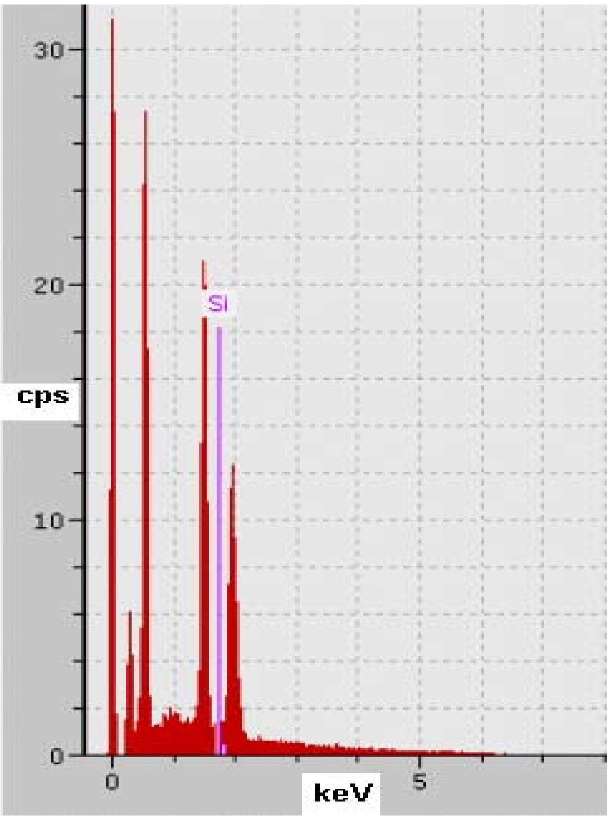

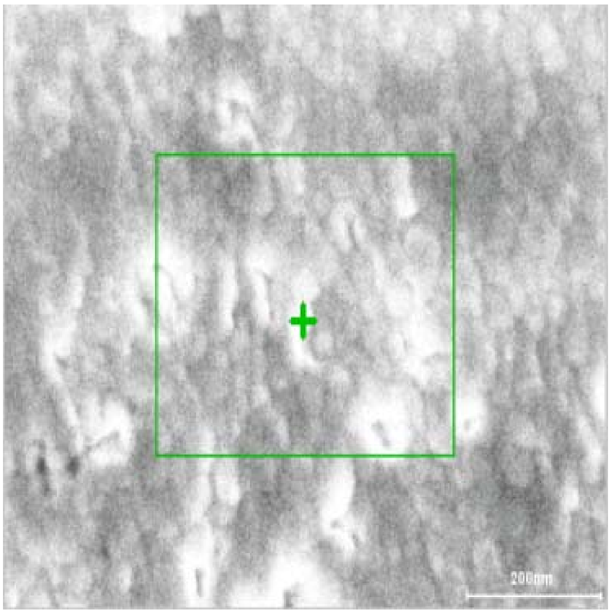
200nm

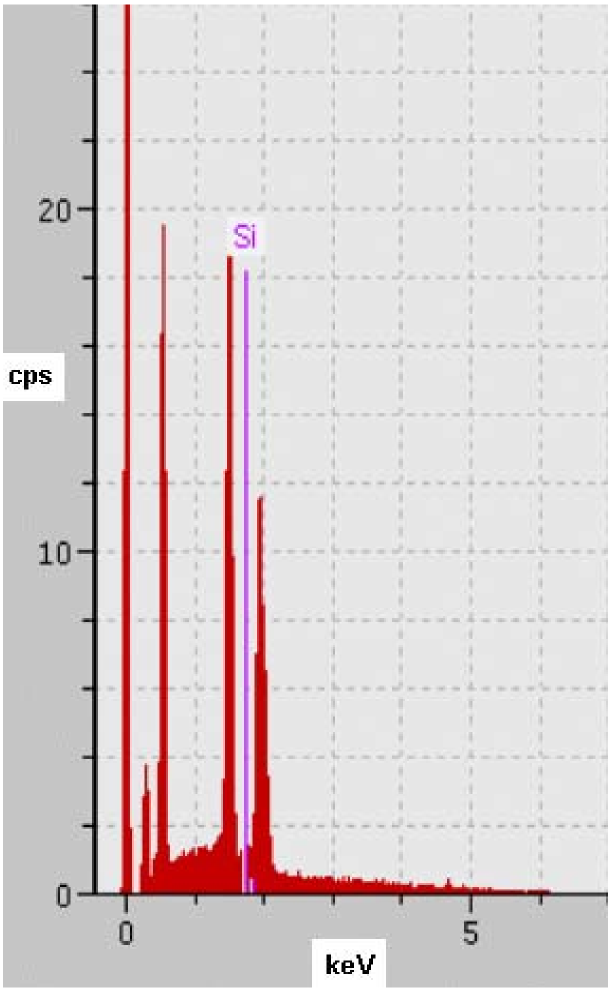
cps
20
10
0
Si
0
5
keV

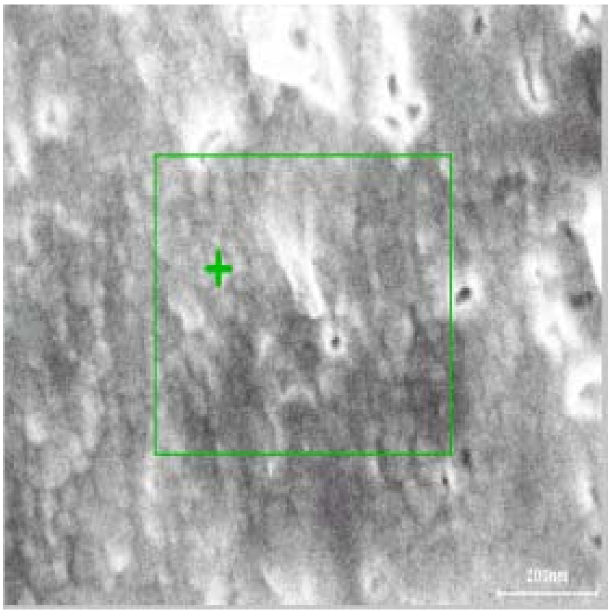
200nm

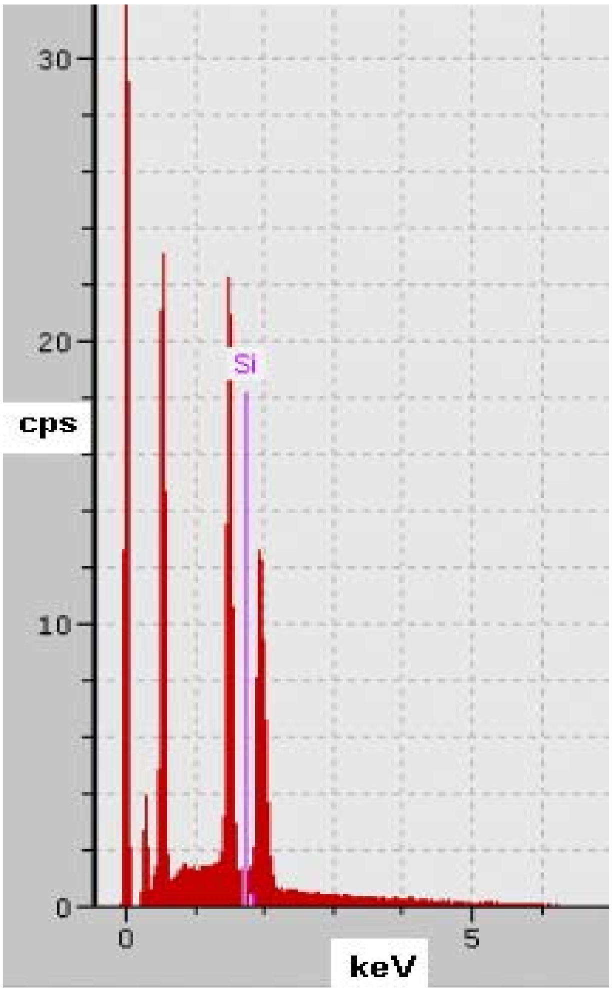
30
20
10
0
cps
Si
0
5
keV

SEM Images and EDS Analysis Taken from 10% Ca Doped Sample

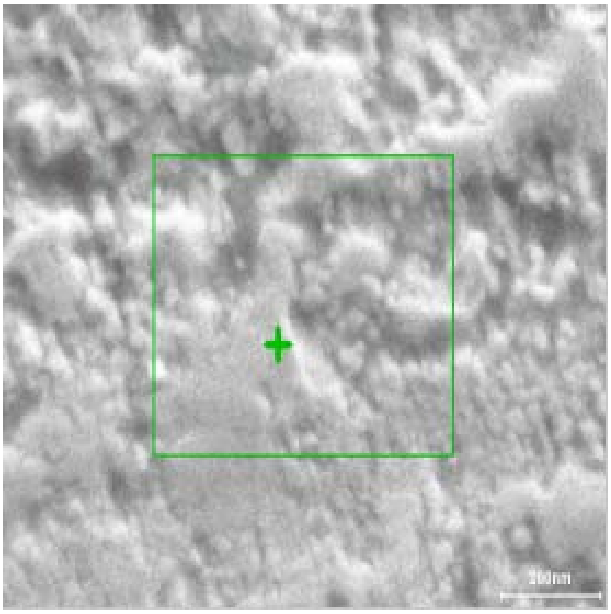

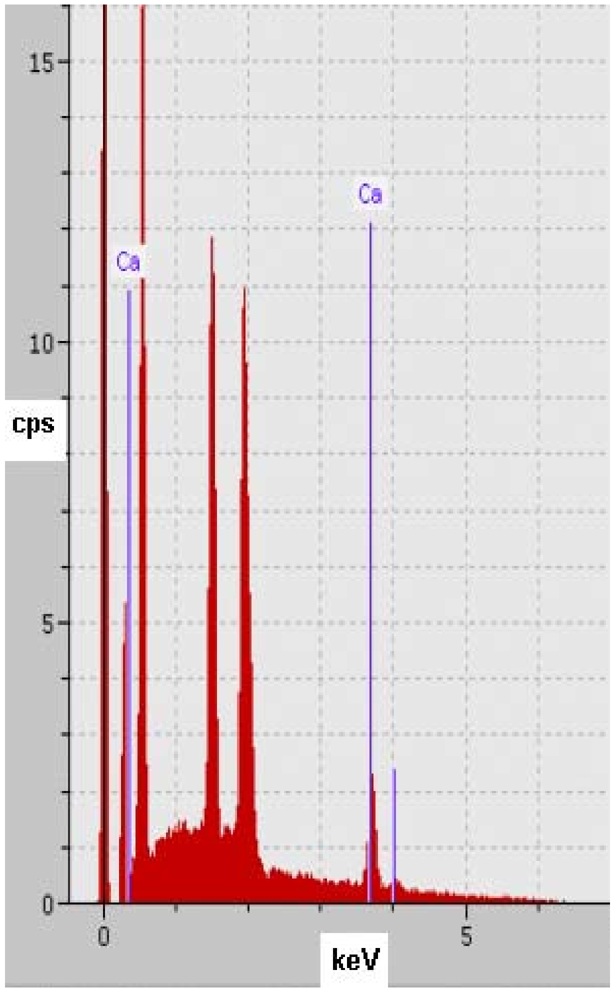

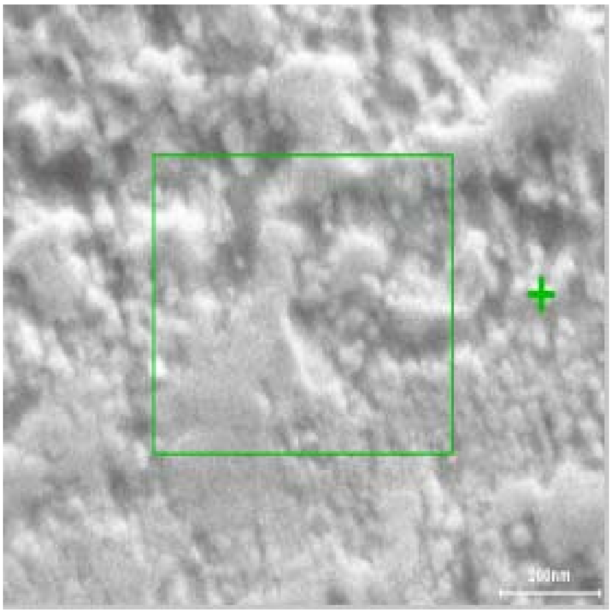
200nm

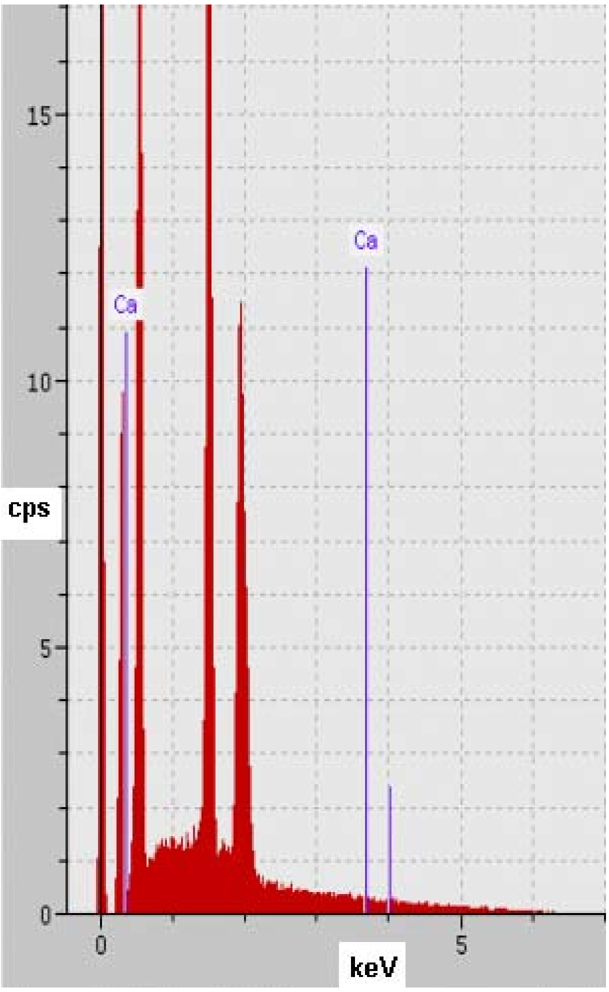
15
10
5
0
cps
Ca
Ca
0
5
keV

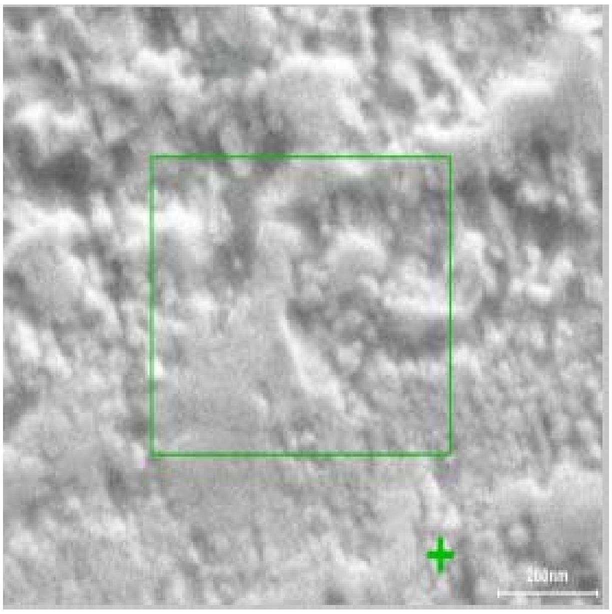

200nm

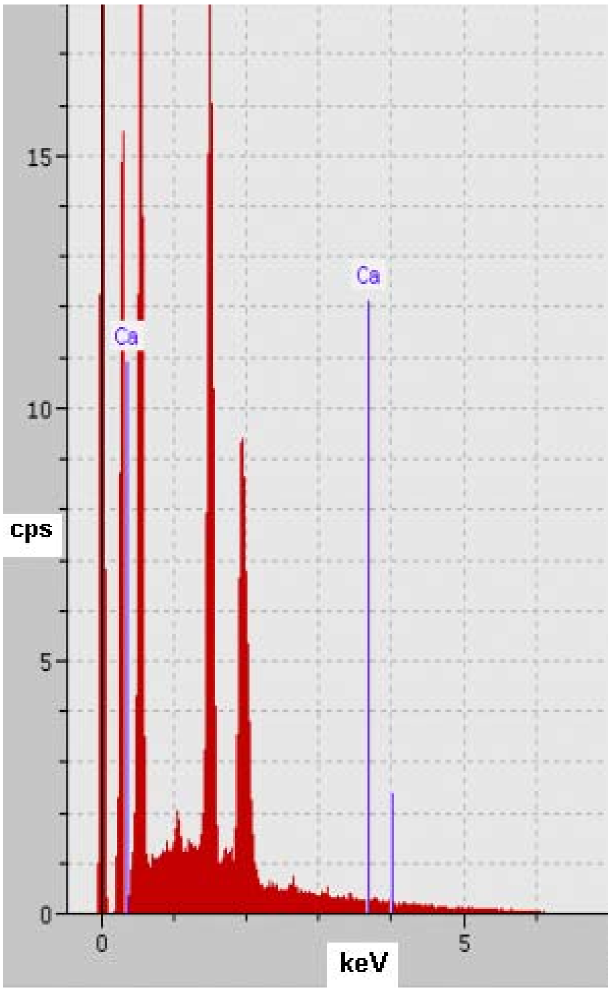

cps
15
10
5
0
Ca
Ca
0
5
keV

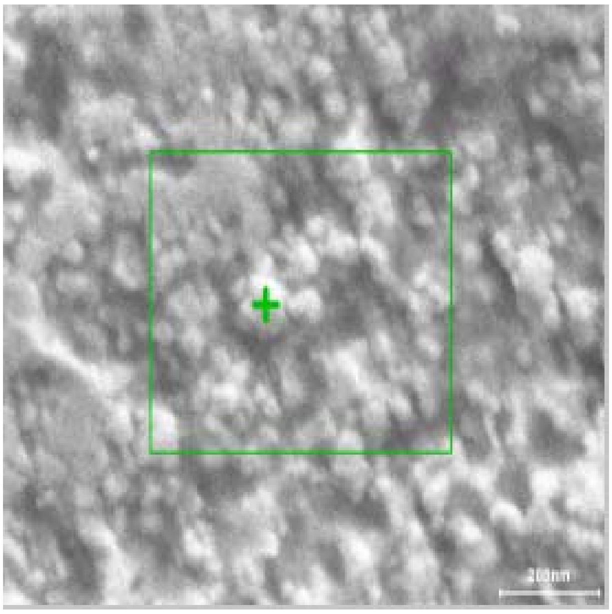
200nm

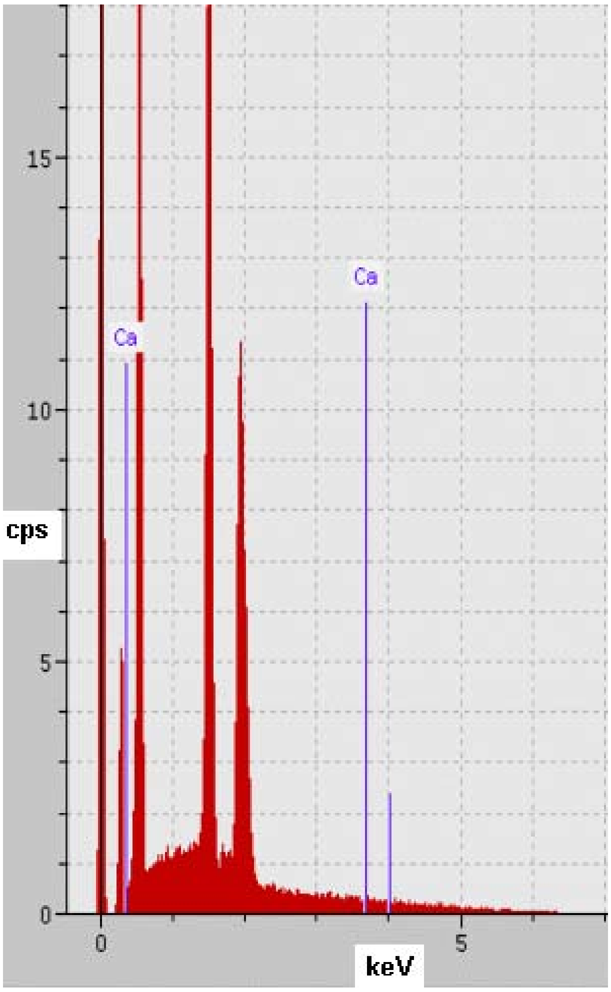
Ca
Ca
cps
keV
0
5
10
15
0
5

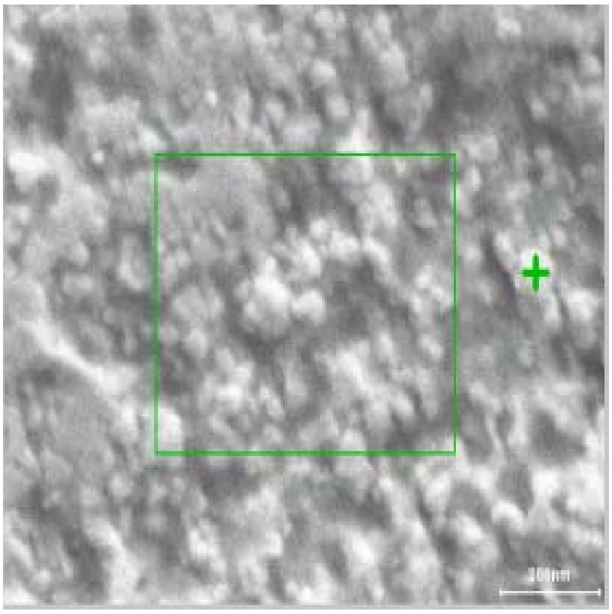
300nm

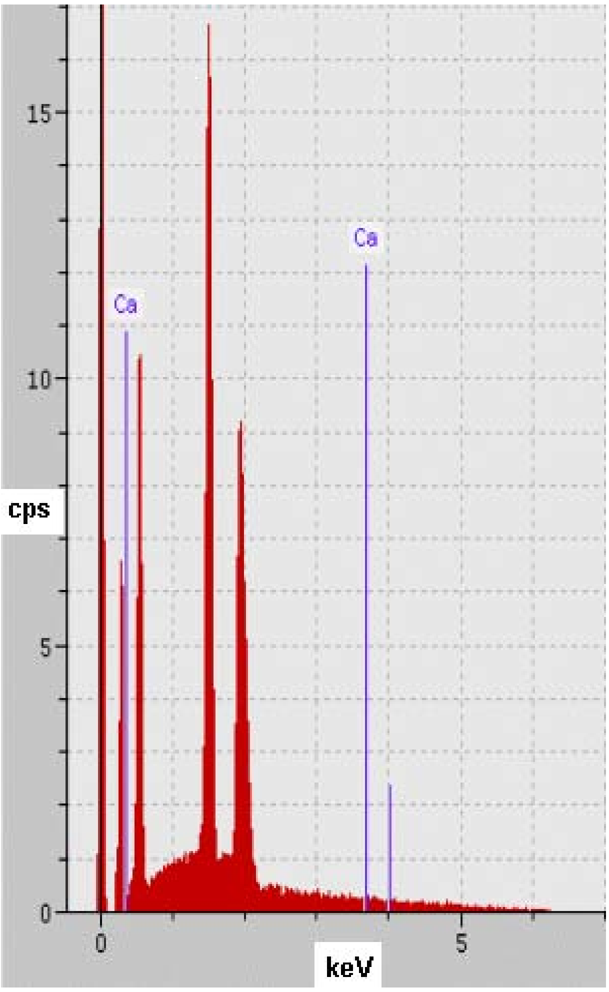
cps
15
10
5
0
Ca
Ca
0
5
keV

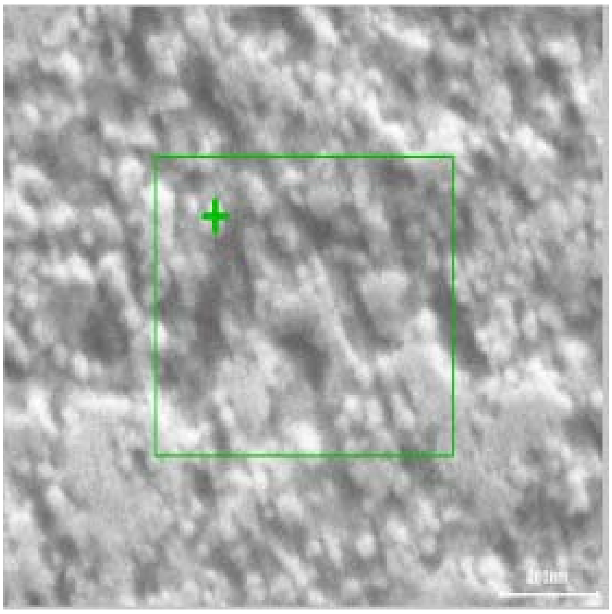

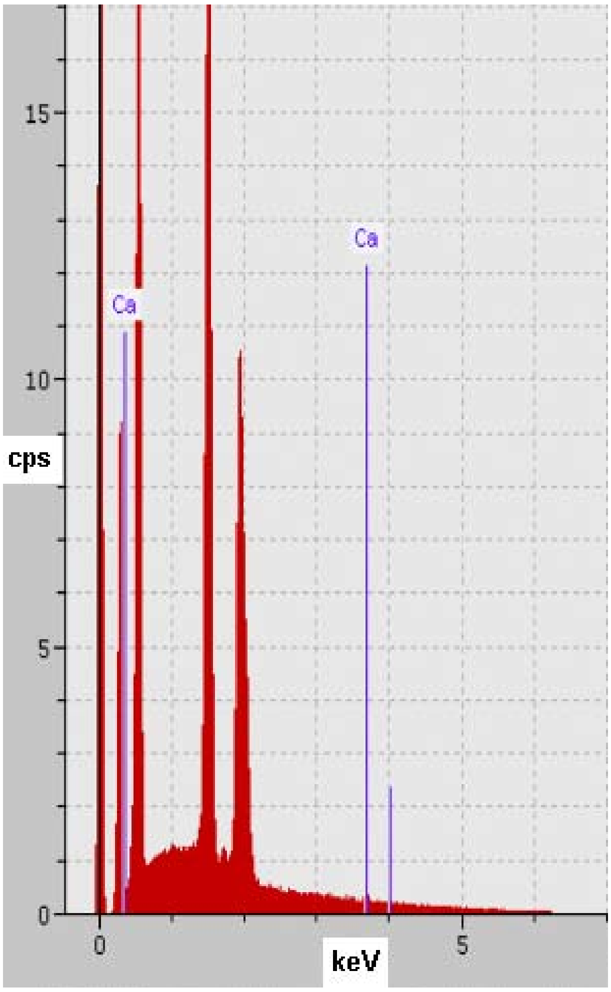

cps
15
10
5
0
Ca
Ca
0
5
keV

SEM Images and EDS Analysis Taken from 15% Ca+Si Doped Sample

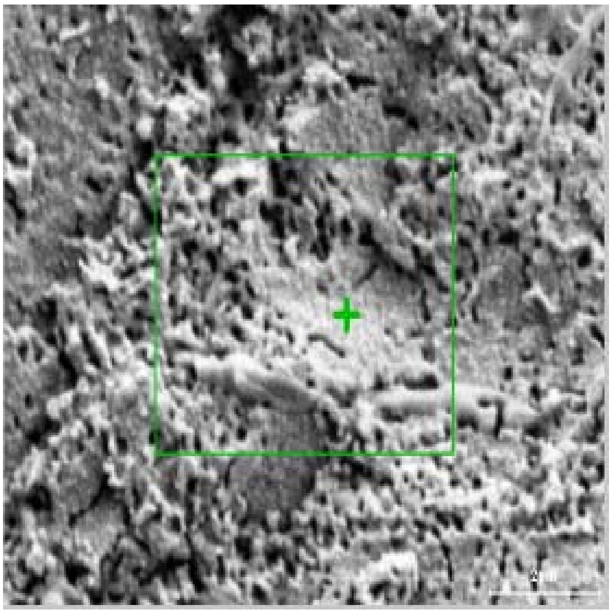

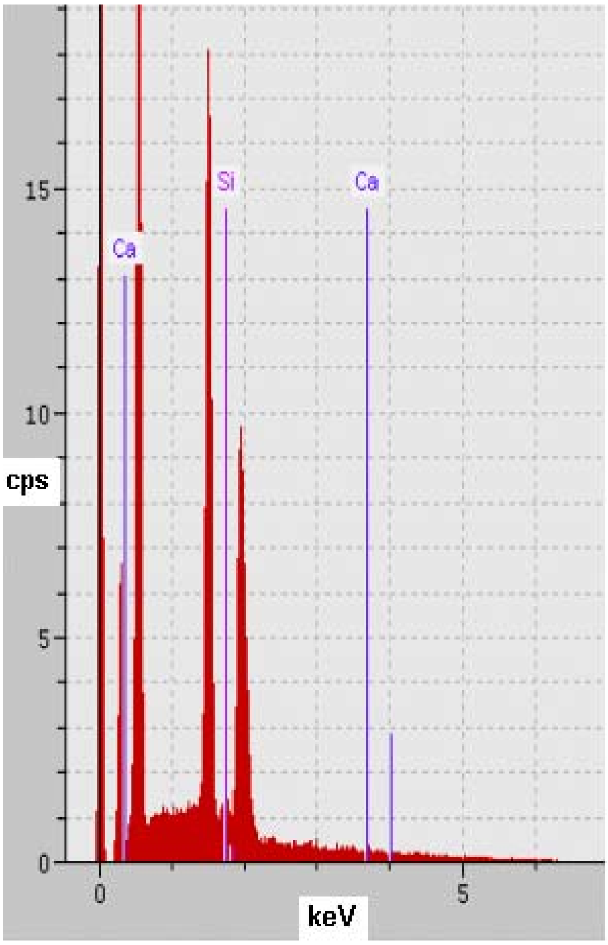

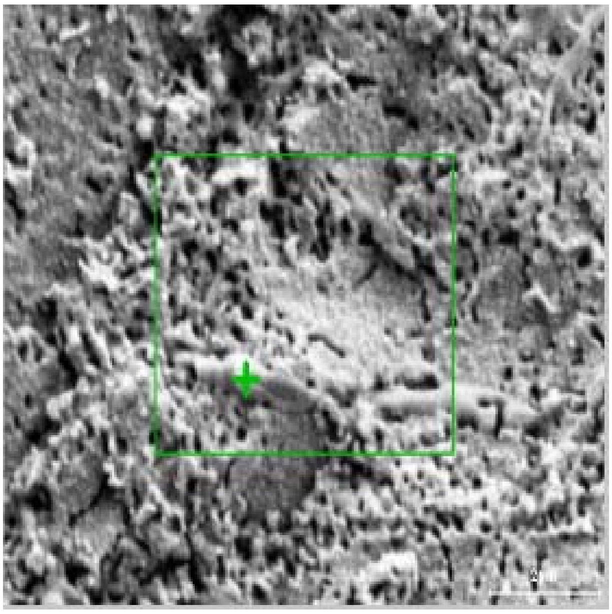

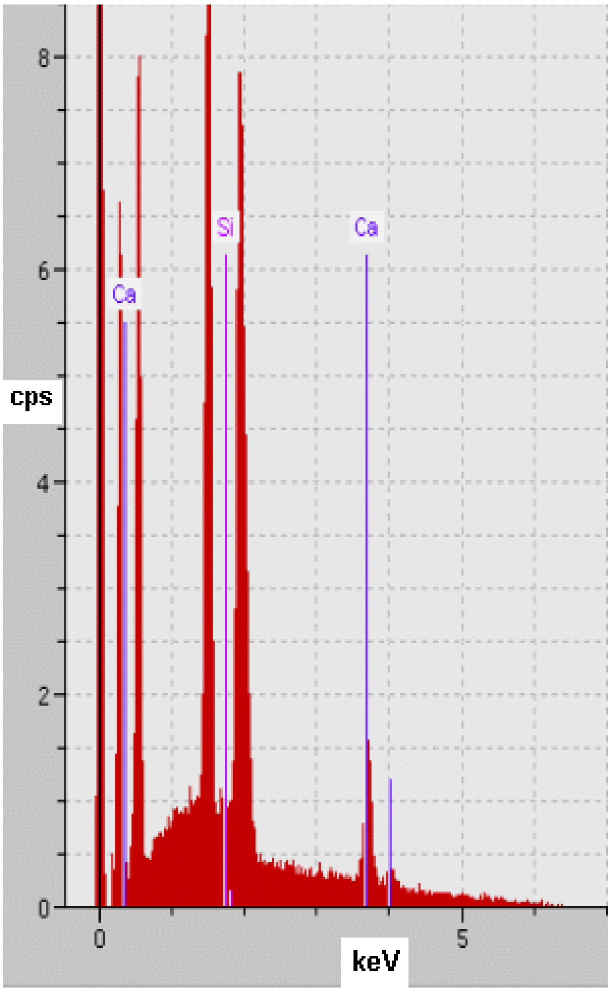
8
6
4
2
0
cps
Ca
Si
Ca
0
5
keV

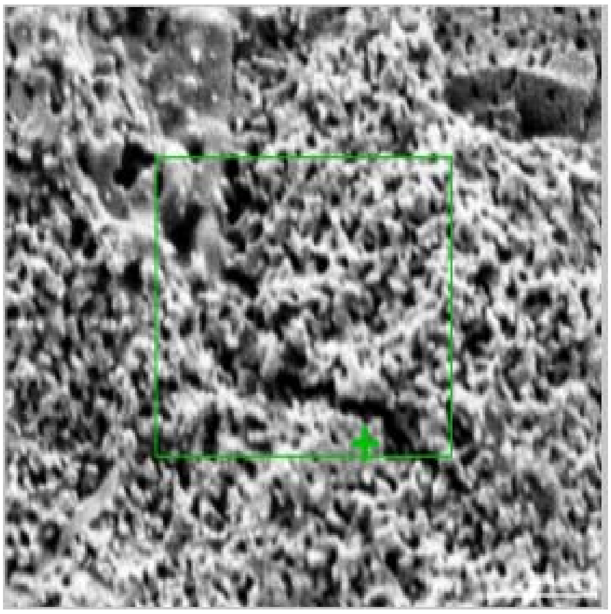

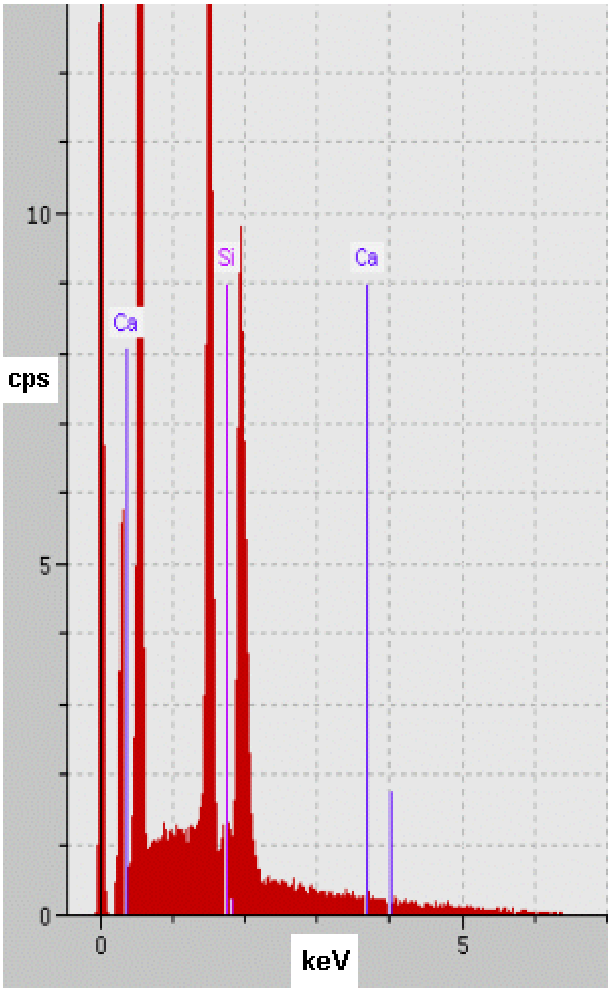
10
5
0
cps
Ca
Si
Ca
0
5
keV

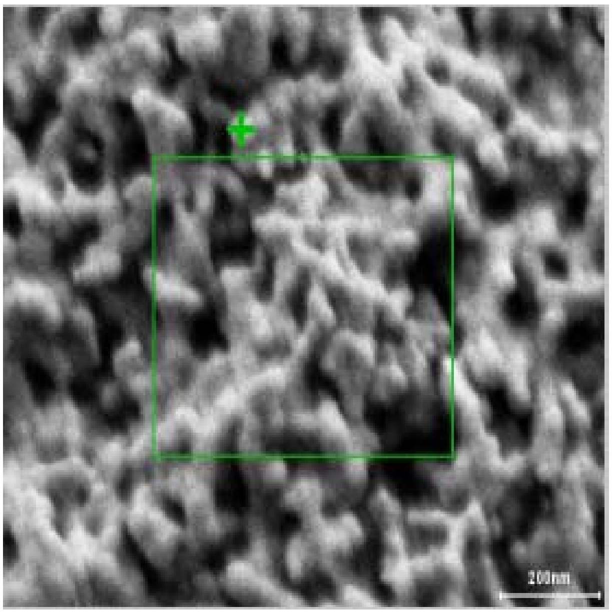
200nm

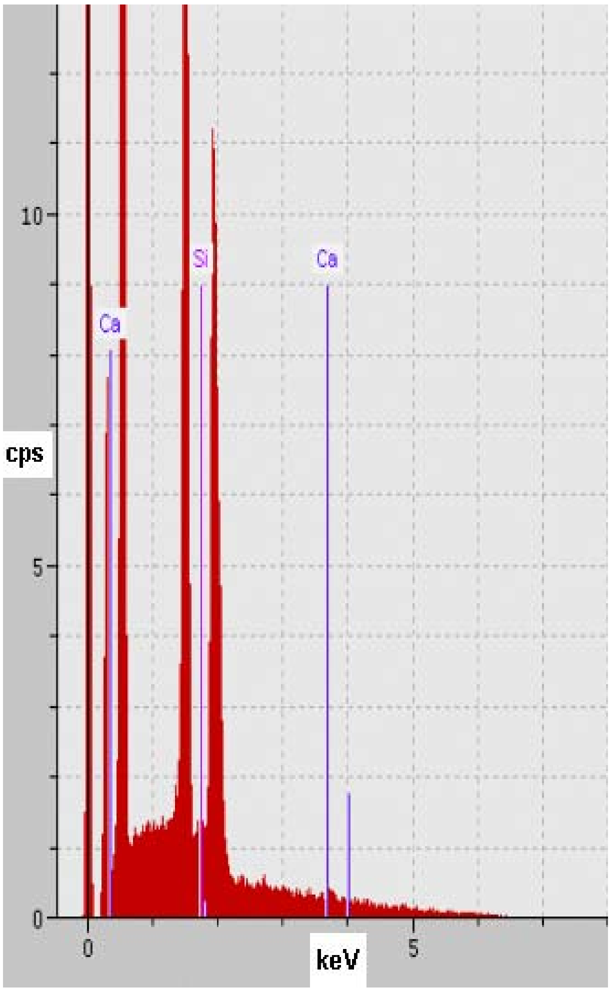
cps
10
5
0
Ca
Si
Ca
0
5
keV

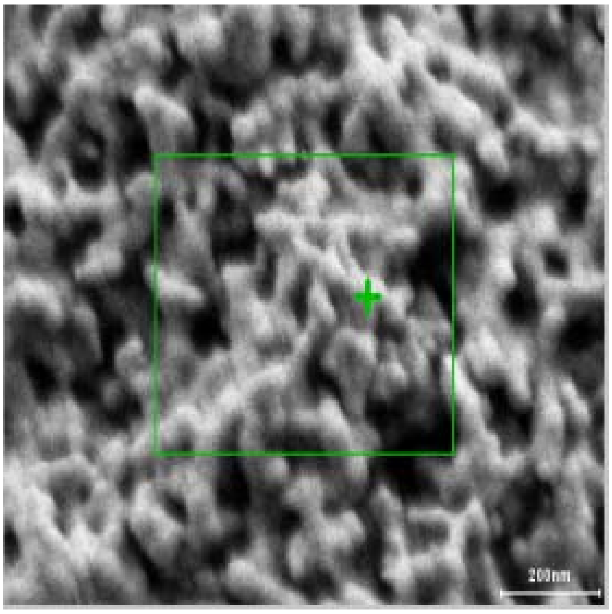
200nm

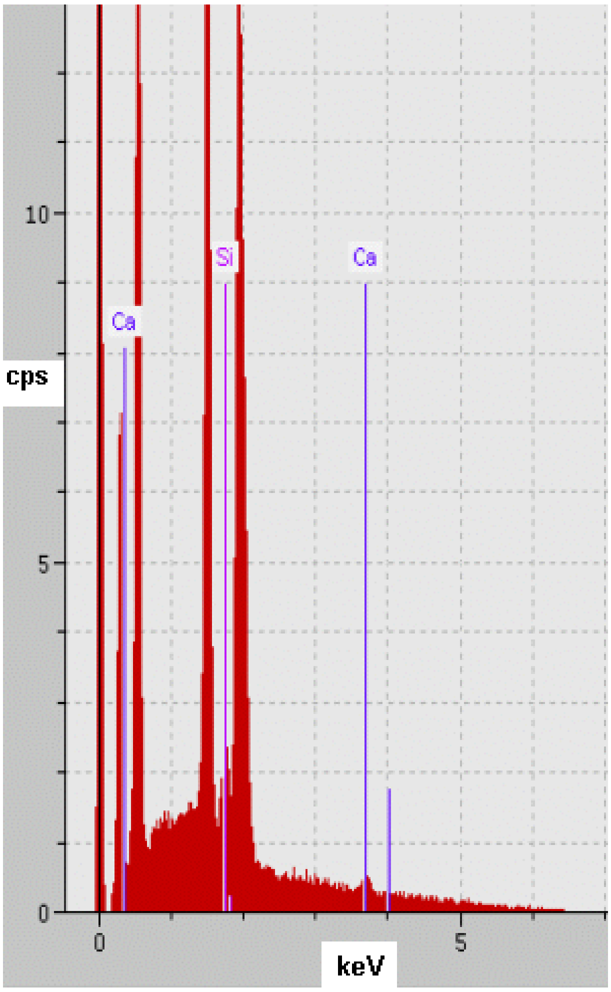
cps
10
5
0
Ca
Si
Ca
0
5
keV

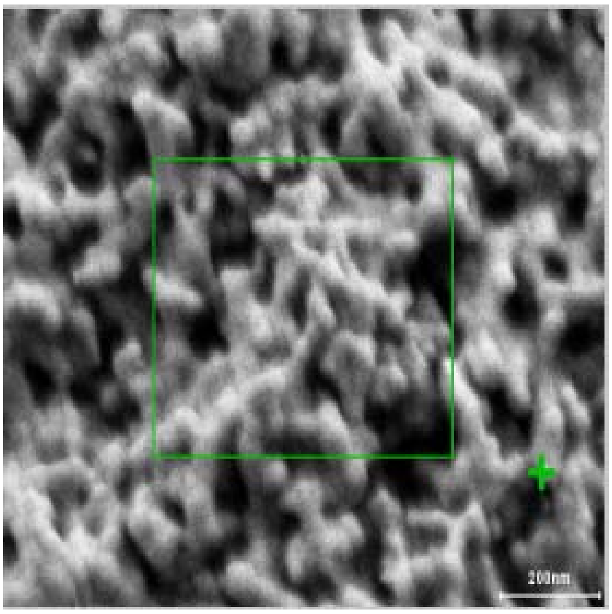
200nm

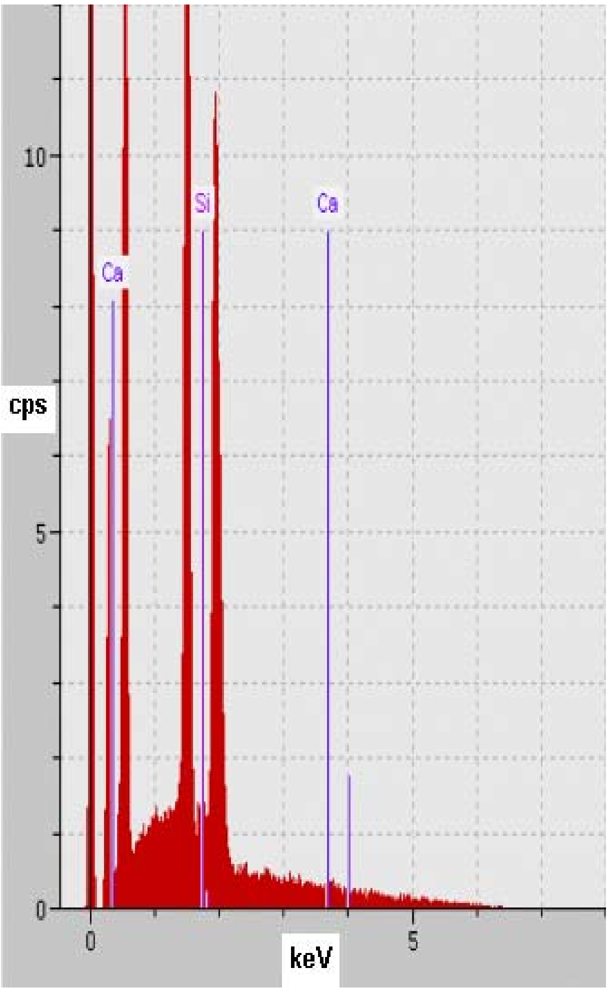
10
5
0
cps
Ca
Si
Ca
0
5
keV

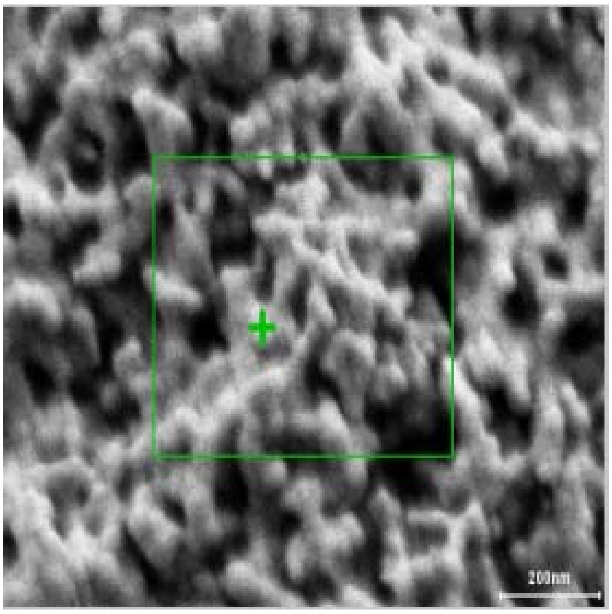
200nm

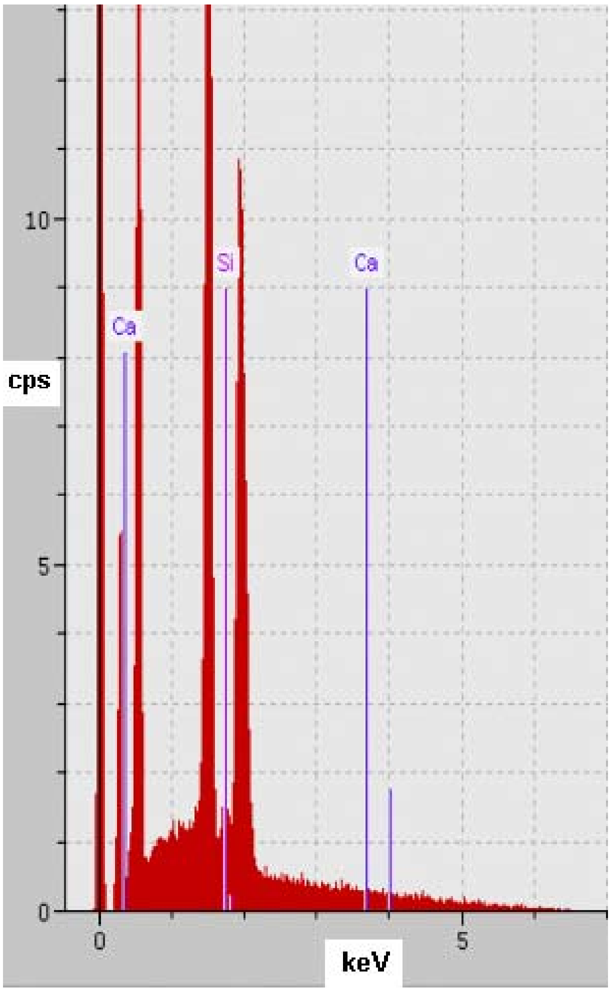
10
5
0
cps
Ca
Si
Ca
0
5
keV

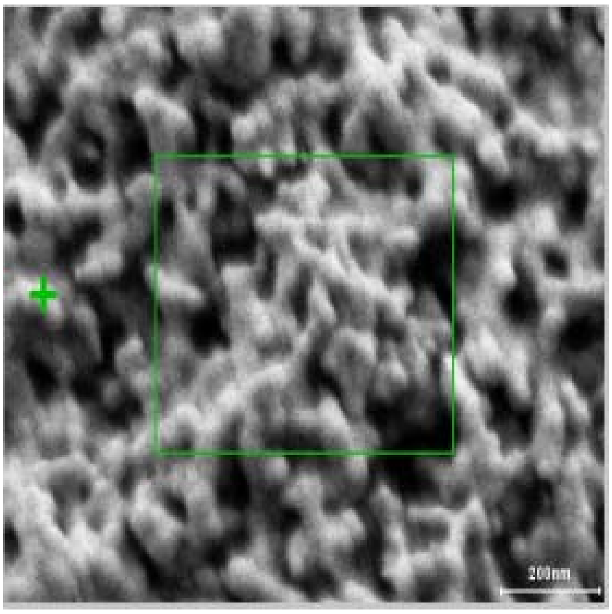
200nm

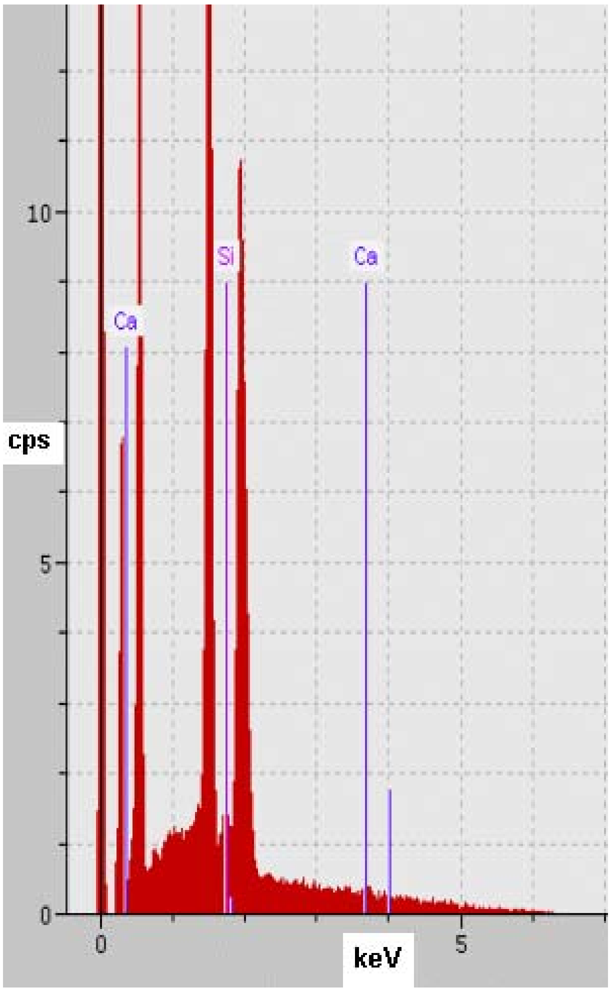
10
5
0
cps
Ca
Si
Ca
0
5
keV

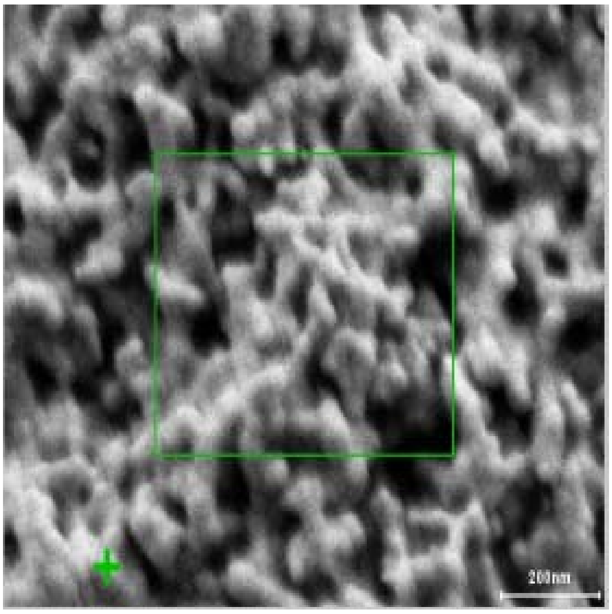
200nm

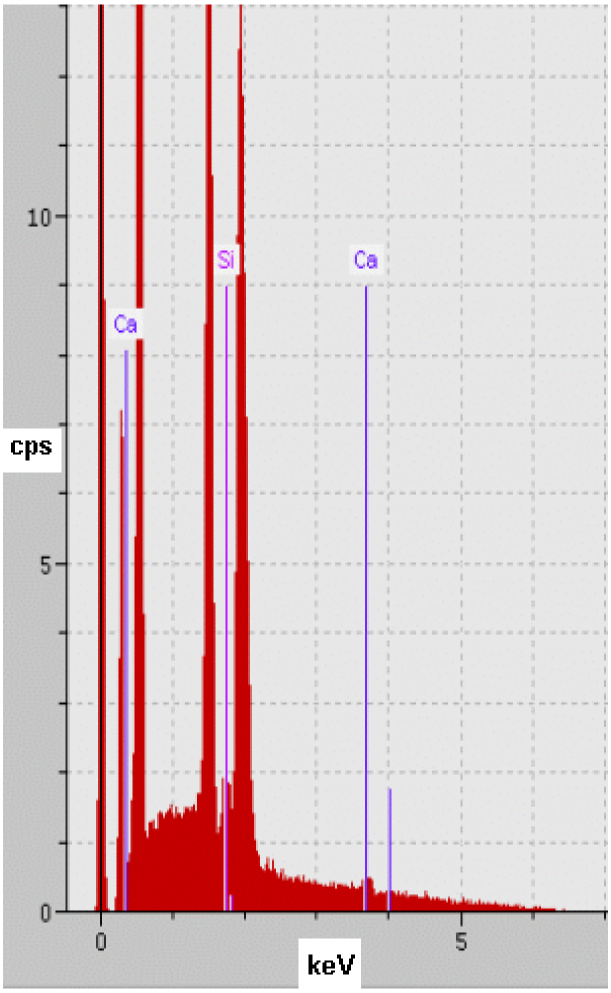
cps
10
5
0
Ca
Si
Ca
0
5
keV

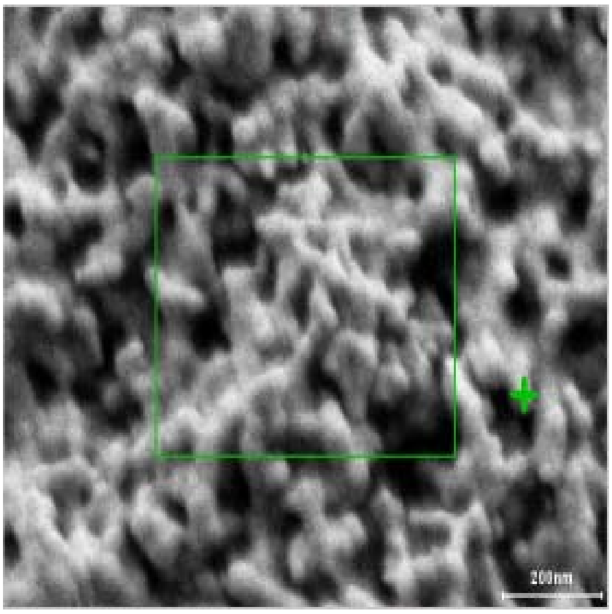
200nm

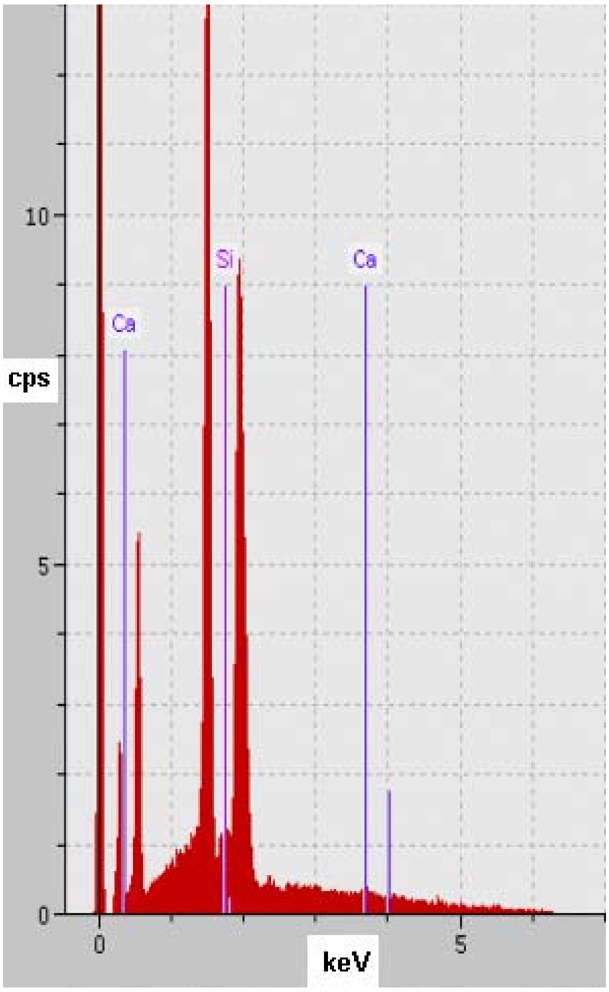
cps
10
5
0
Ca
Si
Ca
0
5
keV

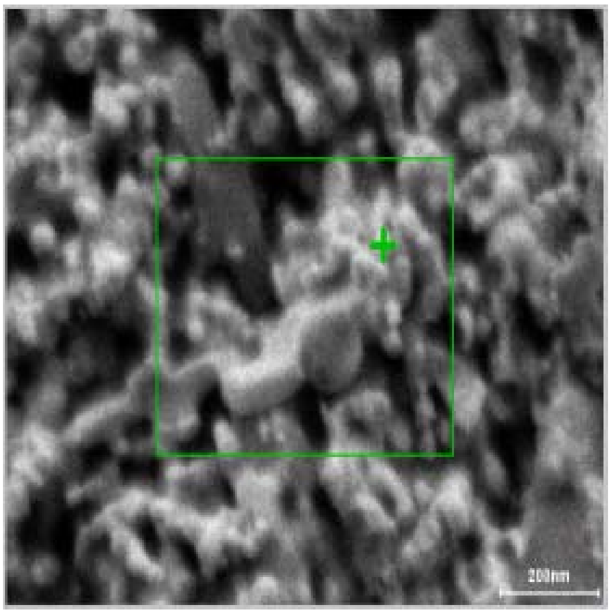
200nm

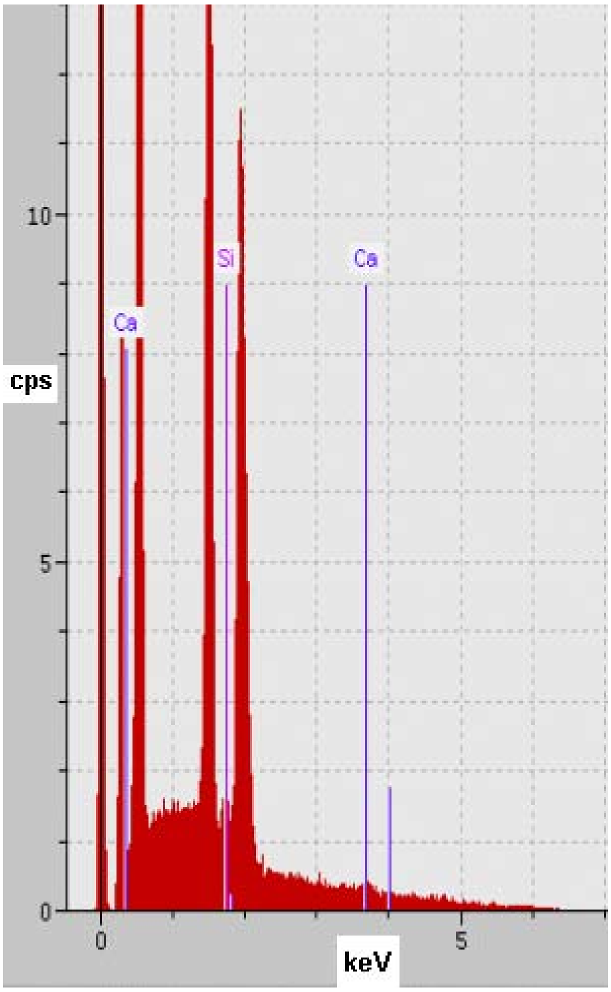
cps
10
5
0
Ca
Si
Ca
0
5
keV

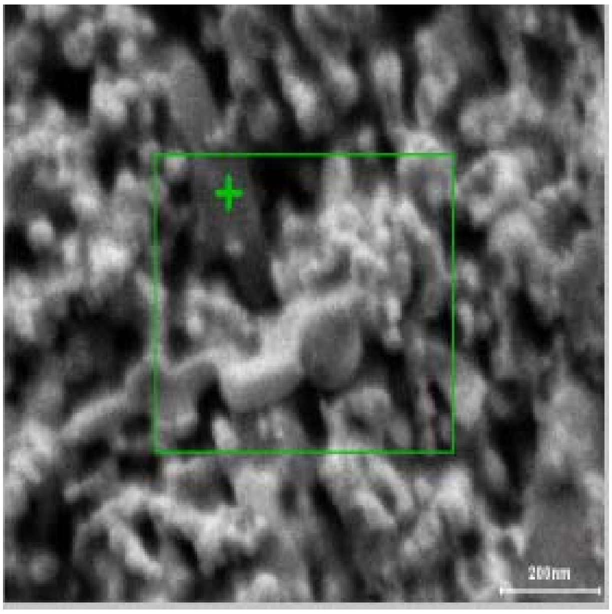
200nm

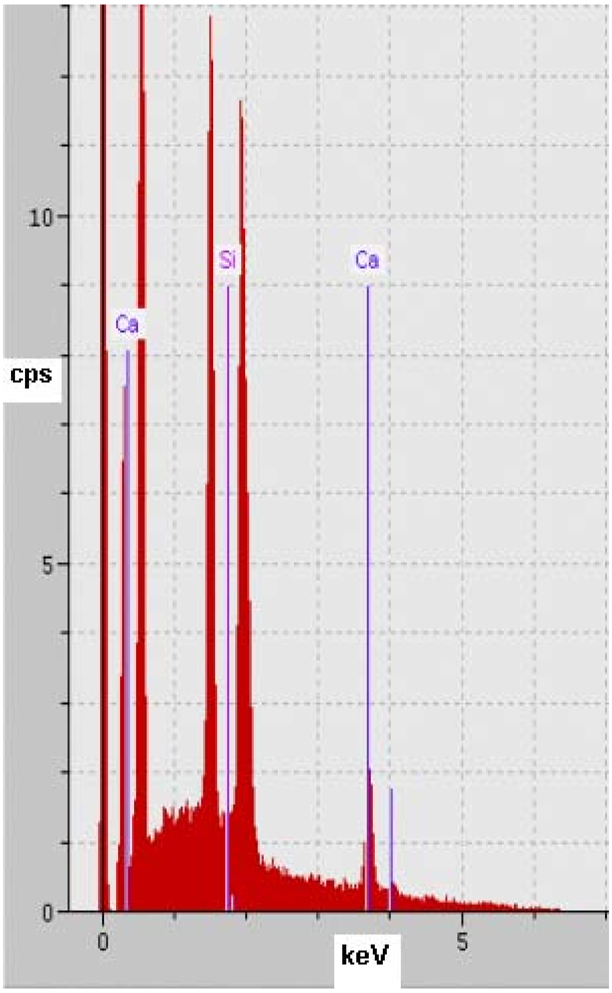
10
5
0
cps
Ca
Si
Ca
0
5
keV

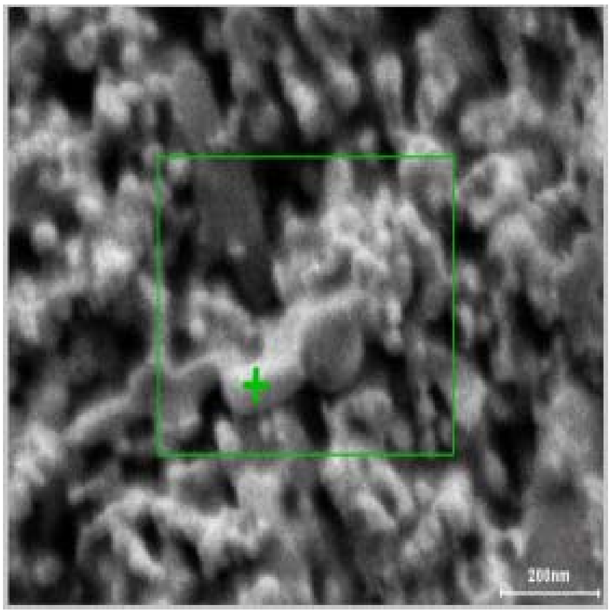
200nm

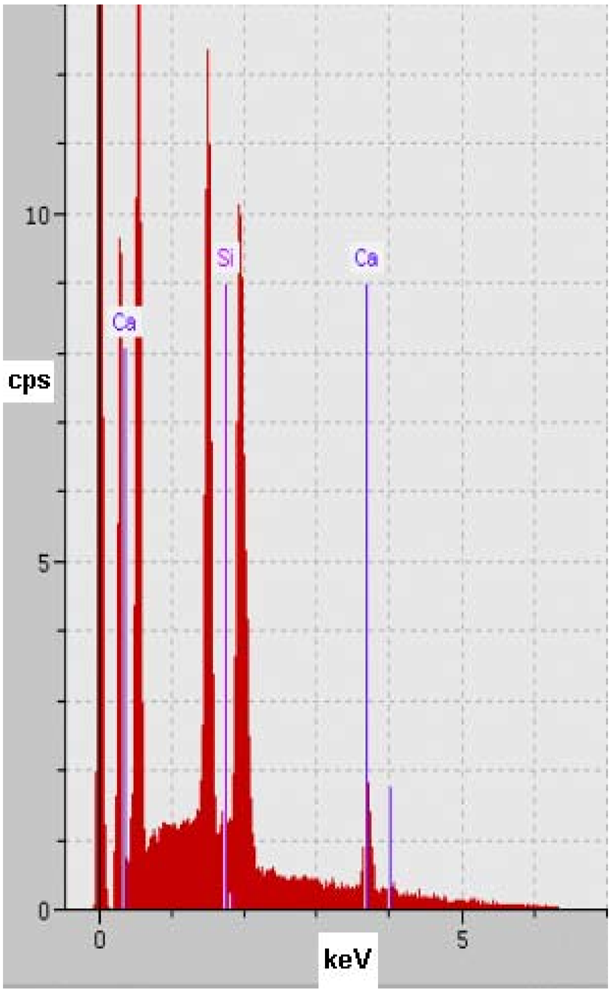
cps
10
5
0
Ca
Si
Ca
0
5
keV

7 REFERENCES

1. J. K. R. Weber, B. Cho, A. D. Hixson, J. G. Abadie, P. C. Nordine, W. M. Kriven, B. R. Johnson and D. Zhu, Growth and Crystallization of YAG- and Mullite-composition Glass Fibers, Journal of the European Ceramic Society **19** (1999) 2543-2550.

2. http://www.td.anl.gov/Programs/ti/lal/

3. X. Xu, Z. Zhao, P. Song, J. Xu and P. Deng, Growth of High-quality Single Crystal of 50 at.% Yb:YAG and Its Spectral Properties, Journal of Alloys and Compounds **364** (2004) 311-314.

4. L. Gao, H. Wang, H. Kawaoka, T. Sekino and K. Niihara, Fabrication of YAG-SiC Nanocomposites by Spark Plasma Sintering, Journal of the European Ceramic Society **22** (2002) 785-789.

5. T.A. Parthasarathy, T. Mah and K. Keller, Creep Mechanism of Polycrystalline Yttrium Aluminum Garnet, Journal of the American Ceramic Society **75** (1992) 1756-1759.

6. K. Keller, T. Mah and T.A. Parthasarathy, Processing and Mechanical Properties of Polycrystalline $Y_3Al_5O_{12}$, Ceramic Engineering and Science Proceeding **12** (1990) 1122-1133.

7. A. Ikesue, I. Furusato and K. Kamata, Fabrication of Polycrystalline, Transparent YAG Ceramics by a Solid-State Reaction Method, Journal of the American Ceramic Society **78** [1] (1995) 225-228.

8. Q. Zhang and F. Saito, Mechanochemical Solid Reaction of Yttrium Oxide Alumina Leading to the Synthesis of Yttrium Aluminum Garnet, Powder Technology **129** (2003) 86-91.

9. S.M. Sim, K.A. Keller and T.I. Mah, Phase Formation in Yttrium Aluminum Garnet Powders Synthesized by Chemical Methods, Journal of Materials Science **35** (2000) 713-717.

10. A. Ikesue, T. Kinoshita, K. Kamata and Y. Yoshida, Fabrication and Optical-Properties of High-Performance Polycrystalline Nd-YAG Ceramics for Solid State Lasers, Journal of the American Ceramic Society **78** (1995) 1033-1040.

11. G.S. Corman, High-temperature Creep of Some Single Crystal Oxides, Ceramic Engineering and Science Proceeding **12** (1991) 1745-1766.

12. T.A. Parthasarathy, T. Mah and K. Keller, High-Temperature Deformation Behaviour of Polycrystalline Yttrium Aluminum Garnet (YAG), Ceramic Engineering and Science Proceeding **12** (1991) 1767-1773.

13. D.R. Messier and G.E. Gazza, Synthesis of $MgAl_2O_4$ and $Y_3Al_5O_{12}$ by Thermal Decomposition of Hydrated Nitrate Mixtures, American Ceramic Society Bulletin **51** (1972) 692-694.

14. L. Wen, X. Sun, Z. Xiu, S. Chen and C. Tsai, Synthesis of Nanocrystalline Yttria Powder and Fabrication of Transparent YAG Ceramics, Journal of the European Ceramic Society **24** (2004) 2681-2688.

15. Y. Hakuta, T. Haganuma, K. Sue, T. Adschiri and K. Arai, Continuous Production of Phosphor YAG:Tb Nanoparticles by Hydrothermal Synthesis in Supercritical Water, Materials Research Bulletin **38** [7] (2003) 1257-1265.

16. Y. Hakuta, K. Seino, H. Ura, T. Adschiri, H. Takizawa and K. Arai, Production of Phosphor (YAG:Tb) Fine Particles by Hydrothermal Synthesis in Supercritical Water, Journal of Materials Chemistry **9** (1999) 2671-2674.

17. T. Takamori and L.D. David, Controlled Nucleation for Hydrothermal Growth of Yttrium-Aluminum Garnet Powders, American Ceramic Society Bulletin **65** (9) (1986)1282-1286.

18. H. Wang, L. Gao and K. Niihara, Synthesis of Nanoscaled Yttrium Aluminum Garnet Powder by the Co-precipitation Method, Materials Science and Engineering A **288** [1] (2000) 1-4.

19. J.-y. Park, S.-G. Oh, U. Paik and S.-K. Moon, Preparation of Aluminum Oxide Particles Using Ammonium Acetate as Precipitating Agent, Materials Letters **56** (2002) 429-434.

20. I. Matsubara, M. Paranthaman, S.W. Allison, M.R. Cates, D.L. Beshears and D.E. Holcomb, Preparation of Cr-Doped $Y_3Al_5O_{12}$ Phosphors by Heterogeneous Precipitation Methods and Their Luminescent Properties, Materials Research Bulletin **35** (2000) 217-224.

21. D. Hreniak and W. Strek, Synthesis and Optical Properties of Nd^{+3}-doped $Y_3Al_5O_{12}$ Nanoceramics, Journal of Alloys and Compounds **341** [1-2] (2002) 183-186.

22. M. Veith, S. Mathur, A. Kareiva, M. Jilavi, M. Zimmer and V. Huch, Low Temperature Synthesis of Nanocrystalline Y3Al5O12 (YAG) and Ce-doped Y3Al5O12 via Different Sol-Gel Methods, Journal of Materials Chemistry **9** (1999) 3069-3079.

23. P. Vaqueiro and M.A. Lopez-Quintela, Influence of Complexing Agents and Ph on Yttrium-Iron Garnet Synthesized by the Sol-Gel Method, Chemistry of Materials **9** (1997) 2836-2841.

24. T. Tachiwaki, M. Yoshinaka, K. Hirota, T. Ikegami and O. Yamaguchi, Novel Synthesis of Y3Al5O12 (YAG) Leading to Transparent Ceramics, Solid State Communications **119** (2001) 603-606.

25. M. A. Gülgün, O. O. Popoola and W. M. Kriven, Chemical Synthesis and Characterization of Calcium Aluminate Powders, Journal of the American Ceramic Society **77** [2] (1994) 531-539.

26. M. Pechini, Method of Preparing Lead and Alkaline-Earth Titanates and Niobates and Coating Method Using the Same to Form a Capacitor, U.S. Pat. No. 3 330 697 July 11, 1967.

27. M. A. Gülgün, M. H. Nguyen and W. M. Kriven, Polymerized Organic-Inorganic Synthesis of Mixed Oxides, Journal of the American Ceramic Society **82** [3] (1999) 556-560.

28. X. Zhang, H. Liu, W. He, J. Wang, X. Li and R. I. Boughton, Synthesis of Monodisperse and Spherical YAG Nanopowder by a Mixed Solvothermal Method, Journal of Alloys and Compounds, **372** [1-2] (2004) 300-303.

29. M. L. Keith and R. Roy, Structural Relations among Double Oxides of Trivalent Elements, Journal of the Mineralogical Society of America, **39** January- February, (1954) Nos. 1 and 2.

30. H. S. Yoder and M. L. Keith, Complete Substitution of Aluminum for Silicon: The System $3MnO.Al_2O_3.3SiO_2$-$3Y_2O_3.5Al_2O_3$, Journal of the Mineralogical Society of America, **36** July- August, (1951) Nos. 7 and 8.

31. J. Carda, M. A. Tena, G. Monros, V. Esteve, M. M. Reventos and J. M. Amigo, A Rietveld Study of the Cation Substitution between Uvarovite and Yttrium-Aluminum Synthetic Garnets, Obtained by Sol-Gel Method, Crystal Research and Technology **29** (1994) 3 387-391.

32. http://unit.aist.go.jp/greenlife/ii/STRUCIMAGES/Grossular.gif

33. M. Yoshimura and W. Suchanek, In Situ Fabrication of Morphology-Controlled Advanced Ceramic Materials by Soft Solution Processing, Solid State Ionics **98** (1997) 197-208.

34. U. Adem, Preparation of $Ba_xSr_{1-x}TiO_3$ Thin Films by Chemical Solution Deposition and Their Electrical Characterization (2003), p.27.

35. http://www.chemat.com/html/solgel.html

36. C.J. Brinker and G.W. Scherer, Sol-Gel Science, Academic Press, (1990) p.4 and p.21-30.

37. X. Li, H. Liu, J. Wang, X. Zhang and H. Cui, Preparation and Properties of YAG Nano-sized Powder from Different Precipitating Agent, Optical Materials **25** [4] (2004) 407-412.

38. D. Segal, Chemical Synthesis of Advanced Ceramic Materials, Cambridge University Press, (1991) p. 23.

39. S-H. Yu, T. Fujino and M. Yoshimura, Hydrothermal Synthesis of $ZnFe_2O_4$ Ultrafine Particles with High Magnetization, Journal of Magnetism and Magnetic Materials **256** (2003) 420-424.

40. Y.C. Zhang, H. Wang, H.Y. Xu, B. Wang, H. Yan, A. Ahniyaz and M. Yoshimura, Low-Temperature Hydrothermal Synthesis of Spinel-Type Lithium Manganese Oxide Nanocrystallites, Solid State Ionics **158** (2003) 113-117.

41. Y.C. Zhang, H. Wang, B. Wang, H.Y. Xu, H. Yan and M. Yoshimura, Hydrothermal Synthesis of Metastable γ-Manganese Sulfide Crystallites, Optical Materials **23** (2003) 433-437.

42. M. Popa, J. Frantti and M. Kakihana, Lanthanum Ferrite $LaFeO_{3+d}$ Nanopowders Obtained by the Polymerizable Complex Method, Solid State Ionics **154-155** (2002) 437-445.

43. M. Popa, J. Frantti and M. Kakihana, Characterization of $LaMeO_3$ (Me: Mn, Co, Fe) Perovskite Powders Obtained by Polymerizable Complex Method, Solid State Ionics **154-155** (2002) 135-141.

44. M. Popa and M. Kakihana, Synthesis of Lanthanum Cobaltite ($LaCoO_3$) by the Polymerizable Complex Route, Solid State Ionics **151** (2002) 251-257.

45. A. Abrue Jr., S.M. Zanetti, M.A.S. Oliveira and G.P. Thim, Effect of Urea on Lead Zirconate Titanate –$Pb(Zr_{0.52}Ti_{0.48})O_3$- Nanopowders Synthesized by the Pechini Method, Journal of the European Ceramic Society **xxx** (2004) xxx-xxx.

46. S. Wu and H. Chen, The Effects of Heat-Treatment Temperature on the Retention Capacities of Spinels Prepared by the Pechini Process, Journal of Power Sources **119-121** (2003) 134-138.

47. Z. Xu, Y. Li, Z. Liu and Z. Xiong, Low-Temperature Synthesis of Nanocrystalline $ZnGa_2O_4:Tb^{3+}$ Phosphors via the Pechini Method, Materials Science and Engineering B **110** (2004) 302-306.

48. B. Cockayne, The Uses and Enigmas of the Al_2O_3-Y_2O_3 Phase System, Journal of the Less-Common Metals, **114** (1985) 199-206.

49. L.E. Olds and H.E. Otto, in E.M. Levin et al. (eds.), Phase Diagrams for Ceramicists, American Ceramics Society, (1987), Fig. 311.

50. N. A. Toropov, I. A. Bondar, F. Ya. Galakhov, X. S. Nikogosyan and N. V. Vinogradova, Phase Diagrams for Ceramists, American Ceramic Society, (1987) Fig. 2344.

51. J.S. Abell, I.R. Harris, B. Cockayne and B. Lent, An Investigation of Phase Stability in the Y_2O_3-Al_2O_3 System, Journal of Materials Science, **9** (1974) 527-537.

52. E. Prince, Neutron Diffraction Measurements on Yttrium-Iron and Yttriumaluminium Garnets, Acta Crystallographica B, **31** (1975) 2233-2240.

53. N.J. Hess, G.D. Maupin, L.A. Chick, D.S. Sunberg, D.E. McCreedy and T.R. Armstrong, Synthesis and Crystallization of Yttrium-Aluminium Garnet and Related Compounds, Journal of Materials Science **29** (1994) 1873-1878.

54. R. Diehl and G. Brandt, Crystal Structure Refinement of $YAlO_3$, a Promising Laser Material, Materials Research Bulletin, **10** (1975) 85-90.

55. F. Bertaut and J. Mareschal, Un Nouveau Type de Structure Hexagonale: Al T O3 (T= Y, Eu, Gd, Tb, Dy, Ho, Er), Comptes Rendus Hebdomadaires des Seances de l' A cademie des Sciences, **257** (1963) 867-870.

56. H. Yamane, M. Omori and T. Hirai, Thermogravimetry and Rietveld Analysis for the High-Temperature X-ray Powder Diffraction Pattern of Y4 Al2 O9, Journal of Materials Science. Letters, **14** (1995) 470-473.

57. I. Warshaw and R. Roy, Stable and Metastable Equilibria in the Systems Y_2O_3-Al_2O_3 and Gd_2O_3-Fe_2O_3, Journal of the American Ceramic Society, **42** [9] (1959) 434-438.

58. I. Papadopoulos, On the Existence and Formation of $Y_4Al_2O_9$, Crystal Research and Technology **26** [4] (1991) 409-411.

59. B.D. Cullity, Elements of X-Ray Diffraction, Addison-Wesley Publishing Company, Inc., (1978) p. 377-379.

60. www.webelements.com

61. J. W. G. A. Vrolijk, S. van den Cruysem and R. Metselaar, The Influence of MgO and SiO_2 Dopants on the Sintering Behaviour of Yttrium Aluminium Garnet Ceramics, Ceramic Processing Science and Technology, American Ceramic Society, (1995) p. 573-577.

62. I.A. Bondar and F. Ya. Galakhov, Phase Diagrams for Ceramists, American Ceramic Society, (1987) Fig. 2586.

63. J.D. Verhoeven, Fundamentals of Physical Metallurgy, John Wiley & Sons, (1975) p. 127-129.